Historical and projected freshwater withdrawals and irrigation consumptive use for Arizona, 1896–2099

Sayantan Majumdar[1], Ryan G. Smith[2], Peter ReVelle[1], Md Fahim Hasan[2], Collin Wogenstahl[3, †], Danielle E. Tadych[3], Laney Meeker[3]

1. Division of Hydrologic Sciences, Desert Research Institute, Reno, Nevada, USA
2. Department of Civil and Environmental Engineering, Colorado State University, Fort Collins, Colorado, USA
3. Arizona Department of Water Resources, Phoenix, Arizona, USA

[†] Formerly at Arizona Department of Water Resources

Corresponding author: sayantan.majumdar@dri.edu

Abstract

Sustainable water management needs spatially resolved withdrawal estimates, yet such data remain scarce worldwide. In Arizona, USA, decades of aquifer overdraft and Colorado River over-allocation have outpaced local withdrawal data, constraining policymaking. We present annual freshwater withdrawal and irrigation consumptive use estimates for Arizona at 2 km resolution over 1896–2099, partitioned by source (groundwater, surface water) and use (irrigation, non-irrigation). A machine learning model trained on flowmeter records (1984–2024) estimated total withdrawal, partitioned into eight withdrawal categories and three consumptive-use products. A stream capture index flags where groundwater withdrawal may deplete surface-water supplies. Because post-2026 Colorado River shortages are not yet set, projections are also provided under eight Central Arizona Project (CAP) shortage scenarios, up to a complete loss of CAP deliveries. Every product carries per-pixel uncertainty, and a well package disaggregates the predictions to ~170,000 registered consumptive wells. Outputs were validated against U.S. Geological Survey, Arizona Department of Water Resources, and CAP records. The dataset supports groundwater modeling, aquifer-depletion assessment, and water-resources planning in Arizona and its transboundary watersheds.

Background & Summary

Arizona depends on groundwater (GW) for ~40% of its total water supply, with the remainder sourced from the Colorado River via the Central Arizona Project (CAP), the Salt River Project (SRP), and local surface-water diversions[1]. The Colorado River System, apportioned among seven western U.S. states (Arizona, California, Colorado, Nevada, New Mexico, Utah, and Wyoming) by the 1922 Colorado River Compact[2] and shared with Mexico under the 1944 U.S.–Mexico Water Treaty[3], has been in a prolonged supply–demand imbalance driven by over-allocation, a 26-year megadrought, and rising demands[4]. Lake Mead and Lake Powell, the two largest Colorado River Basin reservoirs, declined to historically low levels in the early 2020s, triggering unprecedented shortage declarations by the U.S. Bureau of Reclamation (USBR). Arizona holds junior priority rights among the Lower Basin states and therefore bears a disproportionate share of these curtailments. Reductions to the state's Colorado River allocation

began in 2020 and have deepened since: a Tier 0 Drought Contingency Plan (DCP) contribution of 192,000 acre-feet per year in 2020–2021; the first Tier 1 shortage declaration in 2022, which cut the allocation by 512,000 acre-feet (AF) per year (512 thousand acre-feet, kAF, yr^{-1}, or ~630 Mm^3 yr^{-1}, ~18% of Arizona's Colorado River supply); a Tier 2a reduction of 592 kAF yr^{-1} in 2023, alongside a further 355 kAF yr^{-1} of voluntary conservation; and a return to Tier 1 for 2024 through 2026. These shortages fall primarily on CAP agricultural users, who lose access to surface water (SW) and must either fallow land or substitute groundwater pumping, which links Colorado River policy directly to aquifer depletion across central Arizona[5–10].

Decades of groundwater extraction have caused substantial aquifer depletion across the state's Active Management Areas (AMAs) and Irrigation Non-Expansion Areas (INAs), seen as declining water tables and, in some basins, land subsidence[6,11–13]. The 2007 Interim Guidelines and the 2019 DCP that governed the reductions in Colorado River allocation both expired in 2026, and the seven Basin States did not reach consensus on a replacement. In August 2026, the U.S. Department of the Interior therefore adopted a Decision Framework for the coordinated operations of Lake Powell and Lake Mead over 2027–2036[9]. The framework fixes operational sideboards, including an upper limit of 3.0 million acre-feet (MAF) yr^{-1} (3,700 Mm^3 yr^{-1}) on the combined shortage that can be imposed on Arizona, California, and Nevada (the Lower Division States), shared among them under applicable law, but defers the specific shortage volumes and their distribution among those states to Operating Guidelines issued at roughly two-year intervals. The first set, the 2027–2028 Operating Guidelines[14], lowers the Lower Division States' apportionment from 7.5 to 6.25 MAF yr^{-1} in both years, of which 760 kAF yr^{-1} (937 Mm^3 yr^{-1}) falls on Arizona under a Lower Basin implementing agreement. Beyond 2028, surface-water availability in Arizona is therefore bounded but not specified, which sharpens the need for spatially resolved water-use data that can inform both state-level planning and interstate allocation decisions. These dynamics make Arizona a useful case study of how groundwater storage[15–17] responds to coupled climate, land-use, and management drivers[18].

Despite Arizona's extensive water infrastructure, no statewide spatially resolved withdrawal dataset spans the historical-to-future continuum. The USGS National Water Census provides county-level estimates at five-year intervals from 1950[19]. The Arizona Department of Water Resources (ADWR) meters wells within the AMA and INA management areas (~3,000 wells per year, 1984–2024)[20], but coverage outside those areas is sparse. U.S. Geological Survey (USGS) reanalysis products provide Hydrologic Unit Code 12 (HUC12)-scale source-partitioned (GW, SW) monthly estimates of irrigation withdrawals, consumptive use (CU), and public supply (PS) across the conterminous U.S. (CONUS), but cover only 2000–2020[21–25]. Reitz et al. (2023)[26] (referred to as USGS Reitz below) provide CONUS-wide GW and SW monthly irrigation withdrawal rasters (1980–2018), but these are resampled from the USGS county-scale estimates and are not operationally updated. An earlier Arizona study by Majumdar et al. (2022)[11] showed that machine learning can estimate groundwater withdrawal statewide at 2 km resolution for 2002–2020, but did not provide detailed uncertainty quantification, surface-water products, consumptive-use estimates, or future projections[27]. To address these gaps, this study assimilates satellite observations, modeled products, and ground-based measurements within a machine learning framework, and produces a spatially resolved, unified water-use dataset for Arizona spanning 1896–2099.

The dataset comprises 15 gridded product families at 2 km resolution for 1896–2099[28]: nine withdrawal categories (the total plus eight partitions), three irrigation consumptive-use

categories, and three stream capture categories. Three eras are used throughout: hindcast (1896–1983), historical (1984–2025), and projection (2026–2099). Fig 1 summarizes the dataset with the mean annual predicted total withdrawal depth (Fig 1a), the statewide annual time series of groundwater and surface-water withdrawal across the three eras (Fig 1b), era-averaged irrigation and non-irrigation volumes (Fig 1c), and the associated uncertainty (σ_{total}; Methods, Uncertainty quantification). Stream capture, as used here, is the part of a groundwater withdrawal that is ultimately supplied by a hydraulically connected stream or canal, either through induced infiltration from the channel or through reduced groundwater discharge to it, instead of by depletion of aquifer storage; it is also called stream depletion or river capture in the literature[29,30]. The base method is a machine learning model trained on pumping data (metered, estimated, or previously published records) with remote sensing and land use-derived predictors (listed in Table 1). Similar machine learning approaches for water use estimation have been developed across multiple regions in the U.S.[11,31–38] and other countries[39–41].

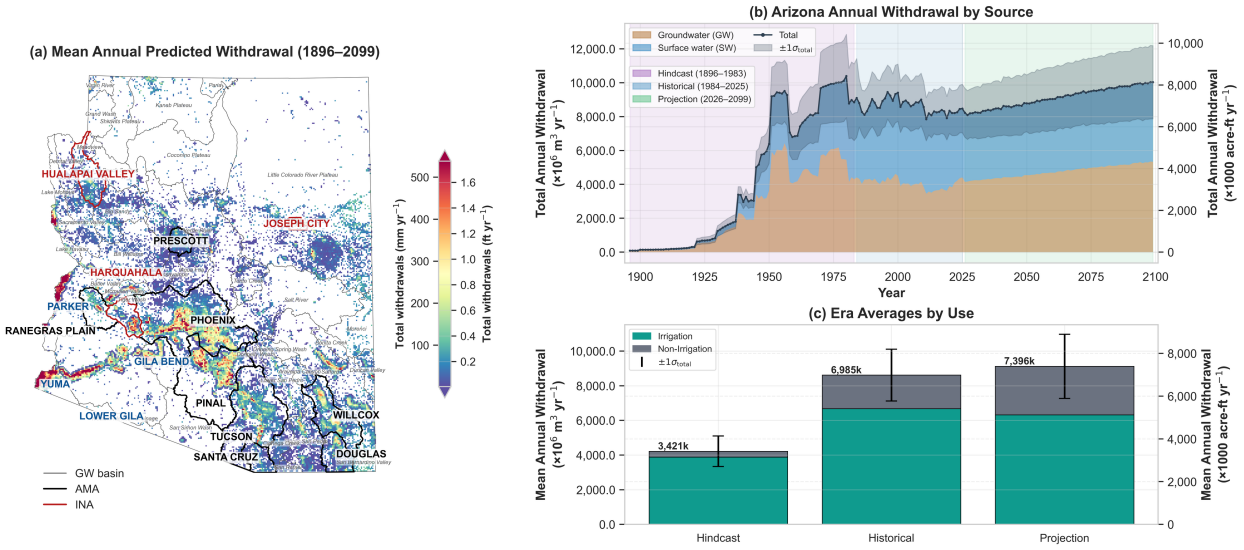


Fig 1. Dataset overview[28]. (a) Mean annual predicted withdrawal depth over 1896–2099, with groundwater basin boundaries and AMA/INA labels. (b) Statewide annual total withdrawal time series, including groundwater and surface water, with $1\sigma_{total}$ from the six-component uncertainty framework and era shading for the hindcast (1896–1983), historical (1984–2025), and projection (2026–2099) eras. (c) Era-average irrigation and non-irrigation withdrawal volumes with $1\sigma_{total}$ error bars. σ_{total} and the uncertainty framework are defined in Methods, Uncertainty quantification.

Methods

Dataset acquisition and harmonization

Dataset inventory

The processing uses three groups of gridded layers on a common 2 km grid over Arizona (Table 1). Group A holds the 22 model predictors used to train and run the machine learning model; group B holds layers used only after prediction, to split the predicted withdrawal by source and use and to compute stream capture; and group C holds layers derived for comparison and not used. Fifteen climate and land-surface bands were downloaded from Google Earth Engine[42,43] (GEE) as tiled GeoTIFFs, and the remaining layers, such as well density, surface-water-rights

density, canal density, watershed streamflow, and water-table depth, were built from point, vector, gage, and raster records and resampled to the same grid. Every layer covers 1896–2099, but only the 1984–2024 metered years supply training labels (Training data); the hindcast and projection years use the same predictors for prediction only. Bands from different sources were joined into continuous series with the overlap-period bias correction described in Three-era data harmonization.

Each band's era-specific sources are as follows. Actual ET came from the USGS Reitz Ensemble[26], OpenET[44,45], and the MACA v2[46] ensemble; reference ET from PRISM Hargreaves[47,48] and OpenET gridMET[49]. Precipitation and mean daily maximum and minimum air temperature datasets were obtained from PRISM and MACA; and the two effective-precipitation (P_{eff}) variants from the U.S. Department of Agriculture Soil Conservation Service (USDA SCS) method[50–52] and from Hasan et al. (2025)[35]. Land cover dataset combined USGS historical LULC[53], NLCD[54,55], and the USGS LULC projections[56], from which the cropland and urban fractions were derived. The irrigated-area fraction dataset came from IrrMapper RF v1.2[57,58] and the groundwater-irrigation fraction from Hung et al. (2025)[59]. The three soil properties datasets were compiled from CSRL/gNATSGO/SSURGO[60,61]. The locally assembled layers were well density, in total and by use category (ADWR Well Registry[62]), HarDWR[63] surface-water-rights density, GRAIN[64] canal density, watershed and canal-weighted streamflow (USGS NWIS[65] and USBR[66,67] gages; Table 2), and 30 m CONUS water-table depth from Ma et al. (2026)[68]. The climate and land-cover fraction layers are annual over 1896–2099; soil properties and water-table depth are static; and the well- and water-rights-density layers grow with infrastructure build-out through 2024 and are then held forward across the projection.

Table 1. Dataset inventory. Layers are grouped by role: (A) the 22 model predictors used to train and run the XGBRF model; (B) layers used only after prediction, in the GW/SW partition and the stream capture index; and (C) layers derived but not used, kept for comparison. For each layer the table gives its native resolution and the dataset from which it was created in each era; the bias corrections between adjacent-era datasets are described in Three-era data harmonization. Only the 1984–2024 metered years are used for training; the other years use the same predictors for prediction.

Layer	Native resolution	Hindcast (1896–1983)	Historical (1984–2025)	Projection (2026–2099)
A. Model predictors (22)				
Actual ET	800 m (Reitz), 30 m (OpenET), 4 km (MACA)	USGS Reitz Ensemble, bias-corrected to OpenET	OpenET Ensemble v2.0/v2.1	MACA v2 ETo × OpenET monthly ETof
Grass reference ET (ETo)	4 km	PRISM Hargreaves, bias-corrected to OpenET gridMET (OpenET gridMET from 1979)	OpenET gridMET	MACA v2 ASCE-PM, bias-corrected to OpenET gridMET
Precipitation	4 km	PRISM	PRISM	MACA v2 40-member ensemble mean

Layer	Native resolution	Hindcast (1896–1983)	Historical (1984–2025)	Projection (2026–2099)
Mean daily maximum and minimum air temperature	4 km	PRISM	PRISM	MACA v2 40-member ensemble mean
Effective precipitation, USDA SCS	2 km (derived)	Derived from PRISM Hargreaves ETo bias-corrected to OpenET gridMET (OpenET gridMET from 1979), PRISM precipitation and SSURGO soils	Derived from OpenET gridMET ETo, PRISM precipitation and SSURGO soils	Derived from MACA v2 ETo and precipitation and SSURGO soils
Cropland and urban fractions; agricultural (AGRI) and urban (URBAN) densities	2 km (derived)	From USGS historical LULC, basin-delta corrected to the 1985 NLCD anchor	From NLCD	From USGS LULC projections, basin-delta corrected to the 2025 NLCD anchor
Irrigated fraction	30 m	Cropland-fraction regression fitted on 1985–2025	IrrMapper RF v1.2	Cropland-fraction regression fitted on 1985–2025
Groundwater irrigation fraction	60 m	Hung et al. (2025), 2000 snapshot	Hung et al. (2025), 2000 / 2005 / 2010 / 2015 snapshots	Hung et al. (2025), 2015 snapshot
Soil depth, available water capacity, saturated hydraulic conductivity	30 m (gNATSGO/SSURGO), 800 m (CSRL)	Static	Static	Static
Water-table depth	30 m	Static, 1913–2023 mean	Static	Static
Well density, total	Point → 2 km	ADWR Well Registry, cumulative from each well's installation year	ADWR Well Registry, cumulative from each well's installation year, through 2024	2024 well field held forward
Surface-water-rights density, total	Point → 2 km	HarDWR, cumulative from each right's priority year	HarDWR, cumulative from each right's priority year	2024 field held forward

Layer	Native resolution	Hindcast (1896–1983)	Historical (1984–2025)	Projection (2026–2099)
Canal density	Vector → 2 km	GRAIN, gated by each segment's first delivery year	GRAIN, gated by each segment's first delivery year	2025 network held forward
Watershed streamflow	Gage → 2 km	USGS NWIS observations; ratio-scaled synthetics and monthly climatology for gaps	USGS NWIS observations	USBR CMIP3 ensemble; historical-ratio estimates at sites without direct projections
Easting, Northing (added at training time)	2 km	Static	Static	Static
B. Used after prediction: GW/SW partition and stream capture				
Well density, irrigation and non-irrigation	Point → 2 km	ADWR Well Registry by declared use, cumulative from each well's installation year	ADWR Well Registry by declared use, through 2024	2024 well field held forward
Surface-water-rights density, irrigation and non-irrigation	Point → 2 km	HarDWR by use, cumulative from each right's priority year	HarDWR by use, cumulative from each right's priority year	2024 field held forward
Canal-weighted streamflow	2 km (derived)	Watershed streamflow redistributed by canal density	Watershed streamflow redistributed by canal density	Watershed streamflow redistributed by canal density
Irrigation pump-capacity fraction	Point → 2 km	ADWR Well Registry pump rates of active wells	ADWR Well Registry pump rates of active wells	2024 well field held forward
LULC class	250 m (USGS), 30 m (NLCD)	USGS historical LULC; 1938 classification for years ≤ 1983	NLCD	Pixel-wise mode of four USGS LULC scenarios (A1B, A2, B1, B2)
C. Derived for comparison, not used				
Effective precipitation, PCML	2 km	Hasan et al. (2025), 2000–2023 mean	Hasan et al. (2025)	Hasan et al. (2025), 2000–2023 mean
Surface-water (SW) density	2 km (derived)	From USGS historical LULC, basin-delta corrected to the	From NLCD	From USGS LULC projections, basin-delta corrected to

Layer	Native resolution	Hindcast (1896–1983)	Historical (1984–2025)	Projection (2026–2099)
		1985 NLCD anchor		the 2025 NLCD anchor

Model predictors

Twenty-two layers are model predictors (Table 1, group A): actual ET, reference ET, precipitation, effective precipitation from the USDA SCS method[50], maximum and minimum air temperature, cropland and urban fractions, agricultural and urban densities, irrigated fraction, groundwater-irrigation fraction, soil depth, available water capacity, saturated hydraulic conductivity, water-table depth, total well density, total surface-water-rights density, canal density, watershed streamflow, and the pixel coordinates (Easting and Northing). Most are derived rather than used as downloaded: the land-cover predictors come from the categorical LULC class, the densities from point and vector records, and the coordinates are added at training time. The remaining layers are not model inputs. The per-category well and surface-water-rights densities, canal-weighted streamflow, irrigation pump-capacity fraction, and raw LULC class (group B) are used only after prediction, to partition withdrawal and to compute stream capture; the PCML effective precipitation[35] and the surface-water density (group C) are kept for comparison.

Three-era data harmonization

The pipeline joined datasets from different eras into continuous 1896–2099 series by bias-correcting each earlier or later dataset to the reference dataset over the years in which the two overlap (Fig 2). For pixel x and calendar month m, a correction ratio was computed as the mean, over the N_m overlap years y, of the reference-to-source ratio, and every image of that month was multiplied by it:

$$r(x, m) = (1 / N_m) \times \Sigma_y R(x, m, y) / S(x, m, y), \quad S'(x, m, y) = r(x, m) \times S(x, m, y)$$

where R is the reference dataset, S the dataset being corrected, and S′ the corrected series. This gives 12 monthly correction grids per variable (the per-pixel, per-month correction hereafter). The correction removes the systematic offset between the two datasets while keeping each dataset's own year-to-year variability, and it assumes that the offset is stable over time, the standard assumption of ratio-based bias correction. The datasets harmonized this way are described below.

Actual evapotranspiration (ET): For 1896–1999, USGS Reitz ET[26] was bias-corrected to OpenET[44] using monthly OpenET/Reitz ratios derived from 228 paired monthly images in the 2000–2018 overlap. OpenET Ensemble v2.0/v2.1 was used directly for 2000–2025. For 2026–2099, monthly crop coefficients (EToF = ET/ETo) derived from the 2000–2025 OpenET/gridMET[49] ratio were applied to MACA v2[46] projected ETo. This keeps the observed spatial pattern of crop water demand while letting the climate signal evolve under the future scenarios.

Grass reference evapotranspiration (ETo): For 1896–1978, PRISM Hargreaves ETo[47,48] was bias-corrected to OpenET gridMET with the per-pixel, per-month correction above, using 564 paired monthly images from the 1979–2025 overlap. OpenET gridMET was used directly for

1979–2025. For 2026–2099, ETo was computed from MACA v2 daily climate variables with the American Society of Civil Engineers (ASCE) standardized Penman–Monteith (ASCE-PM)[69] equation, using the openet-refet-gee[70] Python package. It was then bias-corrected to OpenET gridMET with OpenET's published monthly gridMET correction ratios, so that historical and projected ETo share the same reference. The MACA variables, models, and scenarios are described under Climate projections, below.

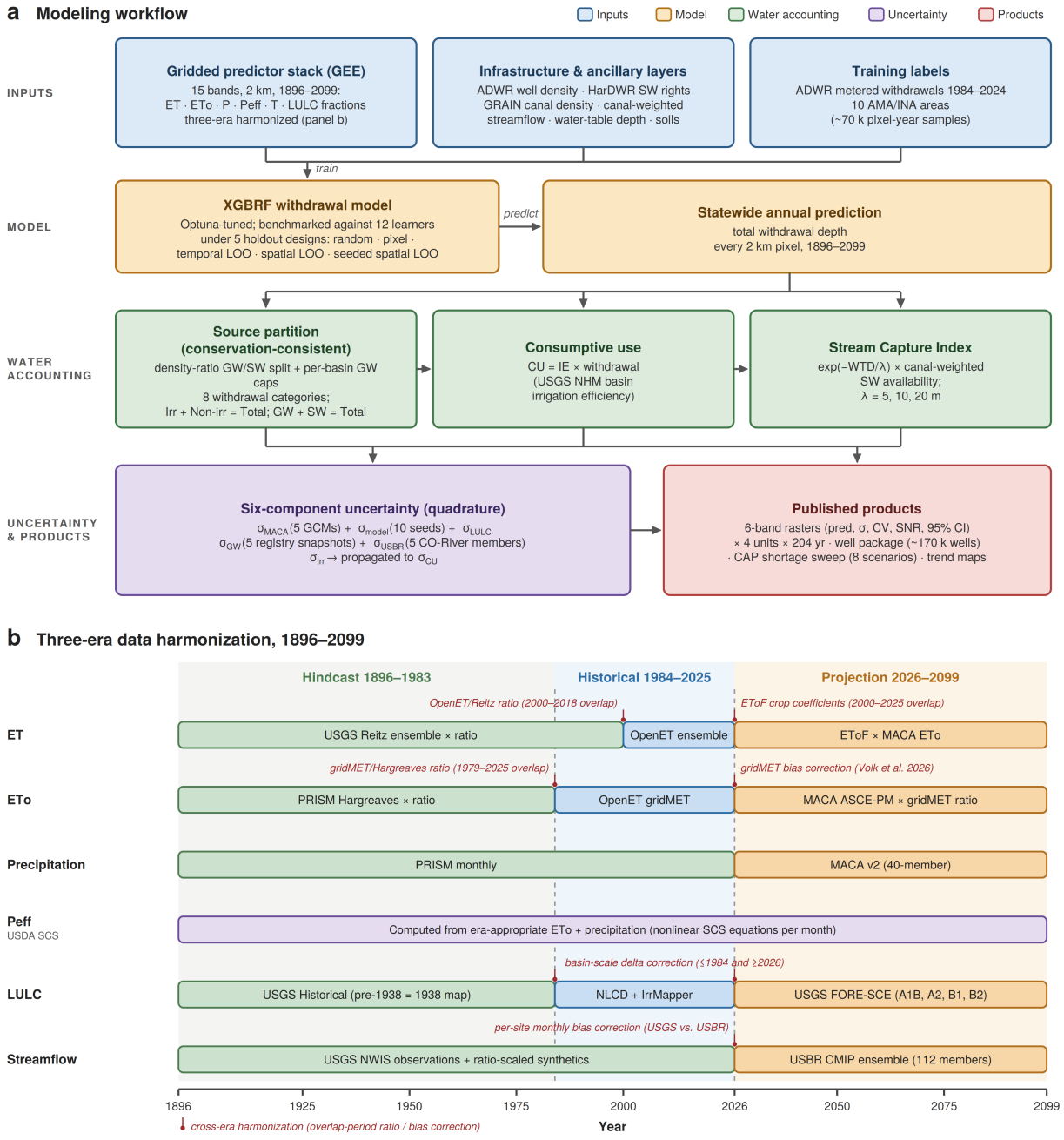


Fig 2. Pipeline workflow and three-era data harmonization. (a) Processing chain from inputs to published products: the harmonized GEE climate and land-surface bands and the infrastructure layers feed the Optuna-tuned[71] XGBoost Random Forests (XGBRF)[72] model trained on ADWR metered records[20] (1984–

2024, AMA and INA areas only); statewide annual predictions are post-processed through the conservation-consistent density-ratio partition, the CU = IE × Withdrawal relationship, and the stream capture calculation, with the six-component uncertainty framework propagated into every published product. (b) Source timeline for the six harmonized dataset families across the hindcast (1896–1983), historical (1984–2025), and projection (2026–2099) eras; annotations mark the overlap-period bias corrections that join adjacent sources (Methods, Three-era data harmonization).

Land use/land cover (LULC): USGS historical LULC[53] (250 m) was used for years ≤ 1984, with the 1938 classification, the earliest available, applied to all pre-1983 years following Reitz et al. (2023)[26]. NLCD (30 m) was used for 1985–2025 and the pixel-wise mode across four USGS LULC projection scenarios (250 m) was used for 2026–2099. The four scenarios correspond to Intergovernmental Panel on Climate Change Special Report on Emissions Scenarios (SRES) storylines that span a range of economic growth and environmental stewardship assumptions. The pixel-wise mode across these four trajectories gives a consensus classification that does not commit the projection to any single scenario.

Each year's classification was recoded into agricultural, urban, and surface-water classes, from which four land-cover predictors were derived. The first two are the cropland and urban fractions, which give the per-pixel area share of the respective classes. The next two are the agricultural and urban densities[11] (AGRI, URBAN), obtained by reducing each class to a binary mask and applying a Gaussian filter (σ = 3 pixels = 6 km) rescaled to [0, 1], so that each pixel value reflects how strongly it sits within surrounding agricultural or urban land. A fifth layer, surface-water density (SW), was derived the same way from the surface-water class with a tighter filter (σ = 1 pixel = 2 km), but it is not used by the model or the partition (Table 1, group C).

NLCD (30 m) and the USGS historical and projected products (250 m) give systematically different basin-level urban and agricultural fractions once aggregated to 2 km, so the land-cover layers were harmonized in a way that mirrors the climate correction. In years outside the NLCD record (≤ 1984 and ≥ 2026), each layer keeps the spatial pattern of the nearest NLCD year (1985 or 2025) and takes only its basin-wide change over time from the USGS product. For pixel p in groundwater basin b, land-cover class c, and year y:

$$\delta(y, b, c) = f(y, b, c) / f(y_0, b, c), \qquad v(p, y) = v_{NLCD}(p) \times \delta(y, b, c)$$

where f is the basin-mean fraction of class c in the USGS product, y_0 is the USGS year next to the NLCD anchor (1984 for the hindcast, 2026 for the projection), v_{NLCD} is the layer value in the NLCD anchor year, and v is clipped to [0, 1]. Because δ = 1 at the boundary year, each series is continuous across it. The correction was applied to the cropland and urban fractions, AGRI, URBAN, and SW.

Irrigated fraction: The irrigated-area fraction was taken directly from IrrMapper RF v1.2[57] (30 m, aggregated to 2 km) over its 1985–2025 coverage. Outside that window it was estimated from the cropland fraction with a single ordinary least-squares linear regression of IrrMapper irrigated fraction on NLCD cropland fraction, fitted on all pixel-year samples with non-zero cropland fraction in 1985–2025. One relationship was fitted statewide, not one per basin or per pixel, because the quantity being transferred is the share of cropland that is irrigated, which is not resolvable at the pixel scale outside the IrrMapper record. The fitted model was then applied

pixel by pixel to the basin-delta-corrected cropland fraction of each hindcast (1896–1984) and projection (2026–2099) year.

Pixels with zero cropland fraction were assigned zero irrigated fraction, and the regression predictions were clipped to [0, 1]. Because the projection cropland fraction is the pixel-wise mode of the four USGS LULC scenarios, the projected irrigated fraction inherits that consensus land-use trajectory.

Effective precipitation: Effective precipitation, the portion of actual ET supplied by precipitation, was computed for all 204 years with the USDA-SCS method[50,51] as implemented in pyCropWat[52]. Monthly precipitation (P) and ETo were converted from mm to inches, and the soil storage depth (d) was computed as

$$d = \mathrm{AWC} \times \mathrm{MAD} \times D_{\mathrm{root}} \quad (1)$$

where AWC is the SSURGO[61] available water capacity, MAD is the maximum allowed depletion factor (set to 1 here), and the root-zone depth (D_{root}) is 2 m or ~6 ft, a typical alfalfa rooting depth[73,74]. The soil storage factor (sf) follows as

$$sf = 0.531747 + 0.295164\,d - 0.057697\,d^2 + 0.003804\,d^3 \quad (2)$$

and the monthly effective precipitation (P_{eff}) is

$$P_{\mathrm{eff}} = sf \times (0.70917\,P^{0.82416} - 0.11556) \times 10^{0.02426\,\mathrm{ETo}} \quad (3)$$

clamped to the physical bounds

$$0 \le P_{\mathrm{eff}} \le \min(P, \mathrm{ETo}) \quad (4)$$

The estimated effective precipitation was then converted back to mm. Equations (1)–(4) were evaluated with era-appropriate inputs: ETo from PRISM Hargreaves (1896–1978), OpenET gridMET (1979–2025), or bias-corrected MACA (2026–2099), and precipitation from PRISM (1896–2025) or the 40-member MACA ensemble mean (2026–2099).

Climate projections: The 2026–2099 climate forcing was built from the MACA v2[46] (Multivariate Adaptive Constructed Analogs) archive, a statistically downscaled CMIP5 daily product for the conterminous United States at 1/24° (~4 km) resolution, resampled to the 2 km analysis grid. Seven daily variables were obtained from MACA: maximum and minimum 2 m air temperature, precipitation, downward shortwave radiation, eastward and northward 10 m wind, and near-surface specific humidity. These supply the two climate-dependent predictors that carry the projection signal, reference evapotranspiration (ETo) and precipitation.

ETo was computed at the daily time step with the ASCE-PM[69] formulation through the openet-refet-gee Python package[70], from MACA daily maximum and minimum temperature, specific humidity, eastward and northward wind, and shortwave radiation, so that its nonlinear dependence on these variables is retained. MACA is statistically downscaled against gridMET, so the computed ETo was bias-corrected to OpenET gridMET ETo[49] with OpenET's published per-pixel, per-month gridMET correction ratios, applied unchanged to every projection year. Holding these ratios fixed assumes that the bias between gridMET and station-based reference ET is stable over time.

Projected precipitation is the 40-member MACA ensemble mean. Because MACA is already bias-corrected against gridMET, no further correction was applied; historical precipitation comes from PRISM. The ensemble comprises 20 CMIP5 GCMs run under two emission pathways (RCP 4.5 and RCP 8.5), giving 40 members.

The 2026–2099 predictors are therefore a multi-model, multi-pathway average. This damps individual-model bias, but it also mutes inter-model extremes. Disagreement between GCMs is quantified separately as σ_{MACA} (Methods, Uncertainty quantification), where the trained model is re-run with five representative GCMs spanning the hot–dry, hot–wet, cool–dry, cool–wet, and central-tendency corners of the projected temperature and precipitation space.

The plausibility of the two emission pathways and the route to a CMIP6/CMIP7[75,76] forcing upgrade are discussed under Emission-pathway choice (RCP 8.5) in Usage Notes, Known limitations.

Ancillary datasets

Canal density and streamflow. Canal density is the number of GRAIN[64] canal segments intersecting each 2 km pixel. Streamflow was assembled from 19 USGS and USBR gage sites falling in 12 of Arizona's 15 surface watersheds[62,65,66] (Table 2). Each gage was assigned by spatial join to the watershed polygon containing it, and gages lying outside every polygon, such as Colorado River above Imperial Dam, were assigned to the nearest watershed. The three watersheds with no gage (Rio Yaqui, San Simon, and Willcox Playa) are ephemeral or endorheic and carry negligible perennial streamflow. Monthly discharge came from USGS NWIS[65] observations where available, with USBR CMIP3 ensemble projections or ratio-scaled synthetic series filling the gaps needed to cover 1896–2099[66,67] (Streamflow projections, below). CAP Canal diversions from the Colorado River are overlaid on pixels within the CAP Service Area[62].

Two streamflow rasters were built on the 2 km grid for every year from 1896 to 2099. The first, watershed streamflow, is the annual gaged flow of each watershed spread evenly over its area and expressed as a depth, so that it has the same units (mm yr^{-1}) as the ET and precipitation bands. For watershed w and year y, with Q the mean annual discharge of its gages (m^3 s^{-1}) and A the watershed area (m^2),

$$\text{flow}(w, y) = Q(w, y) \times 3.15576 \times 10^{10} / A(w)$$

where the constant converts seconds per year to millimeters. Years without a gage record take the site's long-term mean. From 1985 onward, pixels in the CAP service area also receive Colorado River flow from Lees Ferry (09380000) and the CAP Canal at Havasu Pumping Plant (09426650), spread over the CAP service area instead of the watershed.

The second raster, canal-weighted streamflow, moves that watershed-average depth onto the pixels that carry canals, in proportion to each pixel's canal density, without changing the watershed total. For pixel p in watershed w, with c the canal density and N(w) the number of pixels in w,

$$cw(p, y) = \text{flow}(w, y) \times N(w) \times c(p, y) / \Sigma_{p' \in w} c(p', y)$$

Pixels without a canal receive zero, and the CAP overlay is redistributed the same way within the CAP service area. Because canal density is gated by each segment's first delivery year, canal-

weighted streamflow follows the build-out of the delivery network. It is used in the GW/SW partition and the stream capture index and is not a model predictor (Table 1, group B).

Table 2. The 19-site USGS and USBR streamflow gage network underlying the watershed streamflow and canal-weighted streamflow rasters, with each site's watershed assignment.

USGS ID	USBR ID	Site name	Watershed
09380000	00013	Colorado River at Lees Ferry	Colorado River
09429490	00014	Colorado River above Imperial Dam	Colorado River
09444500	00058	San Francisco River at Clifton	Upper Gila River
09448500	00059	Gila River at Head of Safford Valley nr Solomon	Upper Gila River
09497500	00061	Salt River near Chrysotile	Salt River
09498500	00062	Salt River near Roosevelt	Salt River
09499000	00063	Tonto Creek Abv Gun Creek nr Roosevelt	Salt River
09510000	00064	Verde River below Bartlett Dam	Verde River
09508500	00064	Verde R blw Tangle Creek Abv Horseshoe Dam	Verde River
09402300	—	Little Colorado River Abv Mouth nr Desert View	Little Colorado River
09426620	—	Bill Williams River near Parker	Bill Williams River
09512500	—	Agua Fria River near Mayer	Agua Fria River
09415000	—	Virgin River at Littlefield	Virgin River
09489000	—	Santa Cruz River near Laveen	Santa Cruz River
09471000	—	San Pedro River at Charleston	San Pedro River
09520500	—	Lower Gila River near Dome	Lower Gila River
09537500	—	Whitewater Draw near Douglas	Whitewater Draw
09537200	—	Leslie Creek near McNeal	Whitewater Draw
09426650	—	CAP Canal at Havasu Pumping Plant	Colorado River (CAP Diversion)

Canal delivery start dates. A canal segment enters the canal-density raster only from its first delivery year, so that the canal layers follow the growth of the delivery network. That year was taken from documented start dates for named canal systems and, otherwise, from the priority year of the nearest HarDWR[63] surface-water point of diversion or the earliest right in the same groundwater basin. At five basins where deliveries began later than the canals were built, a basin start year was imposed as a lower bound; the CAP canal crossed Tucson AMA in 1985, for example, but Tucson received its first CAP deliveries[77] only in 1990. The five start years are Phoenix AMA, 1868 (canals were dug across the Salt River Valley from 1868[78] and were later consolidated into SRP[79]); Pinal AMA, 1924 (Florence–Casa Grande[80] and San Carlos Irrigation Project[81] deliveries); and Harquahala INA (1985), Ranegras Plain (1989), and Tucson AMA (1990), each the first year of CAP deliveries. The full rules are given in Supplementary Note 6 and Supplementary Table S4.

Streamflow projections. Nine of the 19 gaged sites (Table 2) have direct USBR CMIP ensemble projections. Projections for the other ten were scaled from their nearest USBR site with

per-calendar-month ratios computed over the years in which both sites were gaged. Each site's 1896–2099 series uses USGS observations where they exist, then USBR values bias-corrected to USGS with per-calendar-month factors over the overlap (so the series is continuous), and finally the site's monthly climatology for any remaining gaps.

Well density. Well density, the count of registered wells per pixel, was derived from the ADWR Well Registry[62] (~238,000 registered wells) as one raster per year, with each well counted from its installation year onward and its application date used as a fallback. The rasters therefore follow the build-out of well infrastructure through time instead of representing a single snapshot. Separate irrigation and non-irrigation well-density rasters were produced the same way by classifying each registered well on its declared use code before rasterizing, and these two layers feed the density-ratio GW/SW partition (Methods, Partition calibration and constraints). Registry installation dates extend through 2024, so the projection years (2026–2099) carry the 2024 well field forward, because future drilling is unknown. Registration became mandatory only with the Arizona Groundwater Management Act (GMA) of 1980, so the registry under-represents wells drilled and abandoned before then (Usage Notes, Known limitations).

Soil properties. Soil depth, available water capacity (0–152 cm), and saturated hydraulic conductivity from CSRL, gNATSGO, and SSURGO were used as static predictors[60,61].

Surface-water-rights density. Irrigation and non-irrigation surface-water-rights densities were derived from the HarDWR[63,82] database, which assembles the historical priority and use information of the Arizona surface-water rights system, by counting points of diversion per 2 km pixel from each right's priority year onward. Together with the two well-density rasters described above, these four layers drive the density-ratio GW/SW partition applied at prediction time (Methods, Partition calibration and constraints).

Groundwater irrigation fraction. The Hung et al. (2025)[59] product gives the fraction of irrigation water sourced from groundwater, downscaled globally to 60 m, as snapshots for 2000, 2005, 2010, and 2015. Each prediction year takes the nearest available snapshot: 2000 for years before 2005, 2005 for 2005–2009, 2010 for 2010–2014, and 2015 for 2015 onward. The hindcast therefore uses the 2000 snapshot and the projection the 2015 snapshot. The layer enters the framework as a model predictor.

Training data

The model was trained on ADWR metered groundwater pumping records for 1984–2024 from the AMA and INA management areas, where metering is mandatory. Metered volumes were joined to well locations in the ADWR Well Registry, keeping all consumptive uses and removing non-consumptive categories (monitoring, dewatering, drainage, remediation, and test wells).

Training target. Five steps turned the metered records into the training target. (1) Well records above 5,000 AF yr^{-1} (≈ 6.2 Mm^3 yr^{-1}, about 3,000 gallons per minute pumped year-round) were dropped as aggregated well-field totals or data-entry errors. (2) The remaining volumes were summed per 2 km pixel and year, following Majumdar et al. (2020[31], 2022[11]). (3) Each pixel volume was divided by the 4 km^2 pixel area to give a withdrawal depth in mm, comparable across pixels and with the climate predictors. (4) Pixel depths above 3,000 mm, about twice

Tukey's extreme fence[83] (Q3 + 3 × IQR) and the bound used by Majumdar et al. (2022)[11], were removed as rasterization artifacts. (5) Zero-withdrawal pixels were excluded, because a zero at a pixel that IrrMapper[57] maps as non-irrigated cannot be told apart from an irrigated pixel with no metered record. The resulting depths were paired by pixel and year with the 22 model predictors to form the training set.

Predicting withdrawal directly on the 2 km grid removes the need to link an individual well's point of diversion to a mapped place of use, which field-scale remote-sensing approaches such as Ott et al. (2024)[36] require. A well whose served field lies largely in an adjacent cell leaves its own cell with wells but little mapped irrigated area. On the 2 km grid such mismatches are absorbed by the neighborhood structure of the gridded predictors and by the surface-water availability term used in the partition.

Machine learning model

Model selection, evaluation, and hyperparameter optimization

XGBRF [72,84] was selected as the predictive algorithm from a 13-model benchmark comprising four core baselines (XGBoost[72], LightGBM[85], Random Forests[84], XGBRF) and nine further models (ExtraTrees[86], HistGradientBoosting[87], GradientBoosting[88], AdaBoost, Bagging[89], CatBoost, linear regression, ridge, and lasso[83]). Selection was based on performance across five evaluation strategies.

Random holdout. A grid of five test sizes (10–30 %) × five random seeds gives 25 train/test configurations of the supervised training set. Each model was fitted on each configuration, which tests prediction on randomly withheld samples drawn from the same spatiotemporal distribution as the training data and quantifies sensitivity to the train/test split. Optuna[71] hyperparameter tuning was run only on the first configuration (test size = 10 %, seed = 42); all other configurations reuse those hyperparameters.

Pixel holdout. Each model was tested on a pixel-stratified spatial holdout in which a fraction of the unique pixel locations, identified by their easting and northing coordinates, is withheld across all years. Unlike the random split, where the same pixel can appear in training and test in different years, this strategy evaluates the model at entirely unseen locations. The same test-size × seed grid as the random holdout was used.

Temporal holdout. Each model was tested against eight predefined blocks of years withheld from the 1984–2024 record: seven generalization configurations, T1–T7, and a backward-compatibility baseline that withholds the same years as T1 but under the training configuration of Majumdar et al. (2022)[11]. The seven are T1 (2010–2020), T2 (2015–2024) and T6 (2024 only), which extrapolate forward; T7 (1984–1994), which extrapolates backward; T4 (2007–2010), a mid-record block; T3 (1990–1992, 2005–2007 and 2022–2024), which introduces scattered gaps; and T5 (1985–1989 and 2020–2024), which removes both ends of the record. T5 is the hardest configuration for generalization, because it reproduces the operational case of predicting outside the metered period at both ends. Because the baseline uses a different training configuration, its metrics are not comparable with the others; it is reported separately and excluded from the cross-strategy summary, so the temporal row of Table 8 is the mean over T1–T7.

Spatial leave-one-out (LOO). Each ADWR basin with metered data was withheld in turn while the model trained on the rest of Arizona. This tests generalization to entirely unseen regions, which may differ in hydrogeological setting, land-use pattern, and management regime. Only basins with metered data in 1984–2024 were included.

Seeded spatial LOO. The same leave-one-basin-out design was repeated with 10 % of the withheld basin's samples randomly seeded into the training set, following the Kansas High Plains Aquifer study of Asfaw et al. (2025)[34]. It measures how much a minimal local calibration sample improves cross-basin transfer relative to the fully unseeded case, which is the practical question when applying the framework to a new basin where a small metering campaign is feasible.

Hyperparameters were optimized with Optuna[71] using a Tree-structured Parzen Estimator sampler (50 trials, 5-fold cross-validation) parallelized with Dask[90]. The composite objective combines the cross-validated test normalized root mean square error (NRMSE) with an overfitting penalty and a fold-stability penalty (defined in the paragraph below):

$$J = \mathrm{NRMSE}_{\mathrm{test}} \times [1 + \alpha \times \max(\mathrm{NRMSE}_{\mathrm{test}} / \mathrm{NRMSE}_{\mathrm{train}} - 1, 0)] + \beta \times \mathrm{SD}(\mathrm{NRMSE}_{\mathrm{test}})$$

Here $\mathrm{NRMSE}_{\mathrm{test}}$ and $\mathrm{NRMSE}_{\mathrm{train}}$ are means across the cross-validation folds, $\mathrm{SD}(\mathrm{NRMSE}_{\mathrm{test}})$ is the standard deviation across folds, $\alpha = 0.1$, and $\beta = 0.5\alpha = 0.05$. NRMSE is evaluated in log space when the target is log-transformed and on the original scale otherwise. The ratio form penalizes proportional overfitting, so a 20-fold train-to-test gap costs far more than a 2-fold gap, and the fold-stability term rewards hyperparameters that perform consistently across folds. The inner cross-validation follows the outer holdout design: where a strategy defines a grouping variable, the inner folds are GroupKFold folds on that same variable, by year for the temporal holdout and by pixel coordinates for the pixel holdout, so that a group never appears in both an inner training and an inner validation fold. The random holdout uses repeated k-fold, and the two spatial LOO strategies reuse the tuned hyperparameters.

Model interpretability

The selected XGBRF model was examined with four explainability tools, computed both for each evaluation strategy, on its training and held-out splits, and for the deployed production model fitted on the full metered training set (all AMA/INA well-year samples, 1984–2024). Two ranking diagnostics quantify global feature influence: the model's built-in gain-based feature importance, and model-agnostic permutation importance, which measures the accuracy drop when each predictor is randomly shuffled. SHapley Additive exPlanations (SHAP) values then decompose individual predictions into additive per-feature contributions, summarized as mean |SHAP| rankings and as beeswarm, waterfall, and dependence plots[91]. Accumulated local effects (ALE) curves trace each predictor's marginal, correlation-robust response shape and expose non-monotone or spurious relationships[91,92]. SHAP and ALE were additionally recomputed per era on subsampled statewide prediction features, to show how feature contributions shift across the record. Technical Validation reports the SHAP and ALE diagnostics for the production model; the gain-based and permutation importances, the per-era SHAP analyses, and the dependence plots are provided in the Zenodo archive.

Bias correction

A global linear bias correction[93,94] was applied to each tree-based model: $y_{corrected} = |m \times y_{pred} + b|$, where m and b were fitted by ordinary least squares on the training predictions against the observed values. The absolute value enforces physical non-negativity. The correction was accepted only if the coefficient of determination (R^2), RMSE, and mean absolute error (MAE) all improved on the training set; otherwise the uncorrected predictions were kept. For the deployed XGBRF model the correction met that test on all 70,043 training samples (m = 1.086, b = −23.63 mm; R^2 0.938 → 0.944, RMSE 34.55 → 32.79 mm, MAE 18.60 → 17.85 mm) and is therefore applied to every prediction.

Full-period prediction and partitioning

The evaluation strategies above used train/test splits; for deployment, the XGBRF model was refit on all metered data from 1984 to 2024, with no data withheld, and used to predict annual withdrawal depth (mm) for every 2 km pixel from 1896 to 2099. Predictions are partitioned into eight withdrawal categories using conservation-consistent arithmetic and a density-ratio GW/SW split based on locally observable infrastructure: 1) Irrigation (Total × $irr_{capacity}$), 2) Non-Irrigation (Total − Irrigation), 3) $Irrigation_{GW}$ (Irrigation × GW_{share_irr}), 4) $Irrigation_{SW}$ (Irrigation − $Irrigation_{GW}$), 5) $Non\text{-}Irrigation_{GW}$ (Non-Irrigation × $GW_{share_non_irr}$), 6) $Non\text{-}Irrigation_{SW}$ (Non-Irrigation − $Non\text{-}Irrigation_{GW}$), 7) $Total_{GW}$ ($Irrigation_{GW}$ + $Non\text{-}Irrigation_{GW}$), and 8) $Total_{SW}$ ($Irrigation_{SW}$ + $Non\text{-}Irrigation_{SW}$). The two fractions $irr_{capacity}$ and GW_{share} are defined in the two subsections below.

Irrigation and non-irrigation partitioning. The irrigation share of a pixel's withdrawal is taken as its irrigation pump-capacity fraction, $irr_{capacity}$, not its irrigated-area fraction. For each pixel and year, $irr_{capacity}$ is the summed pump capacity (ADWR Well Registry PUMPRATE, gallons per minute) of the active irrigation wells divided by that of all active consumptive wells, clipped to [0, 1]. A well is active from its installation year, or its application date if that is missing, and non-consumptive wells such as monitoring and test wells are excluded.

Only about 42 % of consumptive wells report a pump rate, and reporting is more complete for irrigation wells (~62 %) than for domestic wells (~39 %). Missing rates were therefore filled with the median rate of the well's own use category, or the overall median where a category reports none. This keeps the contrast between agricultural pumps (median ~900 GPM) and domestic pumps (median ~15 GPM) that makes the capacity ratio a useful proxy for the volume split. Statewide, the result is an irrigation share of ~72 %, consistent with the ADWR 2017 split. Pump capacity is used instead of irrigated area because a 2 km pixel is rarely fully irrigated by area even when nearly all of its pumping is for irrigation.

Groundwater and surface water partitioning. Each pixel's irrigation and non-irrigation withdrawals are then split between groundwater and surface water by comparing the local evidence for each source. Groundwater supply is indicated by the density of registered wells of that use category. Surface-water supply is indicated by the density of surface-water rights of that use category, weighted by how much canal-delivered water is available nearby, as measured by the canal-weighted streamflow (Ancillary datasets). The stronger a pixel's groundwater evidence relative to its surface-water evidence, the larger its groundwater share. The exact expression, and the caps and floors that keep it within physically plausible bounds, are given in Partition

calibration and constraints. Budget closure is enforced by subtraction (Non-Irrigation = Total − Irrigation; Irrigation_{SW} = Irrigation − Irrigation_{GW}), so that Irrigation + Non-Irrigation = Total and Total_{GW} + Total_{SW} = Total hold exactly at every pixel and year. Predictions are set to no-data at pixels with no registered wells.

Three consumptive-use (CU) products are derived as CU = IE × Irrigation Withdrawal, where the irrigation efficiency IE comes from the USGS National Hydrologic Model (NHM) basin-level data[24] (2000–2020). Per-year basin IEs are used within the NHM coverage period, and the long-term basin mean IE is used for all other years. Rasters are written in four units (mm, ft, m^3, AF) for each of the 11 withdrawal and CU products and the three stream capture pools across all 204 years.

CAP delivery perturbation (2020–2099)

Colorado River shortage declarations[9] remove CAP surface water in a way that the climate and land-use predictors cannot anticipate. In a shortage year, CAP-served pixels lean more on groundwater: their total pumping is unchanged, but more of it comes from wells. Because nearly all of Arizona's reductions fall on CAP water users[5], this shift is imposed only at CAP-service-area pixels and only on the GW/SW split; the machine learning total is computed first and is not altered. The adjustment has two parts, both set by the declared Tier or, from 2027, by the Operating Guidelines (Table 3). First, the surface-water term is reduced by a delivery factor, equal to 1 minus the Tier's mandatory cut divided by the 1,850 $Mm^3\ yr^{-1}$ (1,500 $kAF\ yr^{-1}$) CAP design capacity. Because that term is the product of the canal-weighted streamflow and the surface-water-rights density, and the factor is applied to both, the term falls by roughly the factor squared. This is intended, not double counting: the two layers represent different limits, the water available in the canal and the rights that can be served under priority, and a shortage tightens both. Second, well density at CAP pixels is multiplied by a groundwater boost, which has the same effect as raising the groundwater weight. Under Tier 1, for example, the delivery factor is 0.66, so the surface-water term falls to $0.66^2 \approx 0.44$ of its unperturbed value, and the boost of 5.0 raises the effective groundwater weight from its post-CAP value of 0.2 to 1.0. The size of the combined effect is checked against observations, not assumed: together the two parts reproduce the 21–38 % groundwater substitution seen in the 2022–2024 ADWR and USGS aggregates.

Table 3. Central-run CAP delivery perturbation parameters for the shortages declared in 2020–2026 and the 2027–2028 Operating Guidelines, which the central projection holds through 2099. Delivery factor = 1 − mandatory cut / 1,500 kAF (1,850 Mm^3) CAP design capacity. The GW boost scales the well-density columns at CAP pixels, and the target effective GW weight (= 0.2 × boost) lies between the calibrated post-CAP baseline (0.2) and the 1981–1984 GMA-transition level (2.0).

Condition	Mandatory cut ($kAF\ yr^{-1}$)	% of design capacity	Delivery factor	GW boost	Target effective GW weight
Tier 0	192	12.8	0.87	1.0	0.2
Tier 1	512	34.1	0.66	5.0	1.0
Tier 2a	592	39.5	0.61	7.5	1.5
2027–2028 Operating Guidelines	760	50.7	0.49	7.5	1.5

Tier 0 applied in 2020–2021, Tier 1 in 2022, Tier 2a in 2023, and Tier 1 again in 2024–2026[5,9]; Arizona's additional 438 Mm^3 (355 kAF) of voluntary conservation in 2023 is excluded, so that the factors follow the mandatory reductions alone. For 2027 and 2028, the 2027–2028 Operating Guidelines[14] reduce Arizona's apportionment by 937 $Mm^3\ yr^{-1}$ (760 kAF yr^{-1}), a delivery factor of 0.49; the additional voluntary system conservation they call for is excluded in the same way. No cut this deep occurs in the observed record, so the boost is held at the Tier 2a value (7.5), which keeps the 2027 groundwater substitution at the top of the range observed in 2022–2024 (Supplementary Note 7 and Table S5). Because the guidelines cover only 2027 and 2028, the central projection holds this latest official condition from 2029 to 2099 as a stand-in for continued shortage, not as a forecast. The CAP scenario sweep (Technical Validation) brackets it with milder and more severe alternatives.

Partition calibration and constraints

Need for partition-time calibration. No per-pixel measurements exist of how withdrawal splits between groundwater and surface water, or between irrigation and other uses; ADWR and USGS report these splits only as statewide, basin, or HUC12 totals. The partition therefore relies on physical proxies (well density, surface-water-rights density, canal-weighted streamflow, irrigation pump-capacity fraction, and land-cover fractions) whose few free parameters were tuned to reproduce the published historical shares. Only these partition parameters were tuned; the machine learning totals were never adjusted to any agency value.

Density-ratio expression. The groundwater share of a use category at a pixel is

$$GW_{share} = (GW_w \times wd) / (GW_w \times wd + \sigma_{swd})$$

where wd is the well density of that category, σ_{swd} is the surface-water evidence (the surface-water-rights density times the normalized canal-weighted streamflow, Gaussian-smoothed with σ = 4 pixels ≈ 8 km), and GW_w is a groundwater weight, the only free parameter. GW_w changes with era: high before CAP (10, with 30 in 1950–1965 and 15 in 1971–1979), 2.0 during the 1981–1984 GMA transition, and low once CAP water arrived (0.1–0.4, settling at 0.2 from 2008). It was set so that the partitioned statewide totals match the published USGS and ADWR shares (Calibration anchors, below); the full schedule is in Supplementary Table S1.

GW-share caps and floors. The density ratio is known to be biased in two kinds of basin, and both are bounded explicitly. At basins supplied directly from the Colorado River mainstem, federal and tribal deliveries (Colorado River Indian Tribes (CRIT) Priority-1 rights, the Yuma Project, and municipal intakes [95]) bypass both the well registry and the rights raster, so the ratio would push the groundwater share toward 1 where surface water actually dominates; there the groundwater share is capped at 0.10, and at Lower Gila at 0.25 (Table 4). At the canal-served management areas, CAP and SRP municipal deliveries are wholesale allocations that do not appear as points of diversion, so the ratio understates groundwater; per-basin floors are applied at Phoenix, Pinal, Tucson, Harquahala, Prescott, and Ranegras Plain (Supplementary Table S2). Caps and floors are applied twice, to the raw shares and again after the post-1985 surface-water delivery routing.

Table 4. Maximum GW share at Colorado-River-direct basins. A uniform cap of 0.10 applies to every basin in the Colorado-River-direct set; Lower Gila is capped separately at 0.25. The implied SW floor is 1

minus the cap. The cap bounds the density-ratio share and is not an assertion that each basin sits at the bound.

Basin	Cap (max GW share)	Implied SW floor	Physical rationale
Parker	0.10	90 %	CRIT senior Priority-1 rights[95] (~888 Mm^3 yr^{-1} or ~720 kAF yr^{-1}, agriculture-dominant); physical SW share 85–95 %
Yuma	0.10	90 %	Yuma Project + Cocopah/Quechan tribal deliveries[95]; physically 90–98 % SW
Lake Mohave	0.10	90 %	Colorado River direct mainstem municipal supply; ~95–99 % SW
Lake Havasu	0.10	90 %	Mixed municipal (Lake Havasu City) + CAP intake
Detrital Valley	0.10	90 %	Small basin, mixed municipal use
Meadview	0.10	90 %	Small basin, mixed municipal use
Lower Gila	0.25	75 %	Gila River corridor; capped outside the Colorado-River-direct set

Additional partition constraints. Seven further rules handle specific cases in which the density ratio fails: (1) basins with essentially no canal infrastructure have their surface water reassigned to groundwater, so that smoothing cannot carry surface water across basin boundaries; (2) basins that divert directly from the Colorado River or from lakes are exempt from that rule; (3) the volume left over after partitioning is routed to irrigation surface water at canal-served farmland from 1960 onward; (4) before 1948, surface water is restricted to canal and rights pixels; (5) wells missing from the pre-1980 registry are reconstructed; (6) after 1985, pixels next to mapped cropland are treated as cropped; and (7) the irrigation/non-irrigation split is adjusted by basin class, with Phoenix and Tucson AMAs keeping the default pump-capacity split. The thresholds and basin lists for each rule are given in Supplementary Note 4, and the well reconstruction in Supplementary Note 3.

Calibration anchors. The partition parameters were tuned against statewide records for 1915–2019: USGS Open-File Report 94-476 [96] (annual groundwater withdrawals, 1915–1990), the five-yearly USGS Circulars[97] (1950–2015), and ADWR Annual Report[1,5,98] totals (selected years, 1957–2020) together with the 2019 ADWR groundwater and irrigation shares. Agreement with these records (Technical Validation) shows only that the calibration is adequate; it is not an independent test. The independent tests are the cross-validated model performance and the comparisons against USGS NHM, USGS Reitz, the public-supply reanalysis, CAP and SRP delivery records, and the WestWater shortage analysis, all in Technical Validation. Because only statewide totals were used, the spatial pattern of every partitioned product is also independent of the calibration. The full parameter set is given in the Supplementary Information.

Trend analysis

Per-pixel temporal trends were computed for every withdrawal, CU, and stream capture category over four periods: full (1896–2099), hindcast (1896–1983), historical (1984–2025), and

projection (2026–2099). The Mann-Kendall non-parametric test detects monotone change at $\alpha = 0.05$, and Sen's slope gives a robust per-pixel rate of change in four units (mm yr^{-1}, ft yr^{-1}, m^3 yr^{-1}, AF yr^{-1}) matching the depth and volume rasters. Pixels where the Mann-Kendall test is not significant are stippled in the resulting maps (Supplementary Fig. S1), so that significant trends are visually distinct from non-significant noise. Per-basin and per-sub-basin trend statistics (mean Sen's slope, fraction of significant pixels) are written as CSVs alongside the maps, so that users can rank basins by historical or projected rate of change without rerunning the trend computation.

Stream Capture Index

Stream capture is the part of a groundwater withdrawal that is ultimately supplied by a hydraulically connected stream or canal, through induced infiltration from the channel or through reduced groundwater discharge to it, instead of by depletion of aquifer storage. Its per-pixel, per-year apportionment was computed with a process-informed proxy that combines hydraulic connectivity, represented as exponential decay with water-table depth, and surface-water availability, represented by the focal-max-normalized canal-weighted streamflow:

$$\text{capture}_{\text{frac}}(\text{pixel, year}) = \exp(-\text{wtd}_m / \lambda) \times \text{cw}_{\text{norm}}$$
$$\text{capture}(\text{pixel, year}) = \text{Total}_{\text{GW}}(\text{pixel, year}) \times \text{capture}_{\text{frac}}(\text{pixel, year})$$

where wtd_m is the static water-table depth (1913–2023 mean, m) from Ma et al. (2026)[68] and cw_{norm} is the canal-weighted streamflow normalized to [0, 1] within a 5 × 5 pixel window. The first factor represents how well a pumping pixel is connected to surface water: following the stream–aquifer connectivity literature[29,99,100], the share of pumping supplied by capture falls as depth to water increases, at a rate set by the length scale λ. The second factor represents whether there is surface water nearby to capture. Three values of λ (5, 10, and 20 m) bracket the connectivity scale without fitting a parameter; they lie at the shallow end of the ~10–100 m connection depths reported for CONUS[101], so the index emphasizes the most direct connections and is a lower bound. The composite index is introduced in this work and is evaluated in Technical Validation, Stream capture validation.

The stream capture fraction quantifies one pathway only, well-mediated stream depletion at pixels with groundwater withdrawal, and is by construction a lower bound on basin-scale SW–GW interaction. Four other pathways are not represented: direct federal canal diversions outside the ADWR Well Registry, SW-righted wells routed to SW, ephemeral stream–aquifer exchange outside the perennial canal-delivered footprint, and engineered drain networks such as the Wellton-Mohawk system[102]. Seepage from unlined canals, which returns part of the delivered surface water to the aquifer, is likewise not represented, so the index is a gross rather than a net measure of capture.

Uncertainty quantification

Pixel-level uncertainty was quantified through a six-component hybrid framework, with the components combined in quadrature under an assumption of independence:

$$\sigma_{\text{total}} = \sqrt{(\sigma_{\text{MACA}}^2 + \sigma_{\text{model}}^2 + \sigma_{\text{irr}}^2 + \sigma_{\text{LULC}}^2 + \sigma_{\text{GW}}^2 + \sigma_{\text{USBR}}^2)}$$

σ_{MACA}: climate-model spread (2026–2099). The model is re-run with five GCMs chosen to span the Southwest temperature and precipitation projections: CCSM4 (central), CNRM-CM5 (cool-wet), HadGEM2-ES365 (hot-dry), MIROC-ESM-CHEM (hot-wet), and inmcm4 (cool-dry)[46]. σ_{MACA} is the per-pixel standard deviation of the five predictions, and is zero before 2026, when observed climate is used.

σ_{model}: model randomness (1896–2099). Ten XGBRF models with identical hyperparameters but different random seeds (42, 123, 456, 789, 1024, 2048, 3072, 4096, 5120, 6144) are run, and σ_{model} is the per-pixel standard deviation of their predictions.

σ_{irr}: irrigated-area input (1896–2025). For 1985–2025 the model is run with IrrMapper[57] and, separately, with the cropland-fraction regression used outside the IrrMapper record; σ_{irr} is half the difference of the two predictions. Before 1985 the regression estimate is perturbed by ± its RMSE and σ_{irr} is half the resulting range. σ_{irr} is zero after 2025, because the irrigated fraction is then re-derived within each land-use scenario (σ_{LULC}).

σ_{LULC}: land-use scenario spread (2026–2099). Each of the four USGS land-use projection scenarios[56] (A1B, A2, B1, B2) is run through the full chain from land cover to irrigated fraction to withdrawal, and σ_{LULC} is the standard deviation of the four predictions.

σ_{GW}: well-density input (1896–2099). Well density in each prediction year is replaced in turn by the values from each of 2020–2024, and σ_{GW} is the standard deviation of the five resulting predictions. Surface-water-rights density was not perturbed, because it is effectively unchanged in the HarDWR[82] record since ~1996. σ_{GW} does not represent new drilling, well retirement, or redistribution of wells beyond what those years contain.

σ_{USBR}: Upper Colorado River streamflow (1950–2099). MACA covers only the Arizona domain, whereas about 92 % of Lees Ferry inflow originates as Upper Basin snowmelt, so CAP supply uncertainty is represented separately. For each of five USBR CMIP3 ensemble members, the Colorado River flow is scaled in the watershed streamflow predictor at all Colorado-River-served basins (the CAP service area and the mainstem corridor from Parker to Yuma), so the model is re-run, and at CAP service-area pixels also in the canal-weighted streamflow and surface-water-rights density used by the partition. σ_{USBR} is the t-corrected standard deviation of the five predictions. It is zero before 1950, when the USBR ensemble begins, and at CAP pixels before the first CAP deliveries in 1985, so its hindcast-era mean is near zero outside the mainstem corridor (Supplementary Fig. S2). It is small statewide (2–8 % of σ_{total}^2) but larger at Colorado-River-served basins.

Components are classified as sample-based (σ_{model} with N = 10, σ_{GW} and σ_{USBR} with N = 5) or scenario-based (σ_{MACA}, σ_{LULC}, σ_{irr}). Sample-based components use Student's t critical values (t_9 = 2.262 for σ_{model}, t_4 = 2.776 for σ_{GW} and σ_{USBR}) in place of z = 1.96, to account for small-sample estimation uncertainty, applied by inflating σ by t or z before quadrature. Every ensemble member's total prediction is passed through the eight-category partition before the standard deviations are taken, which propagates partition-fraction uncertainty into the per-category σ values.

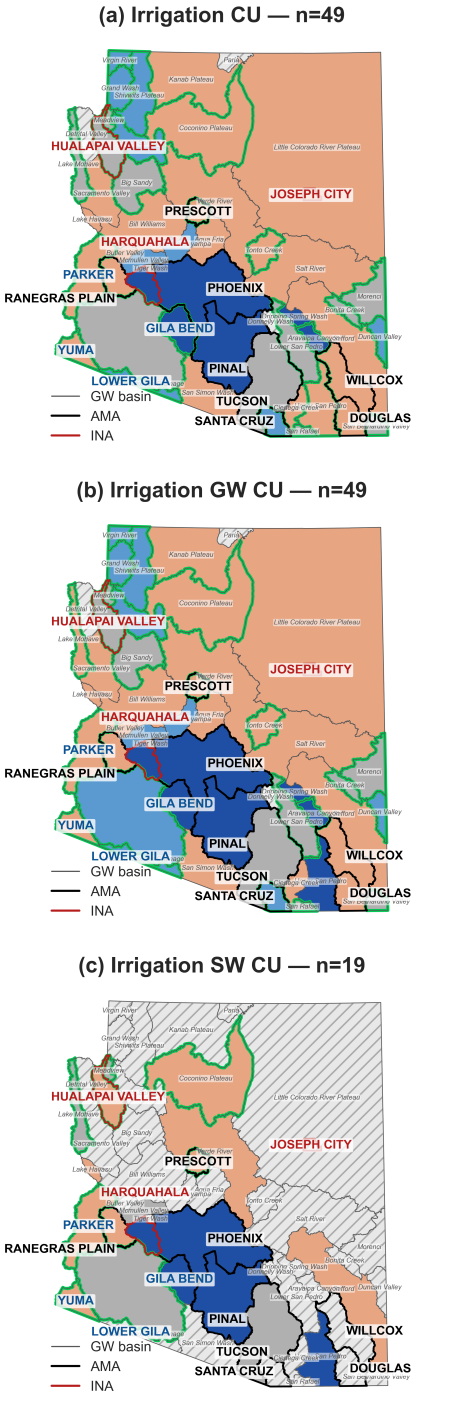
CU uncertainty is computed via error propagation: $\sigma_{CU} = \sqrt{((IE \times \sigma_{wd})^2 + (wd \times \sigma_{IE})^2)}$, where σ_{wd} is per-category withdrawal uncertainty and σ_{IE} is the inter-annual standard deviation of NHM basin-level IE across 2000–2020.

σ_{CU} attribution. To show where consumptive-use uncertainty originates, the per-basin σ_{CU} was decomposed into three drivers and mapped for the projection era (Fig 3). The six withdrawal components were grouped into a management class (σ_{irr}, σ_{LULC}, σ_{GW}: the irrigated-area, land-use, and well-infrastructure reconstruction uncertainties), a climate class (σ_{MACA} and σ_{USBR}: Arizona-local downscaled climate plus UCRB streamflow), and a model class (σ_{model}, the XGBRF seed ensemble).

Each class was propagated to consumptive use through CU = IE × Withdrawal, with the irrigation-efficiency uncertainty placed in the management class: $\sigma^2_{CU,mgmt} = (IE \cdot \sigma_{wd,mgmt})^2 + (wd \cdot \sigma_{IE})^2$, $\sigma^2_{CU,clim} = (IE \cdot \sigma_{wd,clim})^2$, and $\sigma^2_{CU,model} = (IE \cdot \sigma_{wd,model})^2$. Each basin is shaded by the management share of its management-plus-climate variance, and basins where σ_{model} exceeds both are outlined in lime green. In the projection era (Fig 3a), σ_{model} is the largest driver of irrigation CU uncertainty in about half of the basins (median share ≈ 45 %); the rest divide between management and climate, and GW-CU (Fig 3b) and SW-CU (Fig 3c) follow their parent withdrawal pools.

All prediction rasters are augmented in place to six-band GeoTIFFs. B1: prediction (original units); B2: σ (uncertainty, same units); B3: coefficient of variation (CV = σ / mean prediction); B4: signal-to-noise ratio (SNR = 1/CV); B5: lower 95 % CI = prediction − 1.96·σ; B6: upper 95 % CI = prediction + 1.96·σ. Era-mean maps of the six σ components and of the total-withdrawal CV are given in Supplementary Figs. S2–S4.

Fig 3. Per-basin σ_{CU} attribution for the projection era (2026–2099). Irrigation consumptive-use uncertainty is decomposed into a management class (irrigation-fraction, land-use, and well-density uncertainties), a climate class (downscaled climate and UCRB streamflow), and a model class (the XGBRF seed ensemble), each propagated to consumptive use through the CU = IE × Withdrawal relationship. Each basin is shaded by its management share of the classifiable (management + climate) variance, and basins where σ_{model} dominates both classes are outlined in lime green, for (a) total irrigation CU, (b) irrigation groundwater CU, and (c) irrigation surface-water CU. Supplementary Fig. S5 gives the same attribution for groundwater and surface-water withdrawal. The per-era variance-share decomposition and the continuous per-year σ-attribution time series are provided in the Zenodo repository.



Stream capture uncertainty. A pixel's capture volume is the product of groundwater pumping ($Total_{GW}$), which carries σ_{total}, and the capture fraction, whose spread comes from the three connectivity scales (λ = 5, 10, and 20 m).

The two are combined so that each bound pairs low pumping with the weakest connection and high pumping with the strongest:

$$Total_{GW,lower} = \max(Total_{GW} - 1.96\sigma, 0)$$
$$Total_{GW,upper} = Total_{GW} + 1.96\sigma$$
$$capture_{lower} = Total_{GW,lower} \times capture_{frac,lower} \quad (\lambda = 5\ m)$$
$$capture_{central} = Total_{GW} \times capture_{frac,central} \quad (\lambda = 10\ m)$$
$$capture_{upper} = Total_{GW,upper} \times capture_{frac,upper} \quad (\lambda = 20\ m)$$

The resulting lower and upper capture-volume bounds are therefore a combined 95 % confidence interval that reflects both the pumping and the connectivity uncertainty, and not a λ-only envelope. A single per-pixel $\sigma_{capture}$ is attached to the central-λ (10 m) capture volume, taken as the half-width of that full propagated interval:

$$\sigma_{capture} = 0.5 \times (capture_{upper} - capture_{lower}) / 1.96$$

With σ = 0 this reduces to the spread from λ alone, so users can separate the pumping and connectivity contributions.

Out-of-distribution (OOD) detection. σ_{total} measures how much the predictions vary, but not whether a pixel's predictors fall outside the range the model was trained on, which is most likely in the deep hindcast and in unmetered basins. To flag such extrapolation, the

squared Mahalanobis distance $d^2 = (x - \mu)^T \Sigma^{-1} (x - \mu)$ between each pixel's predictor vector x and the mean μ and covariance Σ of the training predictors (with 10^{-6} added to the diagonal of Σ) is converted to a probability with the $\chi^2(n_{features})$ cumulative distribution: 0 means in-distribution and values near 1 mean strong extrapolation. Pixels beyond the 99th-percentile χ^2 threshold are also flagged as hard out-of-distribution[103,104]. Era-mean OOD probabilities are mapped in Supplementary Fig. S6.

The detector uses $n_{features} = 17$, the climate and land-use predictors only. The coordinates and the static infrastructure predictors (well density, canal density, streamflow) are excluded, because they would flag every pixel outside the AMAs and INAs on location alone. The resulting yearly probability raster accompanies σ_{total} but does not feed into it; it approaches 1 in the pre-1950 hindcast, where σ_{irr} and σ_{GW} also dominate.

Well-level disaggregation

The well package disaggregates the pixel-level prediction rasters to ~170,000 individual wells from the ADWR Well Registry and writes four GeoParquet files, one per unit convention (mm, ft, m^3, AF), each in long format with one row per well-year (~34.7 million rows × 34 columns). When several wells share a 2 km pixel, the pixel total is split using capacity-proportional weights with a three-tier fallback: (1) mean historical pumping across all metered years (available for ~3,000 wells per year within the AMAs and INAs); (2) pump rate in GPM, converted to AF yr^{-1}, from the Well Registry for unmetered wells (~79,000 wells); (3) an equal share for wells with neither record. Per-well uncertainty columns (σ and lower and upper 95 % CI) are provided for every category and unit; they are obtained by distributing the pixel-level σ of the same category across the wells in that pixel under the correlated-sum rule given below.

The disaggregation covers the same 15 product families as the rasters (nine withdrawal categories, three CU categories, and three stream capture pools), so every well carries a withdrawal, consumptive use, and capture volume, each with its uncertainty.

Per-well uncertainty. A pixel's σ is split among its wells with the same weights as the volume, $\sigma_{well,i} = w_i \times \sigma_{pixel}$, rather than in quadrature, because all wells in a pixel share the same pixel-level uncertainty and are therefore fully correlated. This keeps $\Sigma\sigma_{well,i} = \sigma_{pixel}$. The 95 % bounds are prediction ± 1.96 σ.

Data Records

Repository structure and access

All input and output data (Tables 5–7) are archived on Zenodo (https://doi.org/10.5281/zenodo.19057935)[28] under a CC-BY-4.0 license; the pipeline source code is licensed BSD-3-Clause. The full archive is ~220 GB uncompressed (~20 GB inputs once the external products are downloaded, plus ~200 GB generated outputs), distributed as an ~80 GB LZMA2-compressed 7z deposit. The deposit is organized into three files, so that most users can retrieve the published product without downloading the full reproducibility archive:

1) **az-hydro-headline.7z** (~8.7 GB compressed): a self-contained subset holding every key output, namely the six-band augmented per-pixel, per-year withdrawal, consumptive-use, and stream capture rasters, the GeoParquet well package, the per-basin and per-sub-basin time

series, the CAP shortage-scenario sweep, the era-mean and trend spatial figures, and the validation and intercomparison outputs. This archive covers the needs of most users.

2) **az-hydro-data.7z** (~80 GB compressed; ~220 GB uncompressed: ~20 GB inputs once the external products are downloaded + ~200 GB generated outputs): the full reproducibility archive, with everything in the headline archive plus the raw inputs, cross-validation outputs, the intermediate input stacks, and the per-component UQ rasters.
3) **az-hydro-1.2.0.zip** (~64 MB): the tagged pipeline source-code release, identical to the GitHub repository at the release tag (https://github.com/montimaj/az-hydro/).

Inside each 7z, Data/HEADLINE_README.md (headline archive) or Data/README.md (full archive) gives the complete per-directory inventory and external-source citations.

Input data records (~9 GB on Zenodo; ~20 GB with external downloads)

Table 5. Input data record inventory.

Directory	Contents	Size	Format
Data/Inputs/GEE_Data/	Downloaded GEE tiles (80 km × 80 km, 2 km resolution) for the ML predictors, the 5 σ_{MACA} GCM stacks, and the 4 σ_{LULC} scenario stacks, plus HUC12 polygons	~3.4 GB	GeoTIFF, GeoJSON
Data/Inputs/GW_Data/	ADWR metered records, Well Registry, groundwater basin / sub-basin / CAP / SRP / streamflow / USBR vectors, statewide WTD TIFs[68], and GRAIN canal parquet[64].	~5.8 GB	CSV, Shapefile, GeoJSON, GeoTIFF
Data/Inputs/USGS WU/	NHM HUC12 withdrawals/CU/IE (2000–2020)[21,24,25], USGS Reitz 800 m rasters (actual ET: 1895-2018; irrigation withdrawals: 1980–2018)[26,105], USGS HUC12 public-supply reanalysis data (2000-2020)[22,23]; only the two small statewide aggregated CSVs are redistributed on Zenodo.	~11 GB (external)	CSV, GeoTIFF, Excel

The harmonized predictor stack is additionally published as 12 public GEE ImageCollections under projects/azhydro/assets/ (Table 6), accessible to any authenticated GEE user.

Table 6. Exported GEE assets used in the data processing and pipeline, under projects/azhydro/assets/.

GEE Collection path	Description	Images
gridmet_hargreaves_eto_ratio	Monthly OpenET gridMET/Hargreaves ETo correction ratios (1979–2025 overlap)	12
openet_reitz_et_ratio	Monthly OpenET/USGS Ensemble ET correction ratios (2000–2018 overlap)	12

GEE Collection path	Description	Images
monthly_etof	Monthly crop coefficient climatology (EToF = ET/ETo, 2000–2025)	12
lulc_projection_ensemble	Annual LULC pixel-wise mode across four USGS scenarios (2026–2099)	74
prism_hargreaves_eto	Bias-corrected PRISM Hargreaves ETo, monthly (1896–1978)	996
usgs_adjusted_et	Bias-corrected USGS Reitz ET, monthly (1896–2018)	1,473
maca_monthly_eto_v2	MACA v2 ensemble ETo, monthly (2026–2099)	888
maca_monthly_et_v2	MACA v2 ensemble ET via EToF, monthly (2026–2099)	888
monthly_peff_v2	USDA SCS effective precipitation, monthly (1896–2099)	2,448
maca_gcm_annual_eto	Per-GCM annual ETo for 5 representative GCMs (2026–2099)	370
maca_gcm_annual_et	Per-GCM annual ET for 5 representative GCMs (2026–2099)	370
maca_gcm_annual_peff	Per-GCM annual effective precipitation for 5 representative GCMs (2026–2099)	370

Output data records (~200 GB)

Gridded predictions. The core products are eight withdrawal categories, three irrigation consumptive-use (CU) categories, and three stream capture pools, each in four units (mm, ft, m³, AF) for 204 years (1896–2099). All withdrawal, CU, and capture rasters are six-band augmented GeoTIFFs (prediction, σ, CV, SNR, lower 95 % CI, upper 95 % CI) at 2 km resolution in EPSG:32612 (UTM Zone 12N). Every gridded product is distributed both in the Zenodo archive[28] and as a public GEE ImageCollection under projects/azhydro/assets/az-wu-v1-2/ (Table 7), which powers the interactive AZ-Hydro Explorer (Usage Notes). The four unit conventions are consolidated into one collection per category, so a single augmented category holds 4 × 204 = 816 images.

Table 7. Output data records and exported GEE assets used in the AZ-Hydro Explorer app. All listed GEE assets are under projects/azhydro/assets/az-wu-v1-2/.

Product family	Categories	Total rasters	GEE Collection path
Total withdrawal	1	816	Predicted_Rasters
Withdrawal partitions	8	6,528	Total_GW, Total_SW, Irrigation, Irrigation_GW, Irrigation_SW, Non_Irrigation, Non_Irrigation_GW, Non_Irrigation_SW (each …_Rasters)
Irrigation consumptive use	3	2,448	Irrigation_CU_Rasters, Irrigation_GW_CU_Rasters, Irrigation_SW_CU_Rasters
Stream capture — depth and volume (central λ = 10 m)	3 pools	2,448	Capture__{Total, Irrigation, Non_Irrigation}_Rasters

Product family	Categories	Total rasters	GEE Collection path
Stream capture fraction (3-band, λ = 5 / 10 / 20 m)	3 pools	612	Capture__{Total, Irrigation, Non_Irrigation}_Fraction
Out-of-distribution probability	1	204	OOD_Rasters
CAP shortage scenario (8 scenarios × 2 windows)	—	16	CAP_Scenario__Pixel_Rasters

Stream capture. Per-pixel, per-year pumping-induced stream-depletion products for three pools (Total, Irrigation, Non-Irrigation). Each pool consists of a dimensionless three-band fraction raster, with the three connectivity scales λ = 5, 10, and 20 m as bands, plus six-band augmented depth and volume rasters at the central λ = 10 m, in which the lower and upper CI bands fold in the three-λ connectivity envelope together with the propagated σ_{total}.

Uncertainty and trend analysis. Per-component σ rasters (σ_{MACA}, σ_{model}, σ_{irr}, σ_{LULC}, σ_{GW}, σ_{USBR}) for each year, plus combined σ_{total} (2-band: σ, CV), per-category σ_{total}, and σ_{CU} rasters; a temporal-average Mean_CV.tif summarizes the spatial pattern of relative uncertainty. The six-component budget is further summarized by per-component σ maps (era means in Supplementary Figs. S2 and S3) and per-era, per-basin variance-attribution maps that decompose σ_{total} into management, climate, and model shares for both withdrawal and consumptive use, with the per-year σ-attribution series in Sigma_Attribution_Timeseries.csv. Temporal change is characterized by Mann-Kendall / Sen's-slope trend analysis, delivered as per-basin and per-sub-basin trend maps and CSVs for the hindcast, historical, projection, and full 1896–2099 windows.

Out-of-distribution probability rasters. Continuous per-year rasters (OOD_Flag_{year}.tif, values in [0, 1]) giving each pixel's OOD probability, i.e., the $\chi^2(17)$ CDF of the squared Mahalanobis distance between the pixel's 17-feature climate/land-use vector and the training feature distribution (*Methods, Out-of-distribution detection*), where 0 indicates in-distribution and values approaching 1 indicate strong feature-space extrapolation. Per-year summary statistics are provided in OOD_Rasters/OOD_Summary.csv.

Well-level GeoParquet files. Well_Package_{mm,ft,m3,AF}.parquet (four files, one per unit convention; ~2.1 GB each) contain ~170,000 wells × 204 years in long format, with per-row prediction and σ columns for all 15 categories (9 withdrawal + 3 consumptive-use + 3 surface-water-capture); 95 % CI bounds are derived downstream as prediction ± 1.96 σ. The same per-well estimates are additionally served on GEE as 15 per-category FeatureCollections (Well_Package__<category>). Supporting vector layers, such as groundwater basins (Groundwater_Basin), ADWR sub-basins (ADWR_Groundwater_Subbasin), the 2024 Well Registry (Well_Registry_2024), and the CAP service area (CAP) are likewise served as FeatureCollections under the same GEE collection path (projects/azhydro/assets/az-wu-v1-2/).

Summary statistics, model artifacts, intermediate files, and visualizations. Alongside the gridded products, the Zenodo archive includes per-basin and per-sub-basin CSV time series (volume in m^3 and AF, mean depth in mm) for every product, cross-strategy evaluation and intercomparison metrics CSVs, and the trained model artifacts (XGBRF model files, Optuna study databases, and tuned hyperparameters for all evaluation strategies). It also includes the

intermediate files generated during pipeline execution, including the mosaicked and reprojected GEE input stacks, rasterized ADWR training targets, assembled ML-ready DataFrames, reprojected vector layers (basins, wells, CAP/SRP, streamflow in a consistent CRS), and per-year observed withdrawal depth rasters (~14 GB GEE mosaics, ~14 GB observed GW rasters and vectors, ~8 GB reprojected vectors). These are accompanied by all 600 DPI figures (as PNGs) generated at each pipeline stage: exploratory data analysis, model evaluation and comparison across the cross-validation strategies, ML interpretability (feature importance, permutation importance, ALE, SHAP), full-period prediction time series and era-mean spatial maps with per-pixel uncertainty, the uncertainty-attribution and trend products described above, and independent validation against USGS products. The largest single output block is the model-evaluation archive (~121 GB across the five strategies and 13 models); the Step 3 prediction, uncertainty, and augmented-raster products account for ~40 GB.

Providing both the intermediate files and the visualizations lets users inspect, verify, or reuse any stage of the processing chain without re-running the full pipeline, which requires ~220 GB of disk space, access to GEE, and substantial computation time. This lowers the barrier to reproducibility checks, supports derivative analyses that build on individual pipeline components, and lets end users evaluate data quality at every processing step instead of only at the final output.

Data Overview

The dataset is organized around six elements. Each is summarized below with its corresponding figure, and specified in full in Methods.

(1) Physics-informed inputs. The input layers were engineered to keep physically meaningful signals in the model. Pump capacities from the well registry set the irrigation and non-irrigation split of the predicted withdrawals; canal-weighted streamflow, smoothed across canal service areas, represents surface-water availability; surface-water-rights densities are split by use category; hydroclimate and land-use inputs are bias-corrected across the three eras; and a high-resolution water-table depth raster represents groundwater accessibility.

(2) Density-ratio GW/SW partitioning with locally observable infrastructure. Total withdrawals are partitioned into eight categories along two axes, by use type (irrigation, non-irrigation) and by source (GW, SW). The GW/SW split weighs ADWR well density[62] against Harmonized Database of Western U.S. Water Rights (HarDWR)[63,82] surface-water-rights density, modulated by Global Registry of Agricultural Irrigation Networks (GRAIN)[64] canal-weighted streamflow[65,66]. Budget closure is enforced algebraically through subtraction-based partitioning (Non-Irrigation = Total − Irrigation, Irrigation_{SW} = Irrigation − Irrigation_{GW}), which guarantees Irrigation + Non-Irrigation = Total and Total_{GW} + Total_{SW} = Total at every pixel and every year (Fig 2). Era-mean partitioned groundwater and surface-water withdrawals are shown in Fig 4, and irrigation and non-irrigation withdrawals in Supplementary Fig. S7.

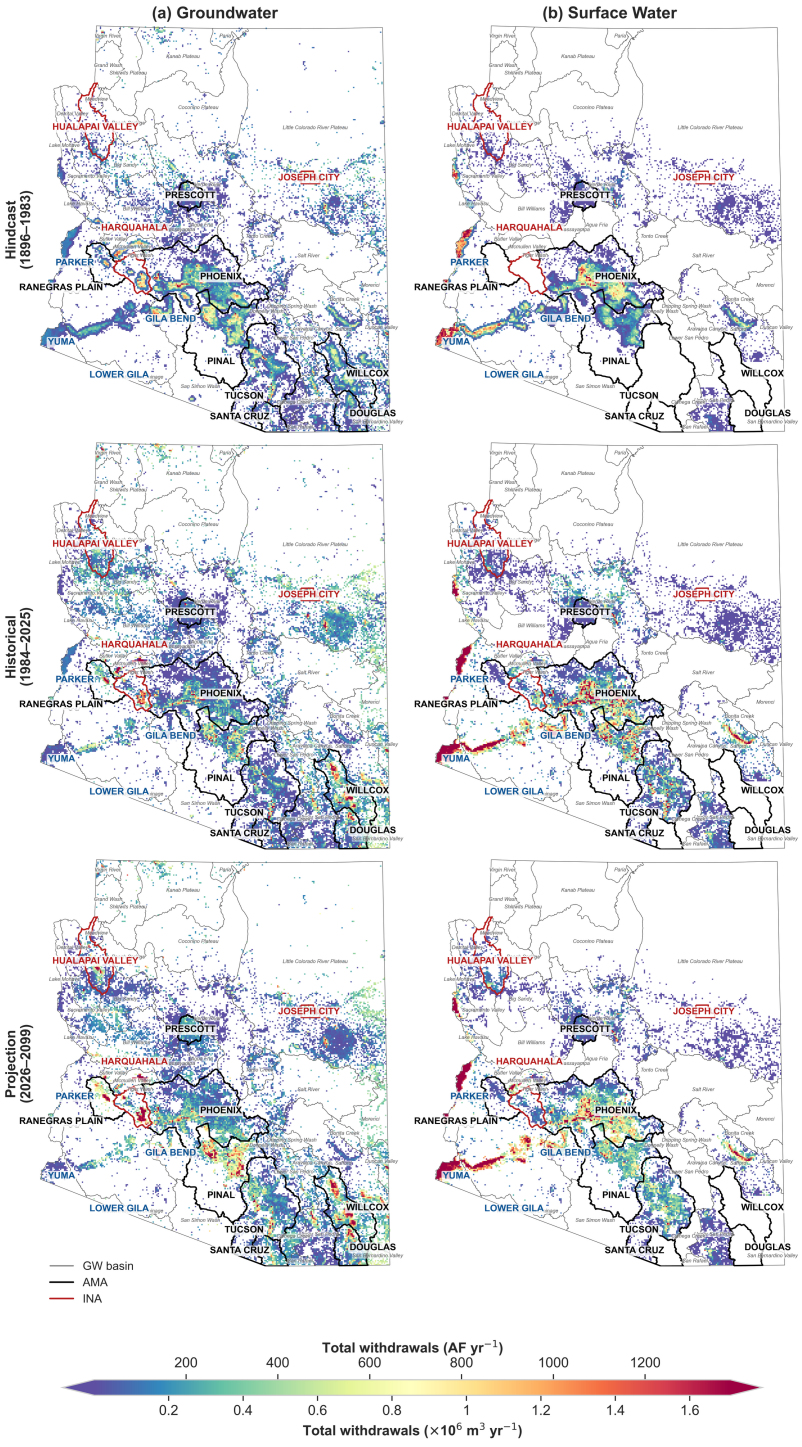


Fig 4. Era-mean partitioned annual withdrawal volumes. Columns are (a) total groundwater and (b) total surface water; rows are the hindcast (1896–1983), historical (1984–2025), and projection (2026–2099) eras, on a single shared volume scale. The groundwater maps concentrate in the alluvial AMA and INA basins, while the surface-water maps trace the SRP and CAP canal corridors and the Colorado River mainstem basins.

(3) A 204-year continuous record with a post-2026 Colorado River shortage-scenario sweep. The dataset spans two centuries by combining a hindcast era (1896–1983), a historical metered era (1984–2025), and a projection era (2026–2099) in one reproducible framework, with the projection driven by 5 GCMs × 2 RCPs (4.5 and 8.5)[46] × 4 USGS LULC scenarios[56] × 112 streamflow ensemble members[66]. The projection is additionally re-partitioned under eight post-

2026 CAP shortage scenarios: DCP Tiers 0, 1, 2a, 2b, and 3, the 2027–2028 Operating Guidelines, the WestWater Research (2026)[8] Basic Coordination scenario, and an extreme shortage scenario. These produce 2 km maps of cumulative additional GW pumping (ΔGW) concentrated along the CAP delivery corridor, for both the 2027–2060 (mid-century; Supplementary Fig. S8) and 2027–2099 (full horizon; Fig 5) reporting windows. The scenario outputs are cross-checked against the WestWater Research (2026)[8] report in Technical Validation.

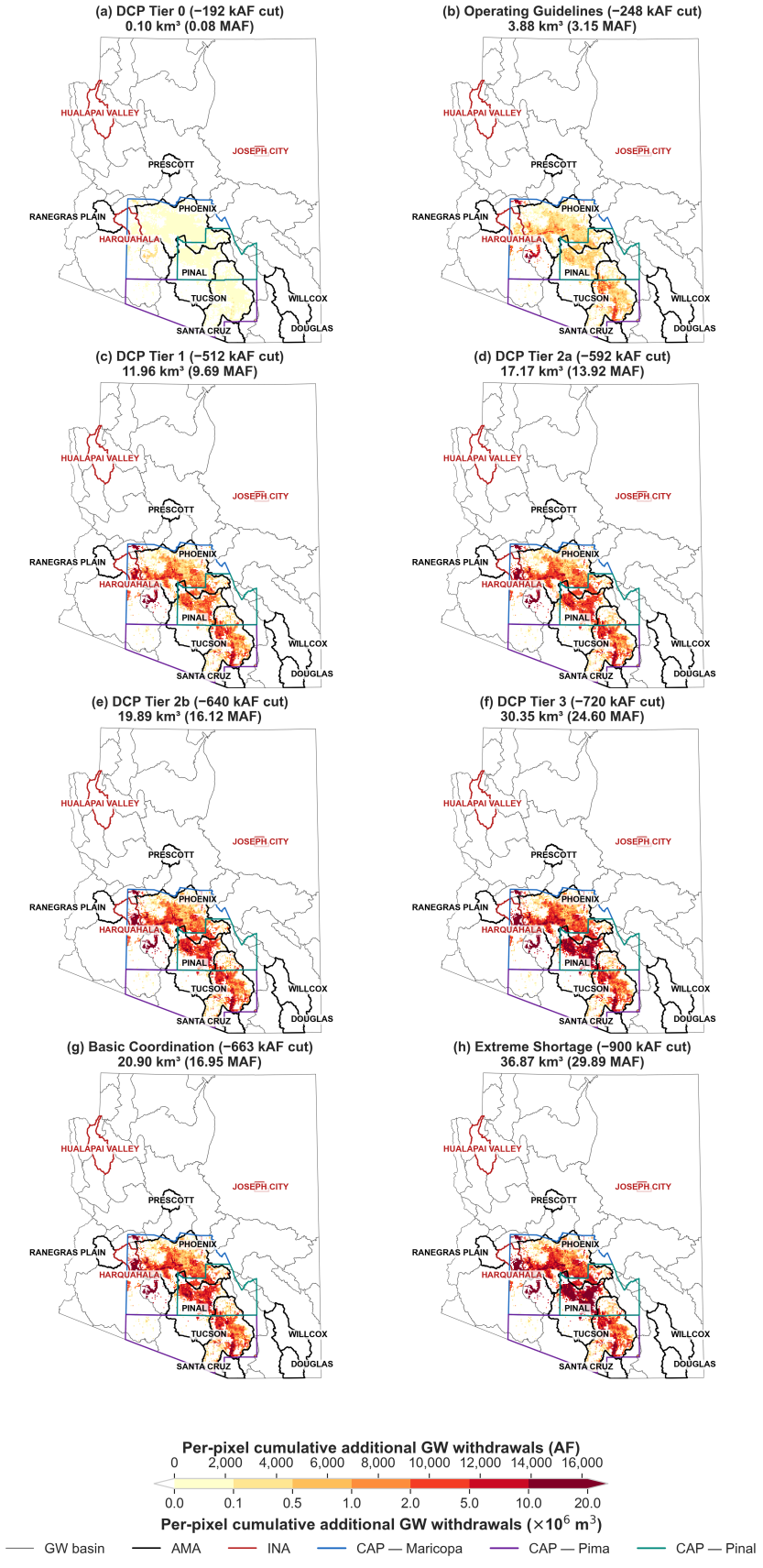


Fig 5. Per-pixel cumulative additional annual GW pumping (ΔGW, AF per pixel) over 2027–2099 for the eight CAP shortage scenarios, relative to the Baseline 900 kAF (~1.1 km^3) reference. Every panel is a difference from the same no-cut Baseline run, which keeps WestWater Research's 900 kAF yr^{-1} post-Tier delivery, and each panel title gives the scenario's cut from that delivery. Panel (b), the 2027–2028 Operating Guidelines, removes 248 kAF yr^{-1}, the part of the guidelines' 760 kAF yr^{-1} Arizona reduction beyond the 512 kAF yr^{-1} Tier 1 cut that the baseline is taken to include. Each DCP tier panel instead removes the tier's full cut from the baseline, so it represents a shortage deeper than the tier itself (Table 12). Pixel values are the basin-level ΔGW distributed proportionally by each pixel's share of Total$_{GW}$, and are not hydraulic-head responses[17]. The 2027–2060 maps are in Supplementary Fig. S8, the cumulative uncertainty and signal-

to-noise maps in Supplementary Figs. S9 and S10, and basin choropleths for both windows are in the Zenodo repository[28].

Continuity across all three eras comes from the three-era data harmonization described in Methods, in which satellite-derived products (OpenET ensemble mean ET[44], OpenET gridMET[49], PRISM[47]) and climate model projections (the MACA v2 CMIP5[46] ensemble) are joined using overlap-period bias-correction ratios computed from paired monthly images.

(4) Statewide irrigation consumptive use for Arizona at 2 km annual resolution, with separate GW-CU and SW-CU components (Fig 6) consistent with the partitioning, per-well disaggregation through the well package, and error propagation. CU is derived as CU = Irrigation Withdrawal × Irrigation Efficiency (IE) using USGS NHM HUC12 IEs[24] aggregated to the ADWR GW basins, with the GW/SW split inherited from the withdrawal-source partition.

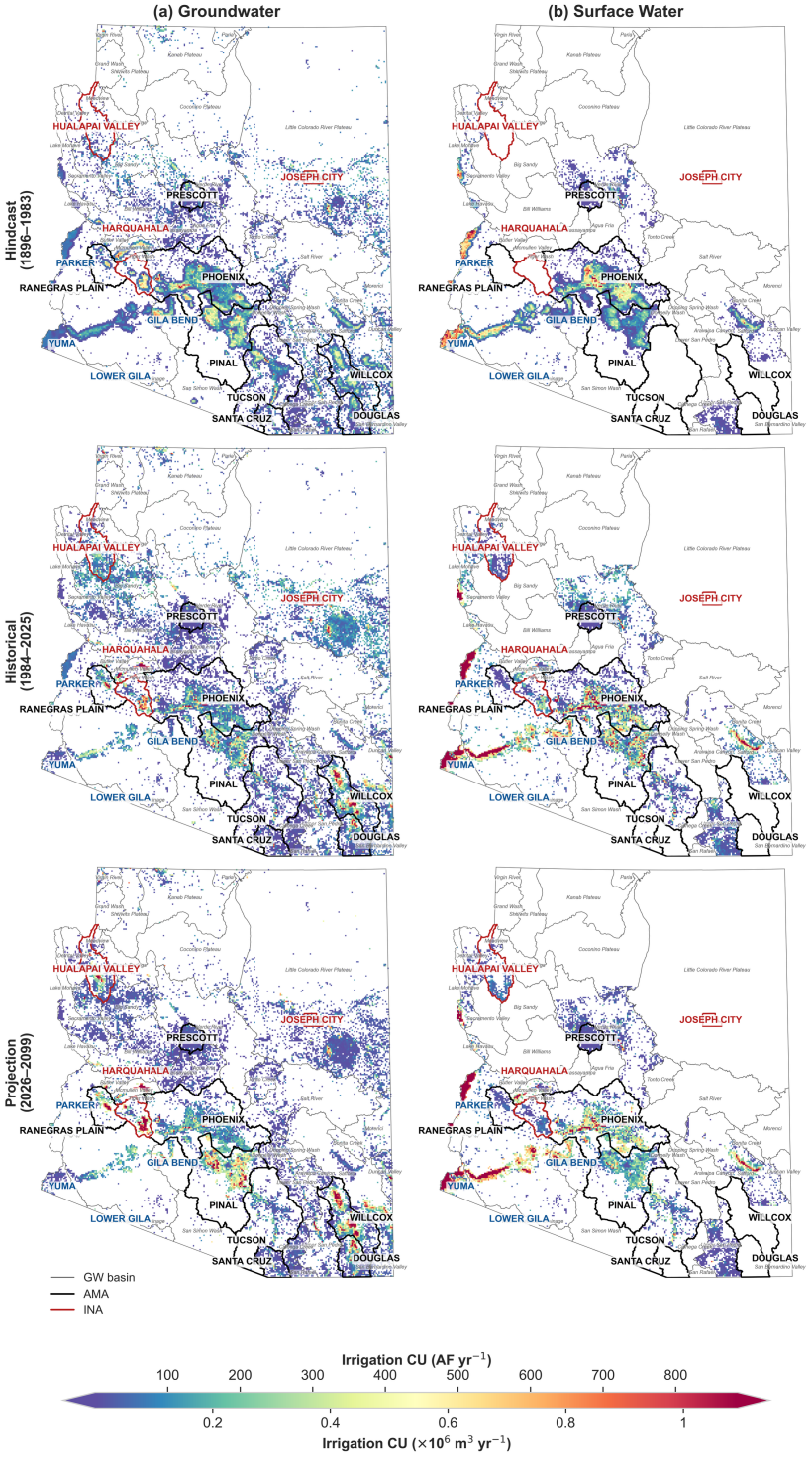


Fig 6. Era-mean annual irrigation consumptive use partitioned into (a) groundwater CU and (b) surface-water CU, with eras as rows (hindcast 1896–1983, historical 1984–2025, projection 2026–2099). The shared color bar shows consumptive-use volumes (m^3, bottom; AF, top).

(5) Per-pixel, per-year stream capture quantification. A process-informed proxy[29,99–101] apportions GW pumping into stream-depletion and storage-mining shares and volumes (Fig 7) at 2 km annual resolution statewide across the 204-year window, with three hydraulic connectivity

scales (λ = 5, 10, and 20 m) producing physically bounded uncertainty intervals. The result is a first-order screen for where well-mediated stream depletion is plausibly significant across the state's groundwater system.

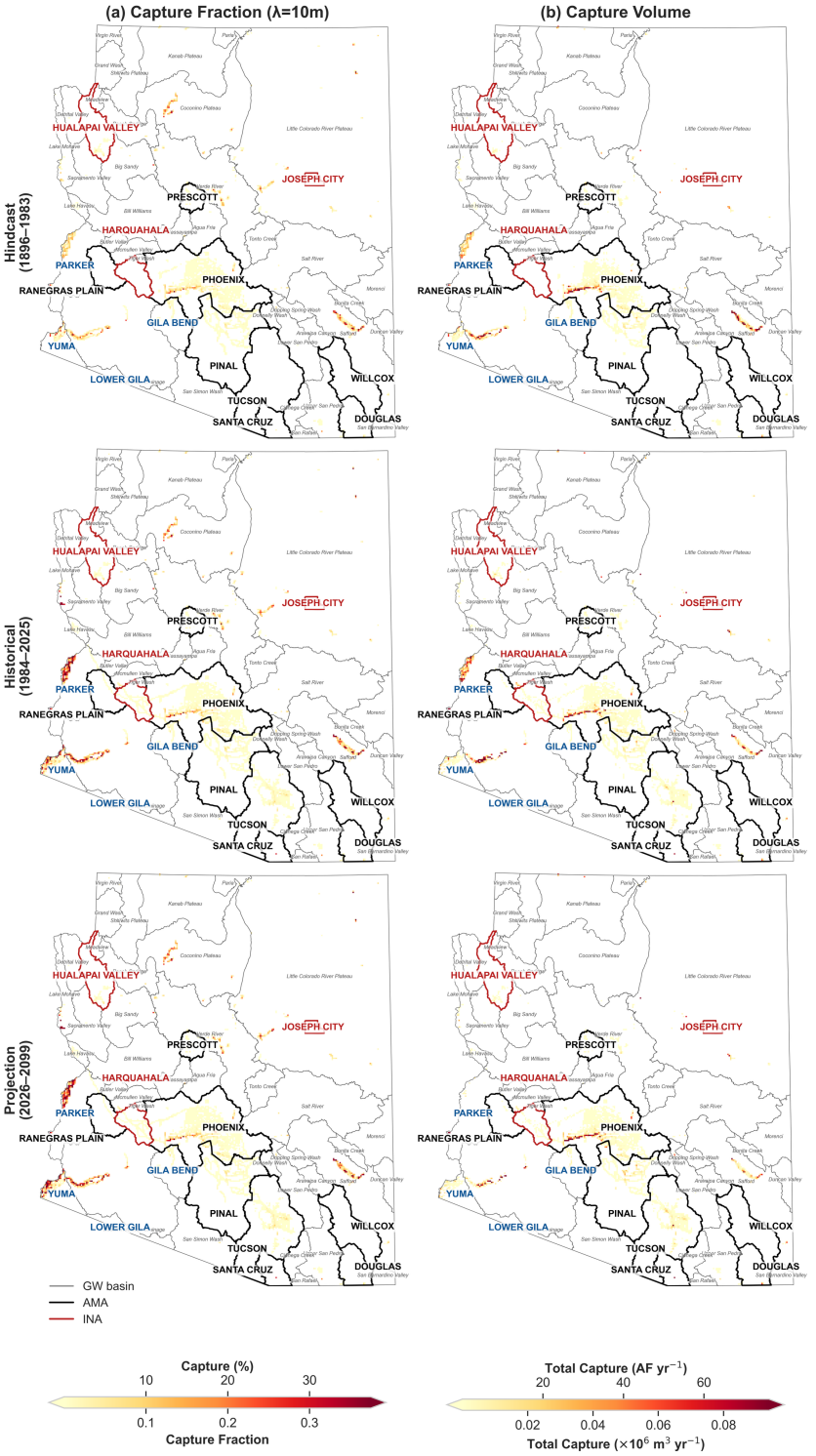


Fig 7. Stream capture fraction and volume era means, with eras as rows (hindcast 1896–1983, historical 1984–2025, projection 2026–2099) and two columns on their own color bars: (a) per-pixel capture fraction at the central connectivity scale (λ = 10 m), and (b) capture volume, which concentrates along the Colorado River mainstem, the Gila corridor, and the CAP and SRP canal-served basins.

(6) Hybrid six-component uncertainty quantification. Every output raster is augmented to a six-band GeoTIFF holding the prediction, its uncertainty (σ), coefficient of variation (CV), signal-to-noise ratio (SNR), and lower and upper 95 % confidence interval (CI) bounds. The uncertainty is separated into six independent components: σ_{MACA} (inter-GCM climate spread[46]), σ_{model} (model randomization seed[72]), σ_{irr} (irrigation-fraction spread[57]), σ_{LULC} (USGS land-use scenarios[56]), σ_{GW} (well-density variability[59]), and σ_{USBR} (streamflow spread at USBR-measured gages[66]). The components are combined in quadrature (σ_{total}; Fig 8), and CU uncertainty is further propagated through the CU = IE × Withdrawal

relationship. Full component definitions and the small-sample corrections are given in Methods, Uncertainty quantification.

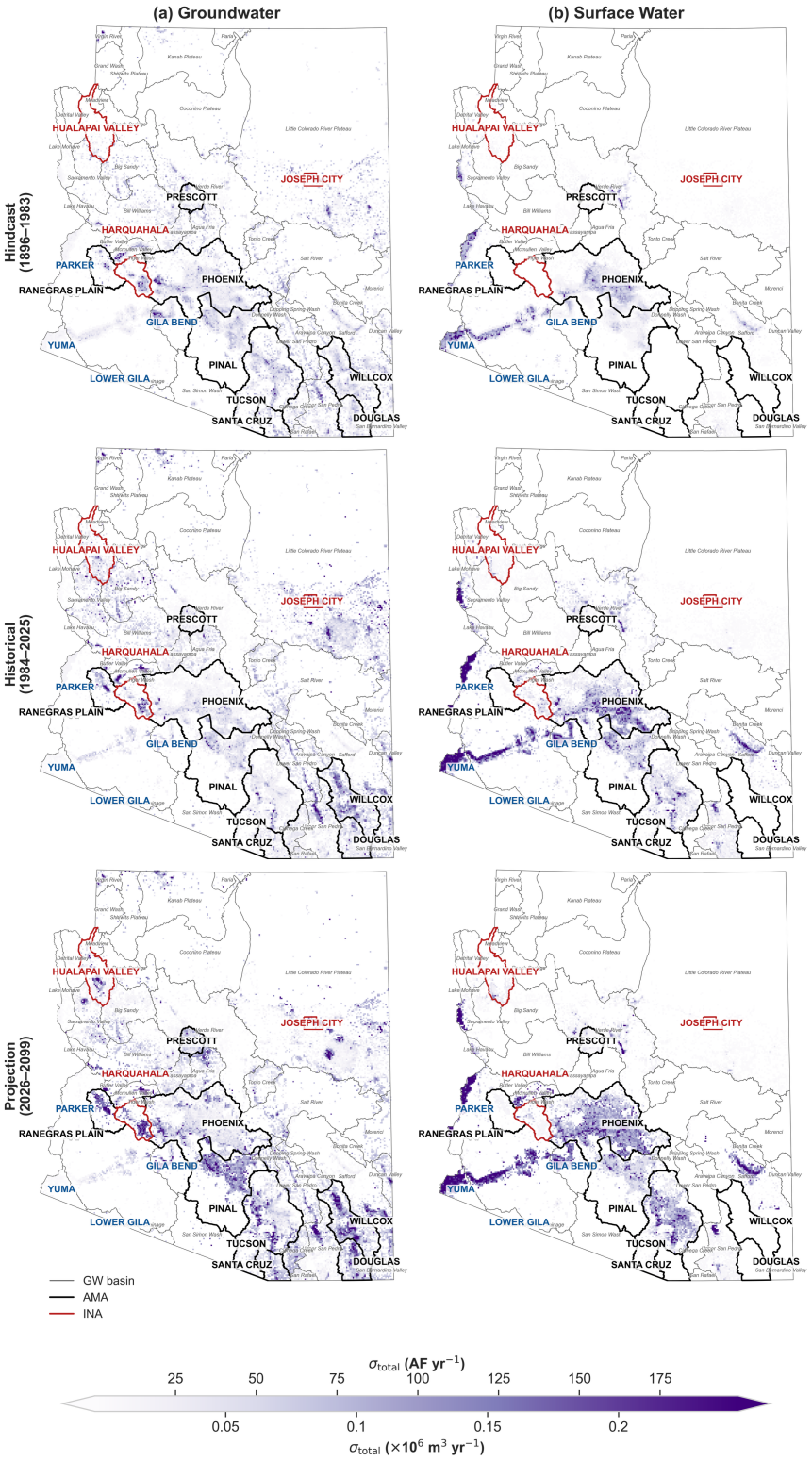


Fig 8. Era-mean annual σ_{total} (quadrature combination of the six uncertainty components) partitioned into (a) groundwater and (b) surface water, with eras as rows (hindcast 1896–1983, historical 1984–2025, projection 2026–2099). The shared color bar shows the per-pixel σ as volume ($\times 10^6$ m^3, bottom; AF, top).

A companion well-level package disaggregates the pixel-level predictions to ~170,000 individual wells from the ADWR Well Registry using capacity-proportional weighting. Per-well uncertainty columns (σ and lower and upper 95 % CI) are included for all categories and units, giving a per-well dataset that links each well's estimated withdrawal, consumptive use, and stream capture to its location, registry attributes, and uncertainty bounds.

The dataset is intended for reuse in groundwater flow modeling [106] (the withdrawal rasters and per-well estimates can serve as pumping boundary conditions, e.g. MODFLOW well-package[107,108] inputs, with per-well uncertainty bounds), aquifer-storage depletion assessment[16,17] when combined with independent recharge estimates, land subsidence analyses[11–13,109], agricultural water management at basin and sub-basin scales[21,73,110], and drought-contingency and Colorado River shortage planning using

the projection-era and CAP shortage-scenario products[6,7]. Projection-era outputs are scenario-dependent and should be treated as exploratory scenario analyses rather than forecasts; the corresponding caveats are detailed in the *Known Limitations* subsection under *Usage Notes*.

Technical Validation

Cross-validated model performance

Model performance was assessed through five evaluation strategies that probe different dimensions of generalization (Table 8, Fig 9). XGBRF ranked among the top performers under every strategy, including the pixel-holdout and temporal-holdout evaluations that test spatial and temporal generalization most directly.

Table 8. Cross-strategy pixel-scale evaluation summary for the selected XGBRF model. Metrics are R^2 (coefficient of determination), RMSE (mm), and NRMSE (% of the training-set mean observed depth, 280.84 mm). Values are mean ± standard deviation across the holdout configurations within each strategy; for the random and pixel holdouts the mean and standard deviation are taken across the five test-size groups, each itself averaged over five seeds. This R^2 follows the scikit-learn formulation[87] and is equivalent to the Nash-Sutcliffe Efficiency (NSE).

Strategy	Test R^2 (=NSE)	Test RMSE (mm)	NRMSE (%)	Notes
Random holdout	0.800 ± 0.006	61.72 ± 0.98	21.98	Mean across 5 test sizes (10–30 %) × 5 seeds
Pixel holdout	0.262 ± 0.013	117.58 ± 0.78	41.87	Same grid; spatial generalization to unseen pixels
Temporal holdout	0.691 ± 0.078	77.69 ± 7.85	27.66	Mean across 7 year-block holdout configurations (T1-T7).
Spatial LOO	−0.458 ± 0.741	159.49 ± 58.21	56.79	Mean across held-out basins (full leave-one-out)
Seeded spatial LOO	0.423 ± 0.092	100.62 ± 20.24	35.83	As above, but with 10 % of the held-out basin's samples seeded into training (local calibration)

The five strategies together show how the model generalizes to unseen random subsets, to unseen locations within known basins, to unseen years both within and beyond the training period, to entirely unseen regions, and to unseen regions with minimal (10 %) local calibration. Held-out basin time series for two representative basins, Phoenix AMA under the T2 forward-extrapolation regime and Harquahala INA under the T5 dual-tail regime, are shown in Fig 9a and Fig 9b. The predictions follow the metered basin totals through both held-out periods, with some overprediction in Fig 9a and some underprediction in Fig 9b.

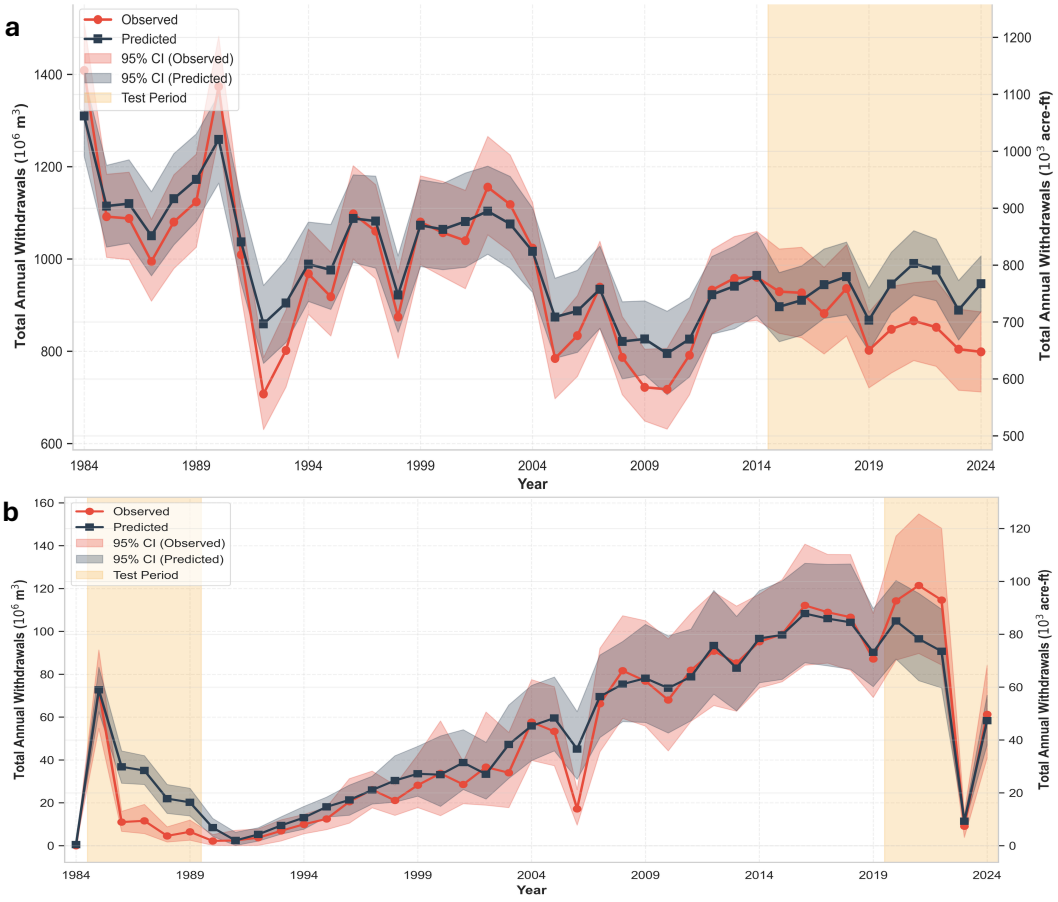


Fig 9. Held-out time series for the selected XGBRF model under two temporal holdout regimes and two management regimes. (a) Phoenix AMA, the largest GW-pumping basin, with mixed municipal and agricultural demand, under the T2 forward-extrapolation configuration (2015–2024 withheld from training). (b) Harquahala INA under the T5 dual-tail configuration (1985–1989 and 2020–2024 withheld simultaneously, forcing backward and forward extrapolation with no early- or late-record anchoring). Each panel shows the observed ADWR basin-summed metered total against the prediction, with the held-out periods shaded. The full per-basin panel sets for all eight temporal holdout configurations, and the seeded and unseeded spatial-LOO products are provided in the Zenodo repository[28].

Model interpretability

The learned relationships of the selected XGBRF model are physically sensible (Fig 10a–c). Crop fraction is the top-ranked predictor by a wide margin (mean |SHAP| ≈ 72 mm; Fig 10c),

followed by irrigation fraction (≈ 31 mm), water-table depth (≈ 27 mm), Northing (≈ 26 mm), agricultural density (≈ 25 mm), and well density (≈ 23 mm).

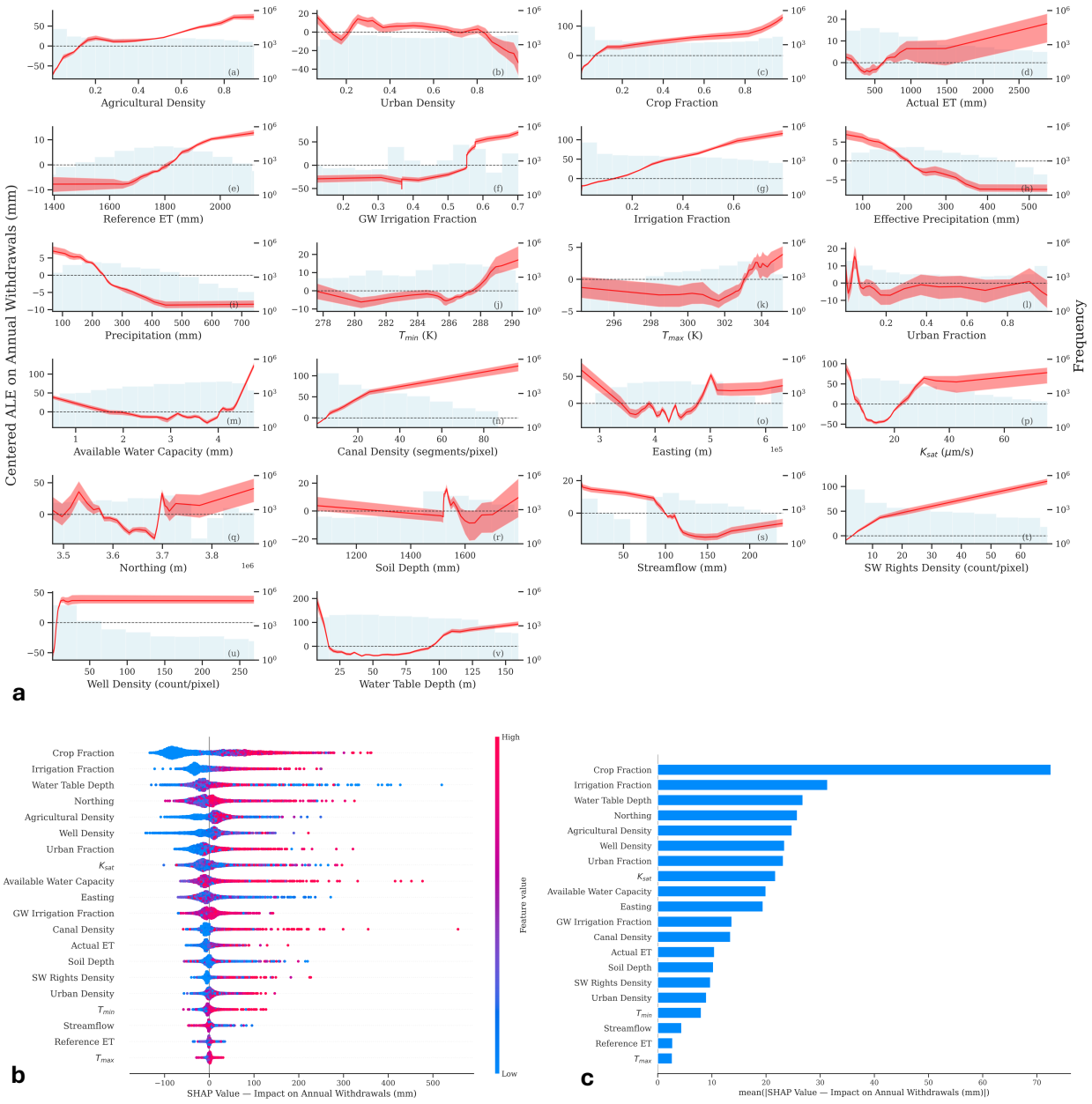


Fig 10. Model interpretability for the selected XGBRF. (a) Accumulated local effects (ALE) on the training data, showing the marginal response of predicted withdrawal depth to each predictor. (b) SHAP summary (beeswarm): predictors ranked by (c) mean absolute SHAP value, each point one test sample colored by feature value, showing both the magnitude and the direction of each predictor's contribution. The permutation importances, per-era SHAP analyses, and per-feature SHAP dependence plots are provided in the Zenodo repository[28].

These top-ranked predictors are the drivers a process-based groundwater pumping model would emphasize: irrigated-land intensity (crop and irrigation fraction), depth to water (a proxy for groundwater accessibility and hydrogeologic setting[68]), and agricultural and well infrastructure

(agricultural and well density). Northing is a spatial coordinate rather than a physical driver, but it absorbs the residual north–south gradient in climate, land use, and management that the other predictors leave unexplained. The accumulated local effects curves (Fig 10a) on the training data show monotone, saturating responses and no spurious oscillations.

Independent validation against USGS products

Model predictions were validated in two stages. Statewide annual totals were first reconciled against the USGS and ADWR reports that informed the partition-parameter calibration. The predictions were then compared against four independent USGS products that were not used in calibration. These products (ML, NHM[21], Reitz[26], PS[22]) have different native resolutions (2 km, HUC12, 800 m), so each was aggregated to a common comparison unit, either GW basin (Table 10) or HUC12 (Fig 11b–f) totals over their common overlap periods. These are model-to-model comparisons rather than comparisons against ground truth, so we report differences rather than errors: root mean square difference (RMSD), mean absolute difference (MAD), and mean bias difference (MBD) use the same formulas as RMSE, MAE, and MBE, with percent difference reported alongside. RMSD, MAD, and MBD are also expressed as percentages, normalized by the reference product, in Fig 11c,e,f.

Statewide agency reconciliation. Modeled total withdrawals were reconciled against the USGS Circulars[97] (published every five years, 1950–2015; Fig 11a) and ADWR reported totals[1] (available only for specific years between 1957 and 2020). Table 9 gives the closures at the anchor years, from the 1955 and 1980 pumping peaks through the 2015 USGS[19] and 2019 ADWR[98] modern record. The two peak years are under-predicted by 6–11 %, because the 2024 Well Registry has lost records for wells abandoned before GMA registration began (Methods, Peak-year well-density infill); every reported total nonetheless falls inside the model's 95 % σ_{total} interval. The deeper 1915–1945 record was checked separately against the USGS OFR 94-476[96] historical GW pumping markers, which the model reproduces within ~6 % at five of them (−0.1 % in 1930, −1.1 % in 1945, +2.0 % in 1925), with larger differences only at 1915 (+8.3 %) and 1920 (−13.9 %). Because these markers are groundwater-only, they are not plotted in the total-withdrawal panel (Fig 11a); the corresponding annual $Total_{GW}$ comparison bars are provided on Zenodo[28]. The ML totals are never adjusted to agency values, but these statewide series anchored the partition-parameter calibration (Methods, Calibration anchors), so Fig 11a and Table 9 demonstrate calibration adequacy. The comparisons in Fig 11b–f are independent of the calibration.

Table 9. Statewide agency reconciliation at the anchor years. Withdrawal volumes are Mm³ with MAF in parentheses; shares are percentages of the statewide total, with differences in percentage points (pp). Every reported total falls inside the model's 95 % σ_{total} interval. These series anchored the partition-parameter calibration (Methods, Calibration anchors), so the table demonstrates calibration adequacy and is not an independent test; the independent comparisons are in Table 10 and Fig 11b–f.

Year	Source and quantity	Reported	Model	Difference
1955	USGS Circular, total withdrawal	9,979 (8.09)	9,364 (7.59)	−6.2 %
1980	USGS Circular, total withdrawal	11,015 (8.93)	10,395 (8.43)	−5.6 %

Year	Source and quantity	Reported	Model	Difference
1980	ADWR, total withdrawal	11,718 (9.50)	10,395 (8.43)	−11.3 %
1990	USGS Circular, total withdrawal	9,362 (7.59)	9,036 (7.33)	−3.5 %
2015	USGS Circular, groundwater withdrawal	3,811 (3.09)	3,653 (2.96)	−4.1 %
2015	USGS Circular, groundwater share	46 %	44.3 %	−1.7 pp
2017	ADWR, total withdrawal	8,634 (7.00)	8,397 (6.81)	−2.7 %
2019	ADWR, groundwater share	41 %	45.9 %	+4.9 pp
2019	ADWR, irrigation share	72 %	74.2 %	+2.2 pp

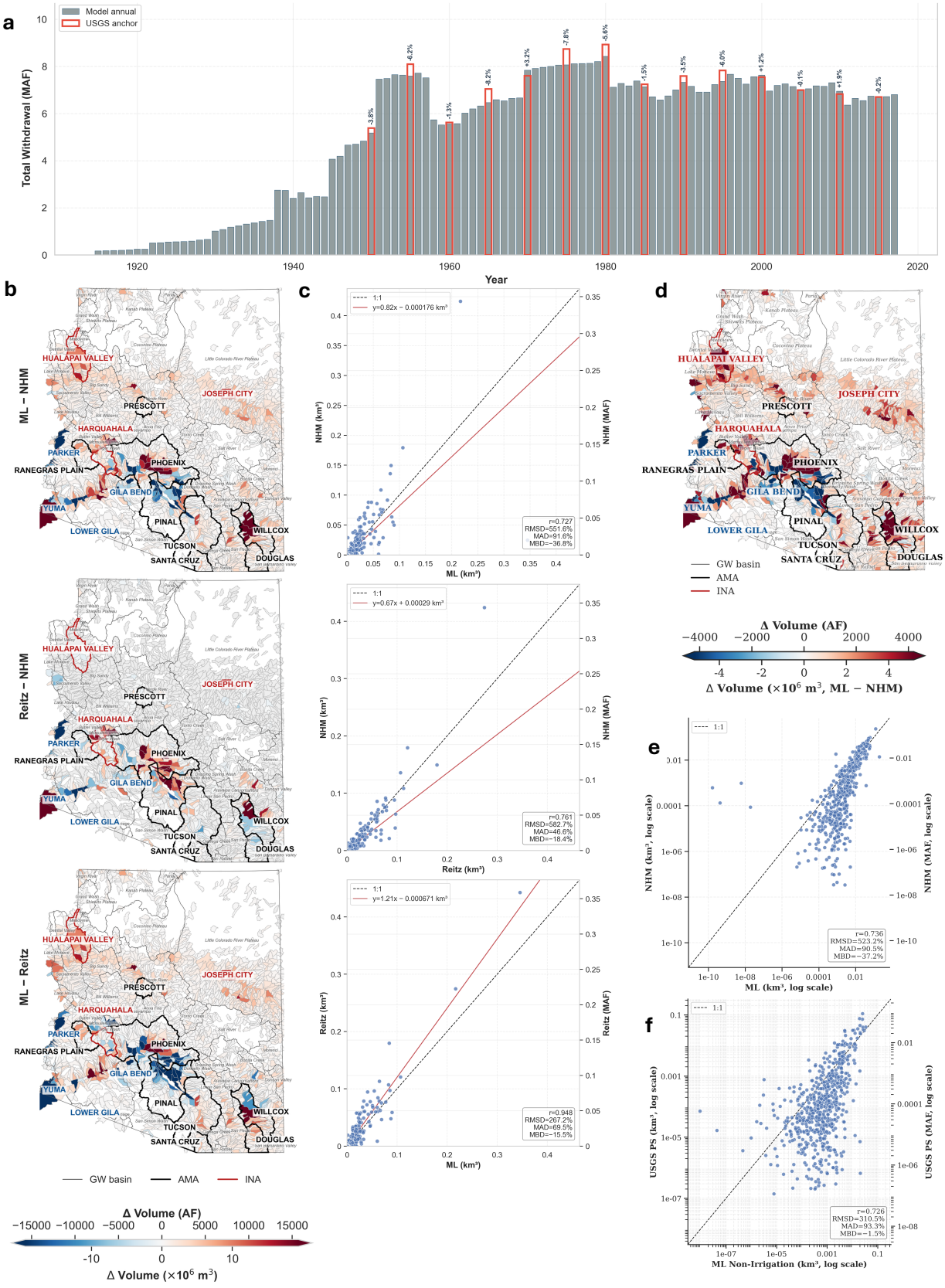
USGS NHM and Reitz irrigation withdrawals. ML irrigation GW and SW predictions were compared against NHM HUC12[24] (2000–2020) and the USGS Reitz [105] irrigation withdrawal estimates (1980–2018) using pairwise metrics (RMSD, MAD, percent difference) and per-basin temporal agreement (Pearson r, NSE). Scatter and difference maps were also computed directly at the HUC12 scale, giving ML vs NHM r = 0.73, ML vs Reitz r = 0.95, and NHM vs Reitz r = 0.76 (Fig 11b,c).

USGS NHM consumptive use. ML irrigation CU was compared against NHM HUC12 CU from the USGS irrigation water use reanalysis product[25] (2000–2020). Statewide ML CU averages 3,858 $Mm^3\ yr^{-1}$ (3.13 MAF yr^{-1}) against NHM's 2,706 $Mm^3\ yr^{-1}$ (2.19 MAF yr^{-1}; +42.6 %), with basin-level RMSD = 63.4 Mm^3, MAD = 35.1 Mm^3 (Table 10), and HUC12 correlation r = 0.74 (Fig 11d,e). Because ML CU applies the NHM-derived basin IEs to the ML withdrawals (CU = IE × Withdrawal), this +42.6 % surplus tracks the parent irrigation-withdrawal surplus (+42.2 %, Table 10) almost exactly. It is inherited from the withdrawal comparison and is not introduced by the CU step.

USGS public supply. ML non-irrigation predictions were compared against the USGS public supply (PS) reanalysis[22,23] (2000–2020). PS is a subset of non-irrigation use, so ML ≥ PS is the expected direction in most basins. The PS metrics in Table 10 diverge strongly because they measure different things. RMSD and MAD average per-basin absolute gaps across all 51 basins, most of which carry negligible non-irrigation volume (49 basins have PS surface water use below 1.2 $Mm^3\ yr^{-1}$, or 1 $kAF\ yr^{-1}$), whereas the percent difference is a statewide-total ratio dominated by the Phoenix and Tucson metropolitan areas and divided by a small reference. The $\text{Non-Irrigation}_{SW}$ row (Table 10) divides a 769 $Mm^3\ yr^{-1}$ surplus by a 119 $Mm^3\ yr^{-1}$ reference, because the USGS PS reanalysis assigns nearly all Arizona municipal supply to groundwater while the ML partition routes CAP and SRP urban deliveries to $\text{Non-Irrigation}_{SW}$. These large PS-row percentages are therefore the expected direction and not a disagreement. At the HUC12 scale (Fig 11f), ML Non-Irrigation tracks the PS spatial pattern closely (r = 0.73) with little systematic bias (MBD = −1.5 %).

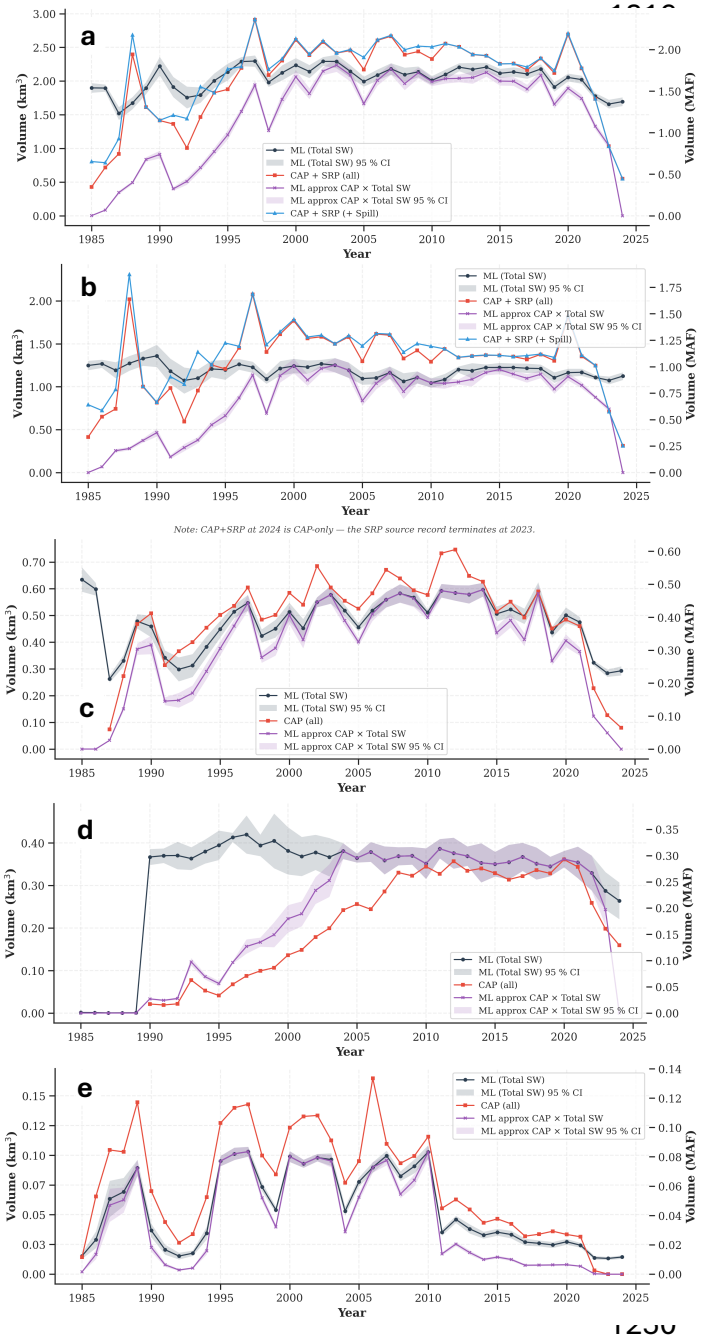
Table 10. Basin-level independent validation metrics. RMSD and MAD are computed across the 51 groundwater basins on each basin's mean-annual volume over the comparison window. The ML and Ref. columns give the statewide mean-annual totals (the sum of the per-basin window means); percent difference (% Diff.) is |ML − Ref.| / Ref. × 100 of those totals, so it measures aggregate statewide bias. ML, Ref., RMSD, and MAD are in $Mm^3\ yr^{-1}$.

Comparison pair	Years	Category	ML	Ref.	RMSD	MAD	% Diff.
ML vs NHM[24]	2000–2020	$Irrigation_{GW}$	2,693	2,102	87.1	42.4	28.1
ML vs NHM[24]	2000–2020	$Irrigation_{SW}$	3,763	2,438	97.8	38.0	54.3
ML vs NHM[24]	2000–2020	Irrigation	6,455	4,540	109.2	59.4	42.2
ML vs Reitz[105]	1980–2018	$Irrigation_{GW}$	3,041	3,020	129.9	58.4	0.7
ML vs Reitz[105]	1980–2018	$Irrigation_{SW}$	3,843	2,901	62.8	30.3	32.5
ML vs Reitz[105]	1980–2018	Irrigation	6,884	5,921	126.6	64.0	16.3
ML vs NHM[25]	2000–2020	CU	3,858	2,706	63.4	35.1	42.6
ML vs PS[23]	2000–2020	Non-Irrigation	2,041	1,175	60.3	28.8	73.7
ML vs PS[23]	2000–2020	$Non\text{-}Irrigation_{GW}$	1,152	1,055	96.2	33.0	9.2
ML vs PS[23]	2000–2020	$Non\text{-}Irrigation_{SW}$	888	119	59.4	14.8	645.5


a
Model annual
USGS anchor
Total Withdrawal (MAF)
Year
b
ML − NHM
Reitz − NHM
ML − Reitz
HUALAPAI VALLEY
JOSEPH CITY
PRESCOTT
HARQUAHALA
PARKER
RANEGRAS PLAIN
PHOENIX
GILA BEND
YUMA
LOWER GILA
PINAL
WILLCOX
TUCSON
SANTA CRUZ
DOUGLAS
GW basin
AMA
INA
Δ Volume (AF)
Δ Volume (×10⁶ m³)
c
1:1
y=0.82x − 0.000176 km³
r=0.727
RMSD=551.6%
MAD=91.6%
MBD=−36.8%
ML (km³)
NHM (km³)
NHM (MAF)
y=0.67x + 0.00029 km³
r=0.761
RMSD=582.7%
MAD=46.6%
MBD=−18.4%
Reitz (km³)
Reitz (MAF)
y=1.21x − 0.000671 km³
r=0.948
RMSD=267.2%
MAD=69.5%
MBD=−15.5%
d
Δ Volume (AF)
Δ Volume (×10⁶ m³, ML − NHM)
e
r=0.736
RMSD=523.2%
MAD=90.5%
MBD=−37.2%
ML (km³, log scale)
NHM (km³, log scale)
NHM (MAF, log scale)
f
r=0.726
RMSD=310.5%
MAD=93.3%
MBD=−1.5%
ML Non-Irrigation (km³, log scale)
USGS PS (km³, log scale)
USGS PS (MAF, log scale)

1207

Fig 11. Independent validation against USGS statewide totals and USGS gridded products. (a) Statewide agency reconciliation bars: ML total withdrawals against USGS reports. (b) HUC12-level mean-annual total-irrigation volume differences (ML − NHM, Reitz − NHM, ML − Reitz). (c) Total-irrigation scatter at the HUC12 scale for the three product pairs (ML vs NHM, NHM vs Reitz, ML vs Reitz). (d) HUC12-level mean-annual irrigation CU volume difference (ML − NHM). (e) Irrigation CU scatter at the HUC12 scale (ML vs NHM, log–log). (f) Non-irrigation scatter at the HUC12 scale (ML vs PS, log–log). GW- and SW-specific versions, basin-scale scatters and difference maps, and per-basin time series are provided in the Zenodo repository[28]; the basin-aggregated statistics are summarized in Table 9.



Surface-water use validation

ML total surface-water predictions are validated against observed CAP and SRP delivery records (1985–2024)[77]. CAP deliveries are filtered to direct use only (excluding managed aquifer recharge). For Phoenix AMA, CAP and SRP deliveries[20] are summed; all other basins use CAP data only.

Fig 12. CAP and SRP delivery-record validation of partitioned surface water (1985–2024). (a) Statewide $Total_{SW}$ time series: the ML central prediction and its 95 % CI ribbon against observed CAP+SRP deliveries. (b–e) Per-basin panels for Phoenix AMA, Pinal AMA, Tucson AMA, and Harquahala INA. The time-series panels also plot an "ML approx CAP" reference, the model $Total_{SW}$ rescaled by each basin's annual CAP direct-delivery ratio relative to its 2000–2009 mean (the peak-CAP era), shown for display only and not part of the partition. Per-basin metrics and scatter plots are in the Zenodo repository.

This validation is independent of training, because the delivery records are never model inputs; the only related predictors are canal density and SW rights, and canal-weighted streamflow is used only during partitioning (Methods, Partition calibration and constraints). Statewide, $Total_{SW}$ closes against the CAP+SRP total within +0.8 % MBE (2,034 vs 2,018 Mm³ yr^{-1}; 1.65 vs 1.64 MAF yr^{-1}), with NSE = 0.34 over the 40-year window: a close match in the long-term mean, with only partial capture of the year-to-year variability.

Per-basin agreement ranges from NSE = 0.73 (MBE = −5.0 %) in Pinal AMA and 0.64 (−26.8 %) in Harquahala INA, through ≈ 0 (−8.0 %) in Phoenix AMA, to −1.81 (+68.5 %) in Tucson AMA, where surface water is over-predicted because imported CAP water there is largely stored as managed aquifer recharge rather than taken as direct delivery. The statewide and per-basin time series are shown in Fig 12a and Fig 12b-e, respectively.

Stream capture validation

No statewide reference dataset for pumping-induced stream depletion exists, so the capture volumes (Fig 7) cannot be compared numerically and were instead evaluated structurally. For a representative year (2017), the per-basin ranking should follow the hydrogeology and the zeros should fall where the physics requires. The results in Table 11 satisfy both requirements.

The Colorado and Gila river-corridor basins rank highest (Yuma 7.6 %, Lower Gila 6.9 %, Lake Mohave 6.1 %, Parker 5.3 %), where shallow water tables over river-recharged alluvium coincide with canal-delivered surface water, whereas basins with no canal infrastructure return exactly zero (Willcox AMA and Butler Valley, the negative controls, where the dual canal gate zeroes the surface-water term). The gate is set on canal infrastructure rather than on distance to a stream because the index measures capture of the surface water actually delivered within a pixel's own supply system, and both negative-control basins are endorheic or ephemeral with no perennial channel from which modeled pumping could capture. Because capture requires both connectivity and a surface-water footprint, neither a shallow water table alone (Safford, 0.6 %) nor large pumping alone produces a high fraction.

Table 11. Per-basin validity check of the stream capture estimates (2017, central λ = 10 m). GW and SW volumes are the partitioned basin totals (kAF with Mm³ equivalents); capture volume = volume-weighted capture fraction × GW volume (AF with Mm³ equivalents); mean water table depth (WTD) is from the static Ma et al. (2026)[68] raster. Willcox AMA and Butler Valley are negative controls with no canal infrastructure.

Basin	GW pumping (kAF / Mm³)	SW withdrawal (kAF / Mm³)	Capture volume (AF / Mm³)	Capture %	Mean WTD (m)	Interpretation
Yuma	6.8 / 8.4	444.2 / 547.9	520 / 0.64	7.61	42	Colorado River alluvium; GW cap (≤ 0.10) routes federal/tribal deliveries to SW
Lower Gila	97.4 / 120.1	512.2 / 631.8	6,701 / 8.27	6.88	55	Gila River corridor
Lake Mohave	2.6 / 3.2	127.9 / 157.8	161 / 0.20	6.14	66	Colorado River mainstem corridor; GW cap ≤ 0.10
Parker	9.2 / 11.3	400.7 / 494.3	491 / 0.61	5.31	51	CRIT senior Priority-1 mainstem; GW cap ≤ 0.10

Basin	GW pumping (kAF / Mm³)	SW withdrawal (kAF / Mm³)	Capture volume (AF / Mm³)	Capture %	Mean WTD (m)	Interpretation
Phoenix AMA	316.7 / 390.6	996.4 / 1229.0	7,037 / 8.68	2.22	64	CAP + SRP corridor; deep WTD
Lake Havasu	0.7 / 0.9	21.7 / 26.8	14 / 0.02	1.94	73	Colorado River adjacent; deep WTD
Safford	151.4 / 186.7	146.4 / 180.6	973 / 1.20	0.64	34	Upper Gila valley; shallowest WTD but small canal footprint
Willcox AMA	333.3 / 411.1	0.0 / 0.0	0 / 0.00	0.00	44	Negative control: canal coverage 0.16 % < 1 % gate threshold
Butler Valley	14.7 / 18.1	0.1 / 0.1	0 / 0.00	0.00	72	Negative control: negligible canal coverage

The high-capture river-corridor basins (Yuma, Lower Gila, Lake Mohave) coincide with the areas that Majumdar et al. (2022)[11] independently identified as posing the highest risk to surface-water supplies, using a geometric screen of shallow wells (≤ 50 m) within the Colorado and Gila River floodplains. That screen also flags the Phoenix, Tucson, and Harquahala areas along the CAP corridor. Our method agrees on the direction of risk there but assigns lower capture volumes (Table 11, Fig 7), because most surface water in those areas is delivered through canals and to SW-righted wells, which the capture numerator excludes. The agreement is out-of-sample, since that study informs no part of the capture computation.

The capture fraction is a lower bound (Methods, Stream Capture Index). A low fraction in a canal-dominated basin therefore means that surface water there is delivered through canals, SW-righted wells, or engineered drains, which the capture numerator excludes, and not that wells in that basin have no effect on streamflow.

CAP shortage-scenario projection (2026–2099)

The same partition framework validated against the observed CAP and SRP records above was also driven forward under eight post-2026 Colorado River shortage scenarios. Five follow the DCP tier structure that was in force through 2026, retained as calibrated magnitude analogs because the 2019 DCP itself lapses at the end of that year: Tiers 0, 1, 2a, 2b, and 3, ranging from a 237 $Mm^3\ yr^{-1}$ (192 $kAF\ yr^{-1}$) to an 888 $Mm^3\ yr^{-1}$ (720 $kAF\ yr^{-1}$) CAP cut. Each tier row removes its full cut from the 1,110 $Mm^3\ yr^{-1}$ (900 $kAF\ yr^{-1}$) baseline delivery. Because that baseline is taken to already reflect the 631 $Mm^3\ yr^{-1}$ (512 $kAF\ yr^{-1}$) Tier 1 cut, the tier rows describe shortages deeper than the tiers themselves; the Tier 1 row, for example, leaves 479 $Mm^3\ yr^{-1}$ (388 $kAF\ yr^{-1}$). A sixth applies the 2027–2028 Operating Guidelines[14]: of their 760 $kAF\ yr^{-1}$ (937 $Mm^3\ yr^{-1}$) Arizona reduction, the 512 $kAF\ yr^{-1}$ Tier 1 cut is taken to be in the baseline, so the row removes the remaining 248 $kAF\ yr^{-1}$ (306 $Mm^3\ yr^{-1}$) and leaves a 652 $kAF\ yr^{-1}$ (804 $Mm^3\ yr^{-1}$) CAP delivery. It is the only row that represents an announced operating condition, and its smaller cut is why its ΔGW falls below that of the Tier 1 row. The remaining two bracket the

deeper end of the range: WestWater Research's[8] Basic Coordination scenario, which leaves a 292 Mm³ yr^{-1} (237 kAF yr^{-1}) CAP delivery and therefore an 818 Mm³ yr^{-1} (663 kAF yr^{-1}) cut from the 1,110 Mm³ yr^{-1} (900 kAF yr^{-1}) baseline delivery; and an Extreme Shortage case of zero delivery, a complete CAP cessation cutting the full 1,110 Mm³ yr^{-1} (900 kAF yr^{-1}). The sweep spans the range the post-2026 sideboards leave open, which permit a Lower Basin shortage of up to 3.0 MAF yr^{-1} allocated by priority under applicable law, and CAP holds the most junior large entitlement in Arizona.

Each scenario mirrors the central-run CAP delivery perturbation (Methods, CAP delivery perturbation) but is referenced to WestWater Research's 1,110 Mm³ yr^{-1} (900 kAF yr^{-1}) post-Tier operating baseline instead of the 1,850 Mm³ (1,500 kAF) design capacity. At CAP-service-area pixels, (1) an additive surface-water cut equal to (1 − delivery factor) × 900 kAF (1,110 Mm³), exactly the cut named in each scenario, is removed from the canal-weighted streamflow, and (2) the well-density columns are scaled by a scenario-specific GW boost mapped to era-analogous GW-weight targets (Table 12). The central projection instead takes the guidelines' full 760 kAF yr^{-1} (937 Mm³ yr^{-1}) reduction from the 1,850 Mm³ (1,500 kAF) design capacity (delivery factor 0.49; Table 3).

The ML total is computed before the perturbation, so only the GW/SW split moves. The per-basin difference in partitioned Total_{GW} between a scenario and the no-cut baseline is the scenario-induced additional pumping, ΔGW. The no-cut baseline keeps the 900 kAF yr^{-1} (1,110 Mm³ yr^{-1}) post-Tier delivery and bypasses the central-run shortage, so every Table 12 value and every scenario map (Fig 5; Supplementary Fig. S8) is measured from that one reference. The scenarios have no uncertainty ensemble of their own: the uncertainty of ΔGW is taken as the central-run σ_{total} of Total_{GW} over the CAP service area, which Supplementary Fig. S9 maps together with the per-pixel signal-to-noise ratio of each scenario (Supplementary Fig. S10). The sweep boosts (Table 12) are larger than the central-run Tier boosts (Table 3) because the sweep is calibrated as a WestWater-anchored stress bracket that reaches the deeper pre-CAP groundwater-substitution regimes, whereas the central run is tuned to the milder observed 2022–2024 substitution. The cumulative statewide ΔGW (Table 12) provides an out-of-sample cross-check against the only published Arizona benchmark, WestWater's projected groundwater plus long-term storage credit (LTSC) drawdown[8].

Table 12. CAP scenario sweep: perturbation parameters and cumulative additional GW pumping (ΔGW, MAF) relative to the no-cut Baseline_900kAF reference, summed over the two reporting windows. The DCP tiers are defined by their cut size and the WestWater scenarios by their remaining annual delivery (cut = 900 kAF yr^{-1} baseline − delivery). Every cut is relative to the 900 kAF yr^{-1} baseline, which is taken to already reflect the 512 kAF yr^{-1} Tier 1 cut. The DCP tier rows therefore describe shortages deeper than the tiers themselves, whereas the 2027–2028 Operating Guidelines row removes only the 248 kAF yr^{-1} by which the guidelines' 760 kAF yr^{-1} Arizona reduction exceeds that cut, which is why its ΔGW is smaller than that of the Tier 1 row. The delivery factor and the well-density GW boost implement each scenario at CAP pixels. Cumulative totals are the time integral of the per-scenario annual ΔGW. Here 1 kAF = 1.233 Mm³ and 1 MAF = 1,233.48 Mm³.

Scenario	CAP delivery (kAF yr^{-1})	CAP cut (kAF yr^{-1})	Delivery factor (× 900 kAF)	GW boost	2027–2060 cum ΔGW (MAF)	2027–2099 cum ΔGW (MAF)	WestWater 2027–2060 anchor (MAF)
DCP Tier 0	708	192	0.787	1.0	0.03	0.08	—
2027–2028 Operating Guidelines	652	248	0.724	2.6	1.30	3.15	—
DCP Tier 1	388	512	0.431	10.0	4.05	9.69	—
DCP Tier 2a	308	592	0.342	18.0	5.89	13.92	—
DCP Tier 2b	260	640	0.289	23.0	6.87	16.12	—
DCP Tier 3	180	720	0.200	50.0	10.69	24.60	—
Basic Coordination	237	663	0.263	25.0	**7.24**	16.95	**8.0 (−9.5 %)**
Extreme Shortage	0	900	0.0	75.0	13.08	29.89	8.7 (+50 %, no-cap framing)

The 2027–2028 Operating Guidelines scenario adds 1,606 Mm³ (1.30 MAF) of groundwater pumping over 2027–2060 and 3,881 Mm³ (3.15 MAF) over 2027–2099 (Table 12), less than the DCP Tier 1 row because only 248 kAF yr^{-1} of the guidelines' reduction lies below the baseline delivery. The Basic Coordination scenario ΔGW reaches 8,930 Mm³ (7.24 MAF) over 2027–2060, within −9.5 % of WestWater's 9,868 Mm³ (8.0 MAF), while the Extreme Shortage ΔGW sits ~50 % above WestWater's 8.7 MAF. The difference arises because the partition framework routes the entire CAP cut to groundwater pumping with no regulatory ceiling, whereas WestWater caps its drawdown at AMA-regulated pumping plus finite LTSC pools and leaves the residual deficit as unmet demand[8]. That residual corresponds to the demand reduction that Sharma et al. (2026)[10] observed at a Pinal County irrigation district that lost nearly all of its CAP supply in 2022–2024, where added pumping replaced only about a quarter of the loss and fallowing and crop switching absorbed the rest. The framework does not model such responses, so the ΔGW of the deeper scenarios is an upper bound on additional pumping.

Physical consistency checks

In addition to the per-pixel budget closure (Methods, Full-period prediction and partitioning), three physical constraints are enforced throughout the pipeline so that the published products are physically meaningful and internally consistent.

Non-negativity. Groundwater withdrawal depth is physically non-negative. Tree-based regressors can produce small negative values near zero as numerical noise at the leaf level, so all predictions are wrapped in an absolute-value transform and the lower 95 % CI bounds are clipped at zero. The transform is applied consistently across the Optuna cross-validation, the uncertainty ensemble generation, and the bias correction, so that all reported metrics and confidence intervals are evaluated on the same post-processed quantity.

Well-density masking. Predictions are set to "no data" at pixels with zero registered wells in the ADWR Well Registry. This prevents the model from generating spurious withdrawal estimates

in areas where no extraction infrastructure exists, including wilderness areas, national forests, and tribal lands without documented wells. The mask is applied after prediction but before partitioning, so all downstream category rasters inherit the same spatial mask.

ET cap. During predictor assembly, actual ET was capped at 2 × ETo (Kc_{max} = 2.0) to remove physically implausible values where ET greatly exceeds atmospheric demand. ET can legitimately exceed ETo for high-Kc crops such as alfalfa, under urban oasis and advection effects[111], and at open-water or riparian pixels, so a factor of 2 was used instead of a strict 1:1 cap. Empirically, ET exceeds ETo only negligibly outside agricultural, urban, and surface-water land uses, which confirms that the factor of 2 is large enough to accommodate legitimate high-ET pixels.

Usage Notes

Accessing the data

All data are available from Zenodo (https://doi.org/10.5281/zenodo.19057935)[28]. Most users need only the headline archive az-hydro-headline.7z (~8.7 GB compressed), which is self-contained and holds every key output: the augmented prediction, consumptive-use, and stream capture rasters, the well-level package, the per-basin and per-sub-basin time series, the CAP shortage-scenario outputs, and the validation, era-mean, and trend figures. Users should extract it and read Data/HEADLINE_README.md for the per-directory inventory.

Reproducing the pipeline from scratch instead requires the full archive az-hydro-data.7z (~80 GB compressed). Users should extract it and place it at the repository root so that Data/Inputs/ and Data/Outputs/ exist. A full setup requires ~220 GB of disk space (~20 GB inputs once the external products are downloaded + ~200 GB outputs + code and figures); users who only need the published prediction products can take the headline archive or skip the ~121 GB model-evaluation archive within the full deposit. For Mac users, the .7z format is not openable by the macOS Archive Utility, so they should use 7-Zip, Keka, or p7zip.

Interactive web exploration

The full gridded prediction stack, the stream capture, the CAP scenario sweep, and the well-level package are also served through an interactive GEE App, AZ-Hydro Explorer, at https://azhydro.projects.earthengine.app/view/azhydro-explorer. The app provides a year slider over 1896–2099, per-category unit/band dropdowns, a side-by-side comparison wipe, and click-driven pixel, basin, sub-basin, and nearest-well time-series charts with 95 % CI envelopes, along with the per-basin × eight-scenario CAP cumulative-drawdown chart. No GEE authentication is required for read-only viewing. Source for the app and the asset-ingest pipeline lives at https://github.com/montimaj/az-hydro/tree/main/gee. The published GEE asset paths under projects/azhydro/assets/az-wu-v1-2/ (*Data Records*) can be loaded directly into any GEE script without redownloading from Zenodo.

Using the well-level package

The four GeoParquet files (Well_Package_{mm,ft,m3,AF}.parquet) are readable with GeoPandas or any GeoParquet-compatible tool and can be loaded directly in recent QGIS releases. Each file is long format, i.e., one row per (well, year) with point geometry, and column

naming follows the pattern {Category}_{unit} for predictions and {Category}_{unit}_sigma for the 1σ uncertainty; 95 % CI bounds are computed on the fly as prediction ± 1.96 σ (clamping the lower bound at zero).

Known limitations

The framework is most reliable inside the 1984–2024 metered window and within morphologically similar basins, and the σ_{total} framework already widens the confidence intervals where the limitations below apply most strongly. Outputs outside that scope should be read as physics-constrained reconstructions and projections, not as validated point estimates. Several limitations follow from the structure of the framework rather than from any single uncertainty component.

Temporal scope. The training era (1984–2024) is the highest-confidence period, where the predictions overlap metered ADWR records and every predictor is observational. The hindcast (1896–1983, and especially pre-1950) extrapolates backward by up to 88 years. Tree-based models cannot extrapolate beyond a predictor's training range and instead plateau at the nearest leaf value[83,84], so these years are reconstructions that hold under the assumption that the 1984–2024 predictor–response relationships are stationary. They are appropriate as a physics-constrained reconstruction and not as a validated estimate for any specific year: pre-1930 Arizona had no Hoover Dam, little SRP build-out, and far fewer wells[9,79]. A per-pixel out-of-distribution detector flags where the extrapolation is most severe (Supplementary Fig. S6), and σ_{irr} and σ_{GW} dominate the deep-hindcast uncertainty as expected. The projection (2026–2099) is climate-scenario-dependent, derived from the MACA v2 40-member ensemble mean (20 GCMs × 2 RCPs)[46] under the CAP shortage set by the 2027–2028 Operating Guidelines, held through 2099 as an assumption[14] that the scenario sweep brackets.

Projection structural-change blindness. σ_{LULC} and σ_{MACA} vary climate and land use across the supplied scenarios but do not vary the learned relationship between predictors and pumping, so the projection cannot represent structural change: crop-mix shifts at constant area[112], on-farm irrigation-technology transitions (below), policy shifts such as basin closures or new metering and conservation rules, step-change events such as a deep Colorado River shortage declaration or dam decommissioning, or emerging demands such as data centers. The post-2026 delivery regime is a specific case. The Decision Framework adopted in August 2026 covers 2027–2036 through Operating Guidelines issued at roughly two-year intervals, and sets a maximum Lower Basin shortage of 3.0 MAF yr^{-1} (3,700 Mm^3 yr^{-1}) without fixing the shortage volumes or their distribution among the Lower Division States[9]. The first Operating Guidelines[14] set them for 2027 and 2028 only, including a 760 kAF yr^{-1} reduction for Arizona. CAP deliveries after 2028 are therefore bounded but not specified, which is why the central projection holds the 2027–2028 condition only as a stand-in and the projection is also delivered as a scenario sweep. The projection answers what water use would be if the 1984–2024 predictor–response relationships continued under the supplied climate and land-use scenarios. It is not a forecast of 2099 water use.

CAP-only footprint of the shortage-scenario sweep. The sweep applies its surface-water cut to the canal-weighted streamflow and its groundwater boost to the well-density columns at CAP-service-area pixels only, so each scenario represents curtailment of CAP deliveries and nothing else. Its deepest case, Extreme Shortage, removes the entire 1,110 Mm^3 yr^{-1} (900 kAF yr^{-1})

baseline delivery and therefore saturates at complete CAP cessation. A Lower Basin shortage approaching the 3.0 MAF yr^{-1} sideboard would exhaust CAP well before reaching that limit and would then fall on the senior mainstem entitlements in the Yuma, Parker, and Lake Mohave basins, which lie outside the perturbed footprint and whose partitioned surface water the sweep leaves unchanged. Shortages deeper than complete CAP cessation are therefore not represented, and the reported ΔGW should be read as the groundwater response to CAP curtailment rather than to a basin-wide reduction. Extending the sweep past that point would require a distribution of Lower Basin shortages among the Lower Division States, which the Decision Framework leaves to be set in the Operating Guidelines.

Emission-pathway choice (RCP 8.5). RCP 8.5 is increasingly regarded as an unlikely business-as-usual case, and its use as a central planning scenario has been cautioned against[76]. Since we average RCP 4.5 and 8.5 across all 40 MACA members, the effective forcing sits between the two and divergence concentrates in the late century. So, users needing a strictly policy-consistent forcing can treat the RCP 8.5 contribution as an upper bound. The ensemble is CMIP5 (MACA v2's basis)[46]; CMIP6 replaced RCPs with SSP–RCP combinations[75] but a subset of its models run hot[113], and CMIP7 scenarios remain under development[76]. Because the bias-correction harmonization is agnostic to the source ensemble, the climate inputs can be regenerated from a CMIP6/CMIP7 downscaled product when one becomes standard, leaving the trained model, partition, and UQ framework unchanged.

Irrigation-efficiency paradox in CU. CU = IE × Irrigation Withdrawal holds the NHM HUC12 irrigation efficiency constant across all years. The crop-area channel of CU change is captured, because the irrigated and crop fractions vary year to year, but the framework does not represent crop-mix shifts at constant area, growing-season extension or double-cropping, intensified application depth, or a shift in IE itself. Those are the mechanisms through which higher on-farm efficiency empirically raises ET, and therefore CU, instead of lowering it, the so-called irrigation efficiency paradox[112,114]. Projected CU is thus a mechanistic projection under constant IE and constant irrigation-system coupling, not a technology-trajectory forecast.

Sparse metering in new ADWR management areas. Ranegras Plain AMA (2026), Willcox AMA (2025), and Hualapai Valley INA (2022) were designated only recently, so ADWR-metered records there are limited to the latest training years and fewer wells per pixel than the seven original AMA/INAs[5,115]. Moreover, the Douglas basin was transitioned from an INA to an AMA in 2022, indicating potential shifts in groundwater management and irrigation practices. Therefore, pre-designation predictions are effectively extrapolations from morphologically similar basins and warrant the same caution as predictions over unmetered basins.

Static water-table-depth raster. The capture fraction and the uncertainty framework treat the Ma et al. (2026)[68] WTD raster as time-invariant, so the $\exp(-wtd_m/\lambda)$ connectivity term does not track water-table change and the proxy is most defensible near the snapshot date. The Well Registry well-depth record was evaluated as a substitute, but it records total drilled depth, typically 2–10 times the water-table depth, which would drive the connectivity term to almost zero everywhere, and it was therefore not used.

Stream capture is a screening proxy. The capture fraction is a first-order screen and not a substitute for a calibrated transient basin model. The existing basin-specific MODFLOW-based groundwater availability studies[106] for Phoenix AMA, Tucson AMA, Pinal AMA, Willcox

AMA, and Yuma are physically rigorous, but each was built with its own calibration targets, parameters, and time horizon, which makes them difficult to intercompare. Our capture fraction gives up that per-basin rigor in exchange for a uniform statewide footprint. It represents one pathway only, well-mediated stream depletion at groundwater pumping pixels, and is by construction a lower bound that omits direct federal and canal diversions, SW-righted wells, ephemeral stream–aquifer exchange, seepage returns from unlined canals, and engineered drains (Methods, Stream Capture Index). It also inherits the static-WTD caveat above.

Structural UQ assumptions. The six uncertainty components are combined via quadrature assuming independence, which may be modestly violated where σ_{MACA}, σ_{USBR}, and σ_{LULC} share structure. Moreover, the GW/SW partition relies on canal density and water-rights densities, which are strong indicators for irrigation surface water but weaker proxies for municipal or industrial surface-water sourcing in basins served by utilities without canal infrastructure.

Code Availability

The project source code and documentation are available at https://github.com/montimaj/az-hydro and archived on Zenodo (https://doi.org/10.5281/zenodo.19057935) under the BSD-3-Clause license.

References

1. ADWR. *Annual Report 2016*. https://www.azwater.gov/sites/default/files/2022-08/Annual_Report_2016%28Final%29.pdf (2016).

2. USBR. *Colorado River Compact, 1922*. https://www.usbr.gov/lc/region/g1000/pdfiles/crcompct.pdf (1922).

3. United States of America & Mexico. *Treaty between the United States of America and Mexico Relating to the Utilization of Waters of the Colorado and Tijuana Rivers and of the Rio Grande*. https://www.usbr.gov/lc/region/pao/pdfiles/mextrety.pdf (1944).

4. Moiz, A. & Mascaro, G. Multiscale Assessment of the Water Balance Components in Arizona Simulated by the National Water Model. *JAWRA Journal of the American Water Resources Association* **62**, (2026).

5. ADWR. *ADWR Annual Report 2025*. https://www.azwater.gov/sites/default/files/2025-08/2025_ADWR_ANNUAL_REPORT_web.pdf (2025).

6. Scanlon, B. R. *et al.* Multidecadal drought impacts on the Lower Colorado Basin with implications for future management. *Commun. Earth Environ.* **6**, 214 (2025).

7. Richter, B. D. *et al.* New water accounting reveals why the Colorado River no longer reaches the sea. *Commun. Earth Environ.* **5**, 134 (2024).

8. WestWater Research. *Economic Impacts to Central Arizona of Reductions in CAP Deliveries. Prepared for the Central Arizona Project.* https://library.cap-az.com/documents/public-information/Economic-Impact-to-CAP.pdf (2026).

9. USBR. *Record of Decision: Decision Framework for Colorado River Guidelines: Coordinated Operations of Lake Powell and Lake Mead (2027–2036)*. https://www.usbr.gov/ColoradoRiverBasin/post2026/decision-doc/P26_RecordofDecision_Final.pdf (2026).

10. Sharma, S. *et al.* Differential impacts of Colorado River shortage operations on agricultural adaptation and groundwater reliance in Central Arizona. *Agric. Water Manag.* **336**, 110842 (2026).

11. Majumdar, S., Smith, R., Conway, B. D. & Lakshmi, V. Advancing remote sensing and machine learning-driven frameworks for groundwater withdrawal estimation in Arizona: Linking land subsidence to groundwater withdrawals. *Hydrol. Process.* **36**, e14757 (2022).

12. Conway, B. D. Land subsidence and earth fissures in south-central and southern Arizona, USA. *Hydrogeol. J.* **24**, 649–655 (2016).

13. Peng, M. *et al.* Mapping land subsidence and aquifer system properties of the Willcox Basin, Arizona, from InSAR observations and independent component analysis. *Remote Sens. Environ.* **271**, 112894 (2022).

14. USBR. *Operating Guidelines: Colorado River Guidelines for Coordinated Operations of Lake Powell and Lake Mead, Operating Years 2027 and 2028*. https://www.usbr.gov/ColoradoRiverBasin/post2026/decision-doc/2027-2028OperatingGuidelines_Final.pdf (2026).

15. Smith, R. & Majumdar, S. Groundwater storage loss associated with land subsidence in Western United States mapped using machine learning. *Water Resour. Res.* **56**, e2019WR026621 (2020).

16. Al Fatta, A., Smith, R., Vajedian, S., Schreuder, W. & Butler Jr, J. J. Quantifying groundwater depletion in an agricultural region using integrated in-situ and satellite-based approaches: insights from the San Luis Valley, CO. *J. Hydrol. (Amst).* 135438 (2026) doi:10.1016/j.jhydrol.2026.135438.

17. Platt, L. C., Weingarten, M., Faunt, C. C., Traum, J. A. & Boyce, S. E. Modeling Future Groundwater Depletion to Evaluate Sustainability Goals Set Under the Sustainable Groundwater Management Act in the Critically Overdrafted Basins of the Central Valley, California, USA (2020–2070). *Water Resour. Res.* **62**, (2026).

18. Hasan, M. F., Smith, R., Vajedian, S., Pommerenke, R. & Majumdar, S. Global land subsidence mapping reveals widespread loss of aquifer storage capacity. *Nat. Commun.* **14**, 6180 (2023).

19. Dieter, C. A. *et al. Estimated Use of Water in the United States County-Level Data for 2015 (Ver. 2.0, June 2018): U.S. Geological Survey Data Release*. https://doi.org/10.5066/F7TB15V5 (2018).

20. ADWR. ADWR Live Queries and Reports. *Arizona Department of Water Resources* https://infoshare.azwater.gov/docushare/dsweb/View/Collection-72 (2020).

21. Martin, D. J. *et al.* Estimating irrigation consumptive use for the conterminous United States: coupling satellite-sourced estimates of actual evapotranspiration with a national hydrologic model. *J. Hydrol.* **662**, 133909 (2025).

22. Alzraiee, A. *et al.* Next Generation Public Supply Water Withdrawal Estimation for the Conterminous United States Using Machine Learning and Operational Frameworks. *Water Resour. Res.* **60**, (2024).

23. Luukkonen, C. L. *et al. Public Supply Water Use Reanalysis for the 2000-2020 Period by HUC12, Month, and Year for the Conterminous United States (Ver. 2.0, August 2024): U.S. Geological Survey Data Release*. https://doi.org/10.5066/P9FUL880 (2023) doi:10.5066/P9FUL880.

24. Haynes, J. V. *et al. Monthly Crop Irrigation Withdrawals and Efficiencies by HUC12 Watershed for Years 2000-2020 within the Conterminous United States (Ver. 2.0, September 2024). U.S. Geological Survey Data Release.* . (2023) doi:10.5066/P9YWR0OJ.

25. Martin, D. J. *et al. Irrigation Water Use Reanalysis for the 2000-20 Period by HUC12, Month, and Year for the Conterminous United States (Ver. 2.0, September 2024): U.S. Geological Survey Data Release*. https://doi.org/10.5066/P9YWR0OJ (2023).

26. Reitz, M., Sanford, W. E. & Saxe, S. Ensemble Estimation of Historical Evapotranspiration for the Conterminous U.S. *Water Resour. Res.* **59**, (2023).

27. Warziniack, T. *et al.* Projections of Freshwater Use in the United States Under Climate Change. *Earths Future* **10**, (2022).

28. Majumdar, S. *et al.* AZ-Hydro — Historical and Projected Arizona Annual Water Use: Software, Input Data, Models, Raster and Well Package Predictions, and Validation at 2 km Resolution (1896–2099). https://doi.org/10.5281/zenodo.19057935 (2026).

29. Barlow, P. M. & Leake, S. A. *Streamflow Depletion by Wells—Understanding and Managing the Effects of Groundwater Pumping on Streamflow: U.S. Geological Survey Circular 1376*. https://pubs.usgs.gov/circ/1376/ (2012).

30. Zipper, S. C. *et al.* Rapid and Accurate Estimates of Streamflow Depletion Caused by Groundwater Pumping Using Analytical Depletion Functions. *Water Resour. Res.* **55**, 5807–5829 (2019).

31. Majumdar, S., Smith, R., Butler, J. J. & Lakshmi, V. Groundwater withdrawal prediction using integrated multitemporal remote sensing data sets and machine learning. *Water Resour. Res.* **56**, e2020WR028059 (2020).

32. Majumdar, S. *et al.* Improving crop-specific groundwater use estimation in the Mississippi Alluvial Plain: Implications for integrated remote sensing and machine learning approaches in data-scarce regions. *J. Hydrol. Reg. Stud.* **52**, 101674 (2024).

33. Majumdar, S., Smith, R. G. & Hasan, M. F. A High-Resolution Data-Driven Monthly Aquaculture and Irrigation Water Use Model in the Mississippi Alluvial Plain. in *IGARSS 2025 - 2025 IEEE International Geoscience and Remote Sensing Symposium* 2686–2691 (IEEE, 2025). doi:10.1109/IGARSS55030.2025.11243173.

34. Asfaw, D. *et al.* Predicting groundwater withdrawals using machine learning with limited metering data: Assessment of training data requirements. *Agric. Water Manag.* **318**, 109691 (2025).

35. Hasan, M. F. *et al.* Satellite data and physics-constrained machine learning for estimating effective precipitation in the Western United States and application for monitoring groundwater irrigation. *Agric. Water Manag.* **319**, 109821 (2025).

36. Ott, T. J. *et al.* Toward field-scale groundwater pumping and improved groundwater management using remote sensing and climate data. *Agric. Water Manag.* **302**, 109000 (2024).

37. Filippelli, S. K. *et al.* Remote sensing of field-scale irrigation withdrawals in the central Ogallala aquifer region. *Agric. Water Manag.* **271**, 107764 (2022).

38. Wei, S., Xu, T., Niu, G.-Y. & Zeng, R. Estimating Irrigation Water Consumption Using Machine Learning and Remote Sensing Data in Kansas High Plains. *Remote Sens.* **14**, 3004 (2022).

39. Zhang, L. *et al.* On the Use of Knowledge-Informed Machine Learning and Multisource Data for Spatially Explicit Estimation of Irrigation Water Withdrawal. *Earths Future* **13**, (2025).

40. Zhang, L., Che, T., Zhang, K., Zheng, D. & Li, X. A novel framework for pixel-wise estimation of irrigation water use by integrating remote sensing and reanalysis data. *Agric. Water Manag.* **323**, 110077 (2026).

41. Kragh, S. J., Schneider, R., Fensholt, R., Stisen, S. & Koch, J. Synthesizing regional irrigation data using machine learning – Towards global upscaling via metamodeling. *Agric. Water Manag.* **311**, 109404 (2025).

42. Gorelick, N. *et al.* Google Earth Engine: Planetary-scale geospatial analysis for everyone. *Remote Sens. Environ.* **202**, 18–27 (2017).

43. Roy, S., Majumdar, S. & Swetnam, T. A community data commons for equitable Earth Science. Preprint at https://doi.org/10.31223/X5WN4J (2026).

44. Melton, F. S. *et al.* OpenET: Filling a Critical Data Gap in Water Management for the Western United States. *JAWRA Journal of the American Water Resources Association* **58**, 971–994 (2022).

45. Volk, J. M. *et al.* Assessing the accuracy of OpenET satellite-based evapotranspiration data to support water resource and land management applications. *Nature Water* **2**, 193–205 (2024).

46. Abatzoglou, J. T. & Brown, T. J. A comparison of statistical downscaling methods suited for wildfire applications. *International Journal of Climatology* **32**, 772–780 (2012).

47. Daly, C. *et al.* Physiographically sensitive mapping of climatological temperature and precipitation across the conterminous United States. *International Journal of Climatology* **28**, 2031–2064 (2008).

48. Luo, Y. *et al.* Short-term forecasting of daily reference evapotranspiration using the Hargreaves–Samani model and temperature forecasts. *Agric. Water Manag.* **136**, 42–51 (2014).

49. Volk, J. M. *et al.* Assessing and correcting bias in gridded reference evapotranspiration over agricultural lands across the contiguous United States. *Agric. Water Manag.* **333**, 110647 (2026).

50. USDA SCS. Chapter 2 Irrigation Water Requirements. in *Part 623 National Engineering Handbook* (USDA Soil Conservation Service, 1993).

51. Muratoglu, A., Bilgen, G. K., Angin, I. & Kodal, S. Performance analyses of effective rainfall estimation methods for accurate quantification of agricultural water footprint. *Water Res.* **238**, 120011 (2023).

52. Majumdar, S. *et al.* pyCropWat: A Python Package for Computing Effective Precipitation Using Google Earth Engine Climate Data (v1.2.1). https://doi.org/10.5281/zenodo.18706481 (2026).

53. Sohl, T. L. *et al.* Modeled historical land use and land cover for the conterminous United States. *J. Land Use Sci.* **11**, 476–499 (2016).

54. USGS. Annual NLCD Collection 1 Science Products: U.S. Geological Survey data release. (2024) doi:10.5066/P94UXNTS.

55. Fleckenstein, R. *et al.* A framework for integrating spatiotemporal deep learning methods with landsat for annual land cover and impervious surface mapping. *Remote Sens. Environ.* **338**, 115347 (2026).

56. Sohl, T. L. *et al. Conterminous United States Land Cover Projections - 1992 to 2100: U.S. Geological Survey Data Release*. (2018) doi:10.5066/P95AK9HP.

57. Ketchum, D. *et al.* IrrMapper: A Machine Learning Approach for High Resolution Mapping of Irrigated Agriculture Across the Western U.S. *Remote Sens. (Basel).* **12**, 2328 (2020).

58. Ketchum, D., Hoylman, Z. H., Huntington, J., Brinkerhoff, D. & Jencso, K. G. Irrigation intensification impacts sustainability of streamflow in the Western United States. *Commun. Earth Environ.* **4**, 479 (2023).

59. Hung, F., Chiarelli, D. D., Famiglietti, J. S. & Müller, M. F. Downscaled global 60-meter resolution estimates of irrigation water sources (2000–2015). *Sci. Data* **12**, 1632 (2025).

60. Walkinshaw, M., O'Geen, A. T. & Beaudette, D. E. Soil Properties. *California Soil Resource Lab* https://casoilresource.lawr.ucdavis.edu/soil-properties/ (2022).

61. Soil Survey Staff, USDA NRCS. Web Soil Survey. https://websoilsurvey.sc.egov.usda.gov/App/HomePage.htm (2025).

62. ADWR. GIS Data and Maps. https://new.azwater.gov/gis (2021).

63. Lisk, M. D. *et al. HarDWR — Harmonized Database of Western U.S. Water Rights (v2.0). MSD-LIVE Data Repository*. https://data.msdlive.org/records/z0h32-ne023 (2024).

64. Suresh, S., Hossain, F., Mishra, V. & Hossain, N. GRAIN – a Global Registry of Agricultural Irrigation Networks. *Earth Syst. Sci. Data* **18**, 1855–1875 (2026).

65. Hodson, T. O., Hariharan, J. A., Black, S. & Horsburgh, J. S. dataretrieval (Python): a Python package for discovering and retrieving water data available from U.S. federal hydrologic web services: U.S. Geological Survey software release. https://doi.org/10.5066/P94I5TX3 (2023).

66. Gangopadhyay, S. & Pruitt, T. *West-Wide Climate Risk Assessments: Bias-Corrected and Spatially Downscaled Surface Water Projections (Technical Memorandum No. 86-68210-2011-01)*. (U.S. Bureau of Reclamation, 2011).

67. USBR. Reclamation Information Sharing Environment (RISE). https://rise-usbr.opendata.arcgis.com/ (2025).

68. Ma, Y. *et al.* High resolution US water table depth estimates reveal quantity of accessible groundwater. *Commun. Earth Environ.* **7**, 45 (2026).

69. ASCE-EWRI. *The ASCE Standardized Reference Evapotranspiration Equation*. (American Society of Civil Engineers, Reston, VA, 2005). doi:10.1061/9780784408056.

70. Morton, C. G. openet-refet-gee 0.7.1. https://pypi.org/project/openet-refet-gee/ (2025).

71. Akiba, T., Sano, S., Yanase, T., Ohta, T. & Koyama, M. Optuna. in *Proceedings of the 25th ACM SIGKDD International Conference on Knowledge Discovery & Data Mining* 2623–2631 (ACM, New York, NY, USA, 2019). doi:10.1145/3292500.3330701.

72. Chen, T. & Guestrin, C. XGBoost: A Scalable Tree Boosting System. in *Proceedings of the 22nd ACM SIGKDD International Conference on Knowledge Discovery and Data Mining* 785–794 (ACM, New York, NY, USA, 2016). doi:10.1145/2939672.2939785.

73. Attalah, S. *et al.* Evaluation and comparison of OpenET models for estimating soil water depletion of irrigated alfalfa in Arizona. *Agric. Water Manag.* **320**, 109850 (2025).

74. Allen, R. G., Pereira, L. S., Raes, D. & Smith, M. *Crop Evapotranspiration - Guidelines for Computing Crop Water Requirements - FAO Irrigation and Drainage Paper 56*. (FAO - Food and Agriculture Organization of the United Nations, Rome, Italy, 1998).

75. O'Neill, B. C. *et al.* The Scenario Model Intercomparison Project (ScenarioMIP) for CMIP6. *Geosci. Model Dev.* **9**, 3461–3482 (2016).

76. Van Vuuren, D. P. *et al.* The Scenario Model Intercomparison Project for CMIP7 (ScenarioMIP-CMIP7). *Geosci. Model Dev.* **19**, 2627–2656 (2026).

77. CAP. Central Arizona Project - CAP. https://www.cap-az.com/ (2026).

78. Autobee, R. *The Salt River Project*. https://www.usbr.gov/projects/pdf.php?id=183 (1993).

79. Salt River Project. A history of canals in Arizona. https://www.srpnet.com/about/history/canal-history (2026).

80. Pima-Maricopa Irrigation Project. *Building the Florence-Casa Grande Project Canals*. https://www.gilariver.com/lessons/sancarloslesson33.pdf (2002).

81. Bureau of Indian Affairs. About the San Carlos Irrigation Project. https://www.bia.gov/programs-services/power-utilities/scip-power/about-scip (2026).

82. Lisk, M. D. *et al.* Harmonized Database of Western U.S. Water Rights (HarDWR) v.1. *Sci. Data* **11**, 598 (2024).

83. Hastie, T., Tibshirani, R. & Friedman, J. *The Elements of Statistical Learning: Data Mining, Inference, and Prediction*. (Springer New York, New York, 2001).

84. Breiman, L. Random Forests. *Mach. Learn.* **45**, 5–32 (2001).

85. Ke, G. *et al.* LightGBM: A Highly Efficient Gradient Boosting Decision Tree. in *Advances in Neural Information Processing Systems* (eds. Guyon, I. et al.) vol. 30 (Curran Associates, Inc., 2017).

86. Geurts, P., Ernst, D. & Wehenkel, L. Extremely randomized trees. *Mach. Learn.* **63**, 3–42 (2006).

87. Pedregosa, F. *et al.* Scikit-learn: Machine Learning in Python. *Journal of Machine Learning Research* **12**, 2825–2830 (2011).

88. Friedman, J. H. Stochastic gradient boosting. *Comput. Stat. Data Anal.* **38**, 367–378 (2002).

89. Breiman, L. Bagging predictors. *Mach. Learn.* **24**, 123–140 (1996).

90. Rocklin, M. Dask: Parallel Computation with Blocked algorithms and Task Scheduling. *Proc. of the 14th Python in Science Conf* http://conference.scipy.org/proceedings/scipy2015/pdfs/matthew_rocklin.pdf (2015).

91. Molnar, C. *Interpretable Machine Learning: A Guide for Making Black Box Models Explainable*. (Leanpub, Munich, Germany, 2022).

92. Clark, S. R., Fu, G. & Janardhanan, S. Explainable AI for Interpreting Spatiotemporal Groundwater Predictions. *Water Resour. Res.* **61**, (2025).

93. Belitz, K. & Stackelberg, P. E. Evaluation of six methods for correcting bias in estimates from ensemble tree machine learning regression models. *Environmental Modelling & Software* **139**, 105006 (2021).

94. Zhang, G. & Lu, Y. Bias-corrected random forests in regression. *J. Appl. Stat.* **39**, 151–160 (2012).

95. USBR. *Colorado River Basin Ten Tribes Partnership Tribal Water Study Report. Chapter 5 – Assessment of Current Tribal Water Use and Projected Future Water Development*. https://www.usbr.gov/lc/region/programs/crbstudy/tws/chapter5.html (2018).

96. Anning, D. W. & Duet, N. R. *Summary of Ground-Water Conditions in Arizona, 1987-90: U.S. Geological Survey Open-File Report 94-476*. (1994) doi:10.3133/ofr94476.

97. USGS. Water Use in the United States. https://www.usgs.gov/mission-areas/water-resources/science/water-use-united-states#publications (2026).

98. ADWR. Annual Report 2020. https://new.azwater.gov/sites/default/files/media/Annual Report_2020_Interactive_Final.pdf (2021).

99. Condon, L. E. & Maxwell, R. M. Simulating the sensitivity of evapotranspiration and streamflow to large-scale groundwater depletion. *Sci. Adv.* **5**, (2019).

100. de Graaf, I. E. M., Gleeson, T., van Beek, L. P. H., Sutanudjaja, E. H. & Bierkens, M. F. P. Environmental flow limits to global groundwater pumping. *Nature* **574**, 90–94 (2019).

101. Yang, C., Condon, L. E. & Maxwell, R. M. Unravelling groundwater–stream connections over the continental United States. *Nature Water* **3**, 70–79 (2025).

102. Moser, T. H. Drainage by Pumped Wells in Wellton-Mohawk District. *Journal of the Irrigation and Drainage Division* **93**, 199–208 (1967).

103. Meyer, H. & Pebesma, E. Predicting into unknown space? Estimating the area of applicability of spatial prediction models. *Methods Ecol. Evol.* **12**, 1620–1633 (2021).

104. Lee, K., Lee, K., Lee, H. & Shin, J. A Simple Unified Framework for Detecting Out-of-Distribution Samples and Adversarial Attacks. in *32nd Conference on Neural Information Processing Systems (NeurIPS 2018)* (Montréal, Canada, 2018). doi:10.48550/arXiv.1807.03888.

105. Reitz, M., Sanford, W. E. & Saxe, S. W. Historical Evapotranspiration for the Conterminous U.S.: U.S. Geological Survey data release. https://doi.org/10.5066/P9EZ3VAS (2023).

106. ADWR. ADWR Developed Groundwater Models. https://www.azwater.gov/hydrology/groundwater-modeling/adwr-models (2026).

107. Harbaugh, A. W., Banta, E. R., Hill, M. C. & McDonald, M. G. *MODFLOW-2005, the U.S. Geological Survey Modular Ground-Water Model -- the Ground-Water Flow*

Process: U.S. Geological Survey Techniques and Methods 6-A16. (2005) doi:10.3133/tm6A16.

108. Hughes, J. D., Langevin, C. D. & Banta, E. R. *Documentation for the MODFLOW 6 Framework*. (2017) doi:10.3133/tm6A57.

109. Hughes, J. D., Leake, S. A., Galloway, D. L. & White, J. T. *Documentation for the Skeletal Storage, Compaction, and Subsidence (CSUB) Package of MODFLOW 6*. (2022) doi:10.3133/tm6A62.

110. Lewis, R. & Sankey, T. ECOSTRESS Evapotranspiration Estimates Across Temporal and Spatial Scales in Arid and Semi-Arid Southern Arizona, USA. *J. Geophys. Res. Biogeosci.* **130** (2025).

111. Kim, Y. *et al.* Thermodynamically constrained surface energy balance using medium-resolution remote sensing for efficient evapotranspiration mapping. *Remote Sens. Environ.* **344**, 115510 (2026).

112. Frisvold, G., Sanchez, C., Gollehon, N., Megdal, S. & Brown, P. Evaluating Gravity-Flow Irrigation with Lessons from Yuma, Arizona, USA. *Sustainability* **10**, 1548 (2018).

113. Hausfather, Z., Marvel, K., Schmidt, G. A., Nielsen-Gammon, J. W. & Zelinka, M. Climate simulations: recognize the 'hot model' problem. *Nature* **605**, 26–29 (2022).

114. Grafton, R. Q. *et al.* The paradox of irrigation efficiency. *Science (1979).* **361**, 748–750 (2018).

115. ADWR. *Arizona Department of Water Resources (ADWR) 2025 - 2029 Strategic Plan*. https://www.azwater.gov/sites/default/files/2025-07/Fiscal%20Year%202026%20Strategic%20Plan.pdf (2025).

Author Contributions

S.M.: Conceptualization, funding acquisition, methodology, investigation, software, data curation, formal analysis, visualization, validation, writing (original draft). **R.G.S.**: Conceptualization, methodology, supervision, funding acquisition, writing (review and editing). **P.R.**: Data curation, methodology, writing (review and editing), funding acquisition. **M.F.H.**: Data curation, writing (review and editing). **C.W., D.E.T., L.M.**: Data curation, writing (review and editing), funding acquisition.

Competing Interests

The authors declare no competing interests.

Acknowledgements

We thank the open-source software and data communities, the OpenET consortium, and the Arizona Department of Water Resources for making their resources and datasets publicly

available, and Google Earth Engine for compute and storage support. S.M. and P.R. acknowledge Dr. Justin L. Huntington, Christopher Pearson, Charles G. Morton, Blake A. Minor, Thomas J. Ott, Dr. Samapriya Roy at the Desert Research Institute, and Dr. David Ketchum at the University of Montana for their contributions to related projects that informed this work. We also thank Rahel Pommerenke at Colorado State University for presenting initial results from this work at the 2025 ESA Living Planet Symposium. Portions of the codebase were developed with the assistance of Anthropic's Claude Opus 4.8/5/5.5, an AI-based coding assistant, used for code generation and refactoring, code review, and documentation; all AI-generated code was reviewed, tested, and validated by the authors, and the scientific methodology, research design, data interpretation, and manuscript writing remain entirely the responsibility of the authors. The views expressed herein are those of the authors and do not necessarily reflect those of the funding agencies.

Funding

This work was supported by NASA (Grant numbers 80NSSC21K0979, 80NSSC23K1453, and 80NSSC26K0983) and the U.S. Army Corps of Engineers (Grant number W912HZ25C0016).

Supplementary Information

Historical and projected freshwater withdrawals and irrigation consumptive use for Arizona, 1896–2099

Sayantan Majumdar[1], Ryan G. Smith[2], Peter ReVelle[1], Md Fahim Hasan[2], Collin Wogenstahl[3, †], Danielle E. Tadych[3], Laney Meeker[3]

1. Division of Hydrologic Sciences, Desert Research Institute, Reno, Nevada, USA
2. Department of Civil and Environmental Engineering, Colorado State University, Fort Collins, Colorado, USA
3. Arizona Department of Water Resources, Phoenix, Arizona, USA

[†] Formerly at Arizona Department of Water Resources

Corresponding author: sayantan.majumdar@dri.edu

This Supplementary Information specifies the parameters of the groundwater/surface-water (GW/SW) partition, of the pre-1980 well-infill reconstruction, and of the canal delivery start dates summarized in Methods. Every parameter below is a module-level constant in azhydro/hydrolibs/partitionops.py (azhydro/hydrolibs/streamflowops.py for the canal dates) in the archived code release[1], and the constant names given here are the identifiers used there, so each value can be located and altered directly. Values are those used to generate all published rasters. Supplementary Figs. S1–S10 map the trend, uncertainty, out-of-distribution, use-type, and CAP scenario products referred to in the main text.

Supplementary Note 1. Era-mapped groundwater weight

The density-ratio expression $GW_{share} = (GW_w \times wd) / (GW_w \times wd + \sigma_{swd})$ has one free parameter, the groundwater weight GW_w. It is mapped to the prediction year as a step function with a single linear ramp (Table S1).

The 1985–1989 segment is the *era ramp* referred to in Methods. Across those five years GW_w interpolates linearly from the GMA-transition value (2.0) to the early-CAP value (0.1), so that the arrival of CAP surface water enters the partition as a gradual transition rather than as a step at a single year.

Table S1. Era-mapped groundwater weight GW_w.

Years	GW_w	Constant
1896–1949	10.0	GW_WEIGHT_PRE_1945, GW_WEIGHT_1930_1935, GW_WEIGHT_1945_1970
1950–1965	30.0	GW_WEIGHT_PEAK_HIGH
1966–1970	10.0	GW_WEIGHT_1945_1970
1971–1979	15.0	GW_WEIGHT_PEAK
1980	10.0	GW_WEIGHT_1945_1970
1981–1984	2.0	GW_WEIGHT_PRE_GMA
1985–1989	2.0 → 0.1, linear	era ramp
1990–1997	0.1	GW_WEIGHT_EARLY_CAP
1998–2007	0.4	GW_WEIGHT_MID_CAP
2008–2099	0.2	GW_WEIGHT_POST_CAP

Supplementary Note 2. Per-basin caps and floors

The density ratio over-attributes groundwater at basins whose surface water arrives by routes that bypass the ADWR Well Registry[2], and under-attributes it at canal-served management areas that retain substantial groundwater pumping inside the canal service area. Caps bound GW_{share} from above at the first group and floors bound it from below at the second. Caps are given in Table 4 of the main text. Floors are given in Table S2.

Both are enforced twice: on the raw density-ratio shares, and again on the final per-pixel irrigation and non-irrigation shares after the post-1985 surface-water delivery routing.

Table S2. Per-basin GW-share floors. Total floors apply across 1896–2099; the irrigation and non-irrigation floors apply from the basin's CAP arrival year onward. Constants: BASIN_GW_FLOOR, BASIN_IRR_GW_FLOOR_POST_CAP, BASIN_NI_GW_FLOOR_POST_CAP.

Basin	Total GW floor	Irrigation GW floor	Non-irrigation GW floor
Phoenix AMA	0.20	0.30	0.10
Pinal AMA	0.30	0.30	0.10
Tucson AMA	0.30	0.40	0.10
Harquahala INA	0.30	0.40	0.15
Prescott AMA	0.64	—	—

Basin	Total GW floor	Irrigation GW floor	Non-irrigation GW floor
Ranegras Plain	0.95	—	—

The Prescott AMA floor of 0.64 is the ADWR-reported total groundwater share for that basin, which is dominated by municipal rather than agricultural pumping. The Ranegras Plain floor of 0.95 reflects a basin that ADWR documents as essentially all groundwater; its apparent canal coverage is the CAP pass-through pipeline serving the three central-county AMAs rather than local delivery, and the 5 % slack accommodates incidental seepage recharge from that pipeline.

At CAP-served management areas two dynamic controls modify these static values. The non-irrigation GW share carries a per-basin, per-year upper bound driven by the observed CAP delivery[3] in that year relative to the basin's 2000–2009 baseline, and the irrigation GW floor rises above its static value as CAP delivery falls, to a maximum of 0.70. A basin is treated as CAP-served from the first year in which its delivery exceeds 5 % of that baseline (CAP_BASIN_NI_PEAK_SW_FRACTION, CAP_BASIN_IRR_FLOOR_MAX_DEFAULT, CAP_BASIN_NI_BASELINE_PERIOD, CAP_BASIN_FIRST_DELIVERY_THRESHOLD).

Supplementary Note 3. Pre-1980 well-infill reconstruction

The ADWR Well Registry records wells that were still registered in 2024. Wells drilled and abandoned before registration became mandatory under the 1980 Groundwater Management Act are largely absent, so the well-density predictor under-represents the 1938–1980 agricultural drilling era. Because well density enters both the model and the GW/SW partition, that absence propagates into the hindcast as an under-prediction of groundwater pumping.

A well-infill reconstruction addresses this by raising the effective well density at pixels that the land-use record identifies as agricultural or urban in the year concerned but that carry few or no registered wells. It is summarized in Methods as the peak-year well-density infill. It runs along two paths, one applied to the model's well-density feature and one to the per-category well densities used in the partition, so that the model and the partition see the same reconstructed infrastructure. Both combine by maximum or by fill rather than by addition, so the reconstruction raises sparse pixels toward a plausible floor and never inflates a pixel that already carries a dense registered well field.

Model-feature path. The effective well density at each pixel is the maximum of three quantities: the registry count for that year; the 2024 registry snapshot scaled by a year factor that reaches 1 at the 1951–1955 and 1970–1980 drilling peaks; and a phantom density

$$\text{phantom_wd} = \text{AGRI} \times M \times k(\text{year}) \times g(\text{year}) \times c(\text{year})$$

where AGRI is the Gaussian-smoothed agricultural density in [0, 1], M = PHANTOM_M_TOTAL = 12.0 is the maximum phantom density in wells per 2 km pixel, k(year) is the temporal strength defined below, g(year) is a binary gate equal to 1 where AGRI meets that year's activation threshold, and c(year) is the canal-served fraction. Pixels that remain at zero but carry cropland or urban signal are then filled with the basin median of the 2024 snapshot, scaled by an infill factor rising from 0.10 at 1938 to 1.0 from 1955 onward.

Partition path. The per-category well densities (total, irrigation, non-irrigation) receive an equivalent reconstruction. Pixels with no registered wells draw a value at random from the distribution of 2024 registered well densities within the same groundwater basin; pixels that carry land-use signal but remain marginal receive the basin median, which represents a typical active well pixel rather than the heaviest. Both are scaled by the same infill factor. The draw uses a deterministic seed derived from the year, the basin and the category, so the reconstruction is reproducible bit for bit across runs: it is stochastic in construction but not in outcome.

The three year-dependent terms are shared by both paths.

Temporal strength *k*(year). Zero before 1938, because the earliest available land-cover classification is the 1938 snapshot[4]; a linear increase from 1938 to 1955 mirroring the growth of agricultural well drilling; a plateau from 1955 to 1980; and a linear decrease from 1980 to 1985 as mandatory registration absorbs the previously unregistered stock. The plateau is interrupted by a V-shaped trough that falls to 0.20 of the plateau value between 1957 and 1960 and recovers by 1965, representing the documented drought-recovery retreat of that period[5].

Activation threshold *g*(year). A pixel becomes eligible when its AGRI exceeds a year-dependent threshold: 0.60 in 1938, declining to 0.40 by 1951, dropping to 0.08 at the 1955 drilling peak, and recovering to 0.30 from 1960 onward. The threshold is lowest at the peak so that eligibility is widest in the years when unregistered drilling was most intense.

Canal-served fraction *c*(year). Pixels within the canal network receive only a fraction of full strength, since surface-water delivery reduces the incentive to drill. That fraction rises to 0.30 at the 1955 boom peak and to a maximum of 0.60 by 1975. Pixels outside the canal network take a value of 1.

Table S3. Well-infill reconstruction constants.

Component	Constant	Value
Temporal strength	PHANTOM_K_RAMP_UP_START	1938
	PHANTOM_K_RAMP_UP_END	1955
	PHANTOM_K_PLATEAU_END	1980
	PHANTOM_K_RAMP_END	1985
Drought trough	PHANTOM_DROUGHT_DIP_START	1957
	PHANTOM_DROUGHT_DIP_MIN_YEAR	1960
	PHANTOM_DROUGHT_DIP_END	1965
	PHANTOM_DROUGHT_DIP_MIN	0.20
Activation threshold	PHANTOM_AGRI_THRESHOLD_EARLY	0.60
	PHANTOM_AGRI_THRESHOLD_MID	0.40
	PHANTOM_AGRI_THRESHOLD_PEAK	0.08
	PHANTOM_AGRI_THRESHOLD_LATE	0.30
	PHANTOM_AGRI_BOOM_START	1951
	PHANTOM_LULC_THRESHOLD	0.20

Component	Constant	Value
Canal-served fraction	PHANTOM_CANAL_BOOM_START	1951
	PHANTOM_CANAL_BOOM_PEAK_YEAR	1955
	PHANTOM_CANAL_BOOM_PEAK	0.30
	PHANTOM_CANAL_RAMP_END	1975
	PHANTOM_CANAL_INCLUDE_MAX	0.60
Infill scale	PHANTOM_INFILL_START	1938
	PHANTOM_INFILL_END	1983
	PHANTOM_INFILL_SCALE_MIN	0.10
	PHANTOM_INFILL_SCALE_RAMP_END	1955
Magnitude	PHANTOM_M_TOTAL	12.0 wells per 2 km pixel

Because the reconstruction is a parameterized reconstruction of records that no longer exist, it is not independently verifiable at the pixel scale. Its statewide effect is calibrated against the USGS Open-File Report 94-476[6] and USGS Circular groundwater markers[7], and it recovers approximately 1,230 Mm^3 (1 MAF) of the otherwise under-predicted peak-era pumping. The σ_{GW} uncertainty component and the out-of-distribution detector both flag the hindcast years in which it is most influential.

Supplementary Note 4. Additional partition constraints and definitions

Methods (Additional partition constraints) summarizes seven rules that handle cases in which the density ratio fails. They are specified here; the terms they use are defined after the list.

(1) Dual canal-infrastructure gate. Basins whose canal coverage is below 1 % of pixels, or whose mean canal-weighted streamflow is ≤ 0, have $Irrigation_{SW}$ reassigned to $Irrigation_{GW}$ and $Non\text{-}Irrigation_{SW}$ to $Non\text{-}Irrigation_{GW}$. This removes spurious surface water at groundwater-only basins such as Willcox, Douglas, and Joseph City, where Gaussian smoothing would otherwise carry a surface-water signal across the boundary from a neighboring canal-served basin.

(2) Whitelists. Colorado-River-direct basins (Parker, Yuma, Lake Mohave, Lake Havasu, Meadview, Detrital Valley) bypass the canal gate, because their riverside diversions do not register as canal pixels. A separate preserve list (Little Colorado River Plateau, Sacramento Valley, Big Sandy, Bill Williams) retains $Non\text{-}Irrigation_{SW}$ at basins with direct lake or river municipal intakes (e.g., Page on Lake Powell, Bullhead City).

(3) Surface-water residual routing. From 1960 onward, the residual between the predicted and partitioned totals is routed to $Irrigation_{SW}$ at canal-served agricultural pixels (Residual routing, below). This lets the post-CAP era reach the USGS-reported $Irrigation_{SW}$ magnitudes[7] (~3,700 Mm^3, or ~3 MAF) without inflating $Irrigation_{GW}$ or $Non\text{-}Irrigation_{SW}$.

(4) Pre-1948 surface-water gate. Before large-scale canal build-out, surface-water shares are restricted to canal and surface-water-rights pixels, consistent with the USGS account that pre-CAP pumping outside the SRP and Yuma areas was almost entirely groundwater[6,7].

(5) Peak-year well-density infill. The well reconstruction of Supplementary Note 3 raises the effective well density at agricultural or urban pixels that carry few or no registered wells, recovering ~1,230 Mm^3 (~1 MAF) of peak-era pumping. In the same peak years, a cropland-proximity dilation reclassifies crop-edge pixels (AGRI > 0.10) as cropped, which recovers expansion-era acreage that the historical USGS LULC[4] appears to underestimate.

(6) Cropland-proximity gate (1986 onward). Pixels with zero crop fraction but AGRI > 0.10, i.e., near mapped cropland, are reclassified from desert to cropped, recovering small or scattered irrigated fields in rural basins (e.g., Willcox, Harquahala, Douglas).

(7) Basin-class modifiers. From 1986 onward the land-use partition override (below) sets the irrigation/non-irrigation split from the cropland and urban fractions everywhere except Phoenix and Tucson AMAs, which keep the default pump-capacity split because most non-agricultural pumping in those metropolitan areas is municipal and industrial. Canal-heavy basins (Lake Havasu, Yuma, Parker, Harquahala, Gila Bend, Hualapai Valley, Prescott, Pinal) receive a crop-fraction floor of 0.3 on post-2010 $\text{Non-Irrigation}_{SW}$ residual routing, while canal-light basins keep strict crop-fraction weighting.

The partition terms used above and in Methods are defined as follows.

Era ramp. The linear interpolation of the groundwater weight across 1985–1989 (Supplementary Note 1). No other partition parameter is ramped between eras.

Residual routing, or excess routing. The partitioned category volumes do not in general sum to the model-predicted total, because the urban-scaling step reduces the non-irrigation share at rural pixels. The residual is the difference between the predicted total and the partitioned total. From 1960 onward it is recovered at canal-served agricultural pixels and routed to irrigation surface water, which allows the post-CAP era to reach the USGS-reported irrigation surface-water magnitudes without inflating irrigation groundwater or non-irrigation surface water. At canal-heavy basins the routed volume is subject to a crop-fraction floor of 0.3 from 2010 onward; at canal-light basins it is weighted strictly by crop fraction, which suppresses routing at desert pixels.

Land-use partition override. From 1986 onward, pixels are classified by cropland fraction *cf* and urban fraction *uf* into four classes — cropland only, mixed land use, urban only, and desert — and the irrigation/non-irrigation split follows the class rather than the default split by pump-capacity fraction. A pixel is treated as mixed rather than cropland-only when *uf* exceeds 0.30 (URBAN_HIGH_THRESHOLD). The override is applied everywhere **except** Phoenix and Tucson AMAs (URBAN_AMA_BASINS), which retain the default split because their metropolitan footprints mean that most non-agricultural pumping is genuinely municipal and industrial. The eight remaining management areas are treated the same as unmanaged areas, which corrects an under-attribution of irrigation share in agricultural basins.

Well-density carry-forward. Registry installation dates end in 2024, so projection years carry the 2024 well field forward. A separate set of constants governs how the 2024 field is applied to hindcast years, including a ramp-down across 1995–2005 and a residual tail of 0.2 (WD_2024_*).

Supplementary Note 5. Complete parameter listing

The partition is governed by a larger set of constants than can usefully be tabulated here. All of them are module-level constants in azhydro/hydrolibs/partitionops.py, grouped by function and commented with the evidence used to set them. The archived code release contains the exact file used to generate every raster, so the complete parameter set is recoverable from the archive and each value can be traced to the outputs it produced.

Supplementary Note 6. Canal delivery start dates

Each GRAIN[8] canal segment enters the canal-density raster from its first delivery year, which is assigned in three steps. (1) If the segment belongs to a named canal system with a documented start date, that date is used (Table S4). (2) Otherwise, the priority year of the nearest HarDWR[9,10] surface-water point of diversion within 20 km is used, taken across all right types so that basins without irrigation points of diversion still receive a date. (3) Failing both, the earliest surface-water-right priority year in the same groundwater basin is used.

Step (2) assumes that a segment was built at about the time of the nearest surface-water right. Over many segments this gives a reasonable picture of how the network grew, but an individual segment can be dated too early, because a canal can exist before deliveries under its current operator begin. The CAP canal crossed Tucson AMA in 1985, for example, but Tucson received its first CAP deliveries in 1990[3]. A lower bound is therefore applied at five basins (Table S4): any segment dated before the basin's first delivery year is moved to that year, and segments already at or after it keep their date. All other basins, including Parker, Yuma, and Safford, keep their assigned dates, because their diversions from local rivers predate any basin-level delivery program. The values are the constants CANAL_FIRST_DELIVERY and BASIN_DELIVERY_START in azhydro/hydrolibs/streamflowops.py, and the sources for the basin start years and the major canal systems are cited in Table S4.

Table S4. Canal delivery start years. Named canal systems take their documented first delivery year; the basin lower bounds advance earlier segment dates within those basins.

Canal system or basin	First delivery year	Notes
Named canal systems		
SRP canals (Arizona, South, Grand, Western, Eastern, Consolidated, Highline, Crosscut)	1868	Salt River Valley canals, dug from 1868 after a canal company formed in December 1867[11,12]
Gila Bend Canal	1887	
Buckeye Canal	1888	Buckeye Canal Co.
Roosevelt Canal	1911	Roosevelt Dam
Yuma Project (Yuma Main, North Gila, South Gila)	1912	
Florence–Casa Grande system	1924	San Carlos Irrigation Project[13,14]

Pima Lateral	1928	San Carlos Irrigation Project extension[14]
Gila Gravity Main Canal	1943	USBR Gila Project
Wellton-Mohawk system (incl. Dome and Thacker laterals)	1952	USBR
Central Arizona Project (Hayden-Rhodes Aqueduct, Buckskin Tunnel)	1985	First CAP deliveries[3]
Santa Rosa Canal	1987	
Basin lower bounds		
Phoenix AMA	1868	Salt River Valley canals dug from 1868, later SRP[11,12]
Pinal AMA	1924	Florence–Casa Grande expansion and San Carlos Irrigation Project deliveries[13,14]
Harquahala INA	1985	First CAP deliveries[3]
Ranegras Plain	1989	First CAP deliveries[3]
Tucson AMA	1990	First CAP deliveries[3]

Supplementary Note 7. CAP groundwater boost beyond the observed shortage tiers

The central CAP delivery perturbation (Methods, CAP delivery perturbation) has two parts at CAP-service-area pixels: a delivery factor on the surface-water term and a groundwater boost on well density. Only Tier 0, Tier 1 and Tier 2a occurred in 2020–2026, and the boosts for those tiers were calibrated against the groundwater substitution seen in the 2022–2024 ADWR and USGS aggregates[7,15] (21–38 % of the cut volume). No observation constrains the boost for the deeper 760 kAF yr^{-1} cut of the 2027–2028 Operating Guidelines[16], which the central projection holds from 2027 to 2099.

The boost was therefore chosen so that the statewide groundwater substitution share stays within the range the calibrated settings reproduce for the observed years. The share is the additional groundwater withdrawal relative to a partition with no CAP cut, divided by the cut volume, computed from the central partition for each year and setting in Table S5.

Table S5. Statewide groundwater substitution share under the central CAP perturbation. ΔGW is the additional groundwater withdrawal relative to a partition with no CAP cut. Constants: CAP_DELIVERY_FACTORS, CAP_CUT_GW_BOOST_FACTORS.

Year and condition	Delivery factor / GW boost	ΔGW (kAF)	Share of cut volume (%)
2022, Tier 1 (512 kAF)	0.66 / 5.0	116	22.7

2023, Tier 2a (592 kAF)	0.61 / 7.5	173	29.2
2024, Tier 1 (512 kAF)	0.66 / 5.0	193	37.7
2027, Operating Guidelines (760 kAF)	0.49 / 5.0	247	32.5
2027, Operating Guidelines (760 kAF), adopted	0.49 / 7.5	290	38.1
2027, Operating Guidelines (760 kAF)	0.49 / 10.0	321	42.2

A boost of 7.5, the value calibrated for Tier 2a, keeps the first projection year at the top of the observed range (38.1 % against a 2022–2024 maximum of 37.7 %) and was adopted; a boost of 10 would exceed it. Under every setting the share rises later in the century (under the Tier 1 settings, from 33.9 % in 2027 to 57.9 % in 2099), because projected withdrawal grows while the cut is applied to the surface-water term as a fraction rather than as a fixed volume.

Supplementary Figures

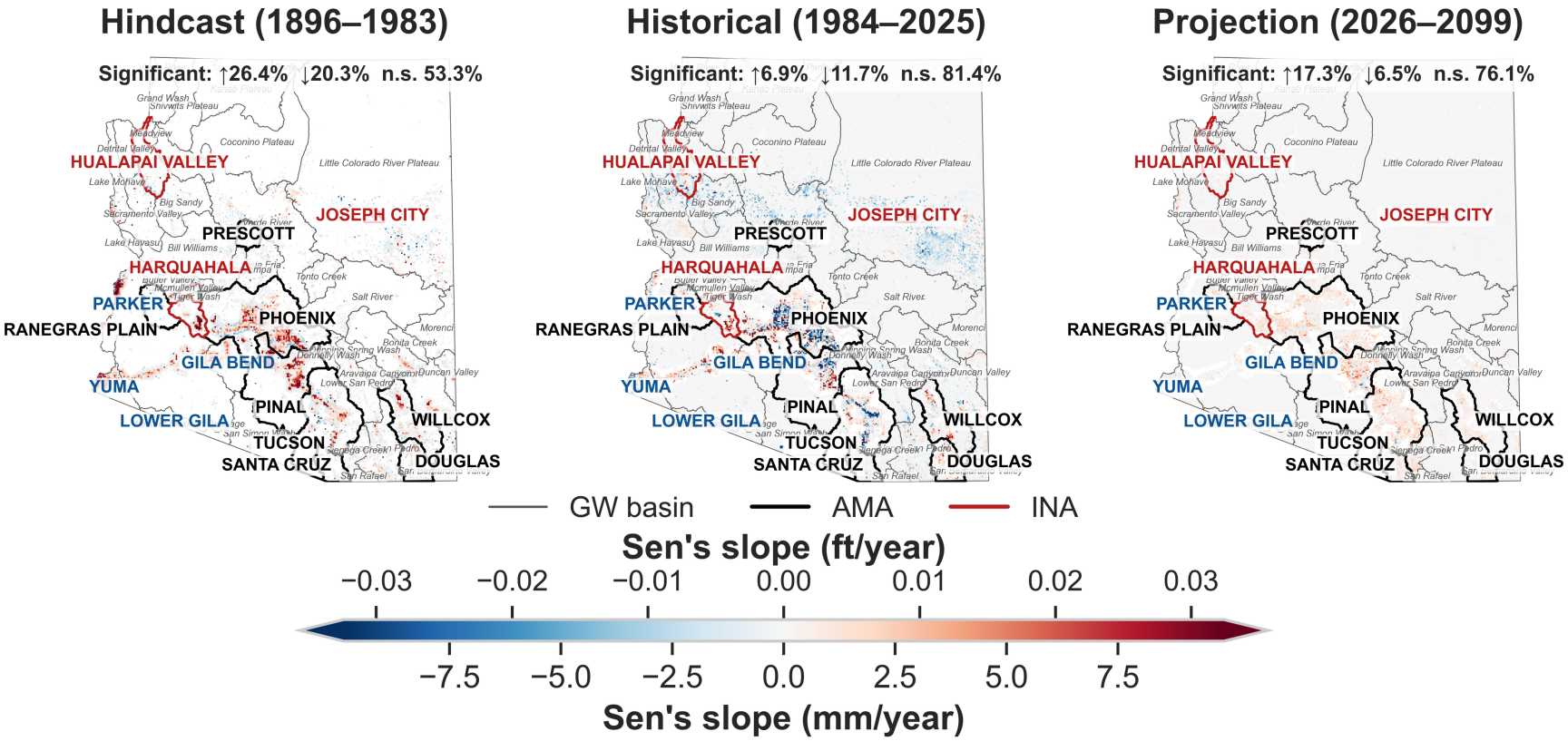


Fig. S1. Sen's-slope trend in annual total withdrawal depth for the hindcast (1896–1983), historical (1984–2025), and projection (2026–2099) eras (left to right). Stippled pixels are not significant under the Mann-Kendall test (α = 0.05), and the shares of pixels with significant increasing, significant decreasing, and non-significant trends are given above each map. Trend maps for the other withdrawal, CU, and capture categories, for the full 1896–2099 window, and at basin scale are in the Zenodo repository[1].

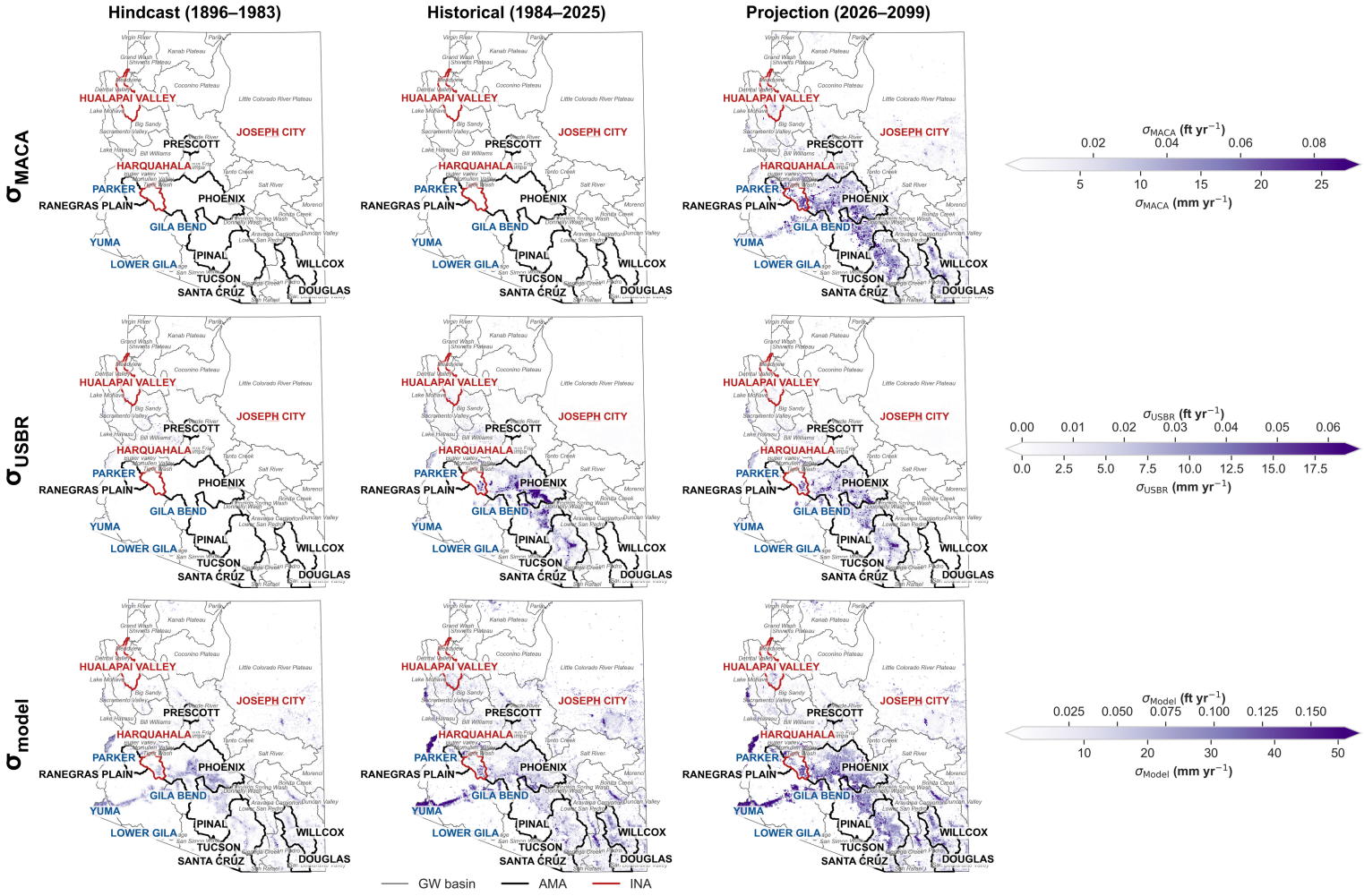


Fig. S2. Era-mean climate and model uncertainty components of annual total withdrawal depth, one per row: σ_{MACA} (top; downscaled-GCM spread, zero before 2026), σ_{USBR} (middle; Upper Colorado River streamflow spread, zero before 1950 and at CAP service-area pixels before 1985), and σ_{model} (bottom; ten-seed XGBRF ensemble), with the hindcast (1896–1983), historical (1984–2025), and projection (2026–2099) eras as columns. Each component has its own color scale (mm yr^{-1}, bottom; ft yr^{-1}, top). The components are defined in Methods, Uncertainty quantification.

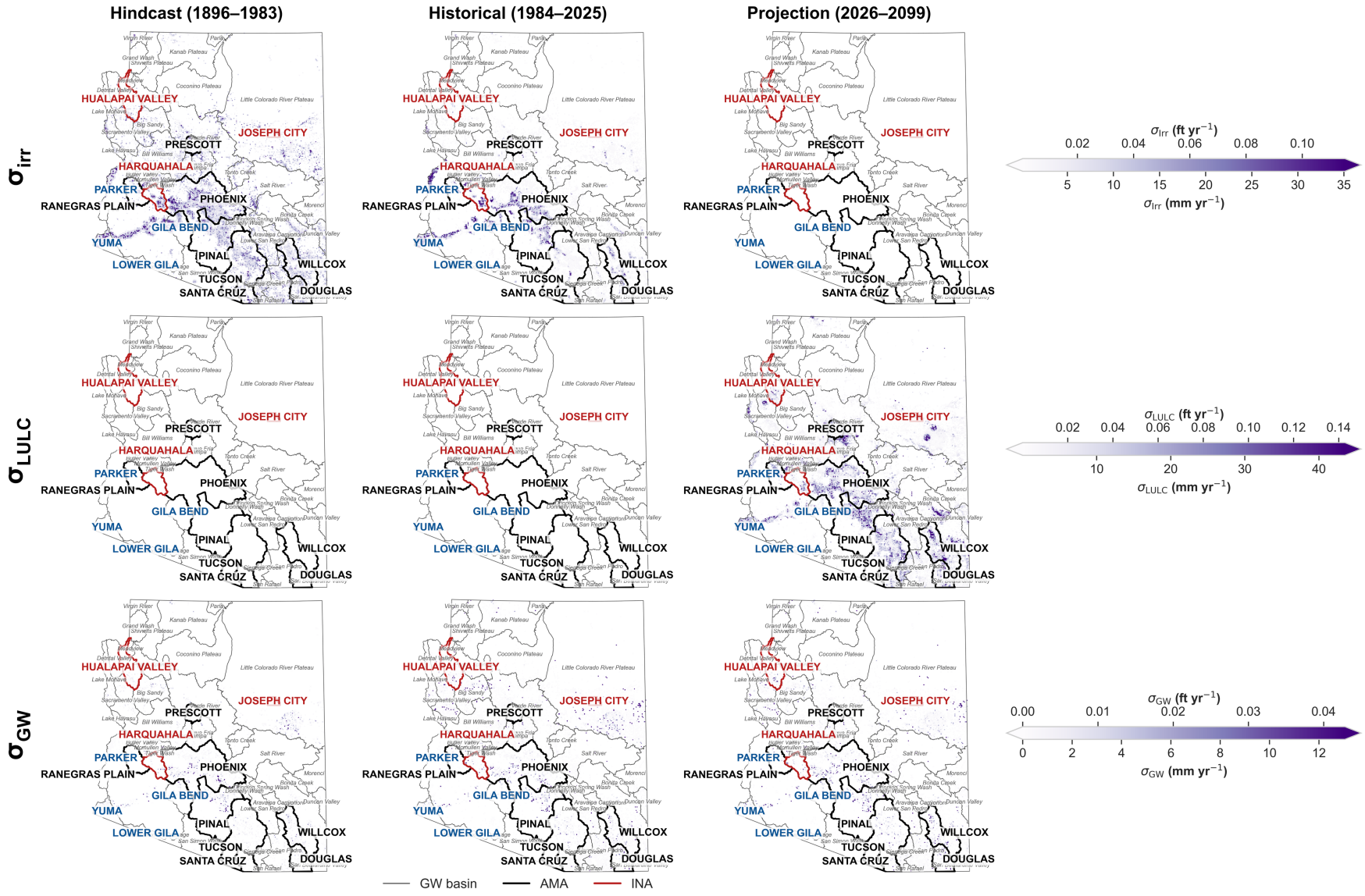


Fig. S3. As Fig. S2, for the management components: σ_{irr} (top; irrigated-area input, zero after 2025), σ_{LULC} (middle; land-use scenario spread, zero before 2026), and σ_{GW} (bottom; well-density input).

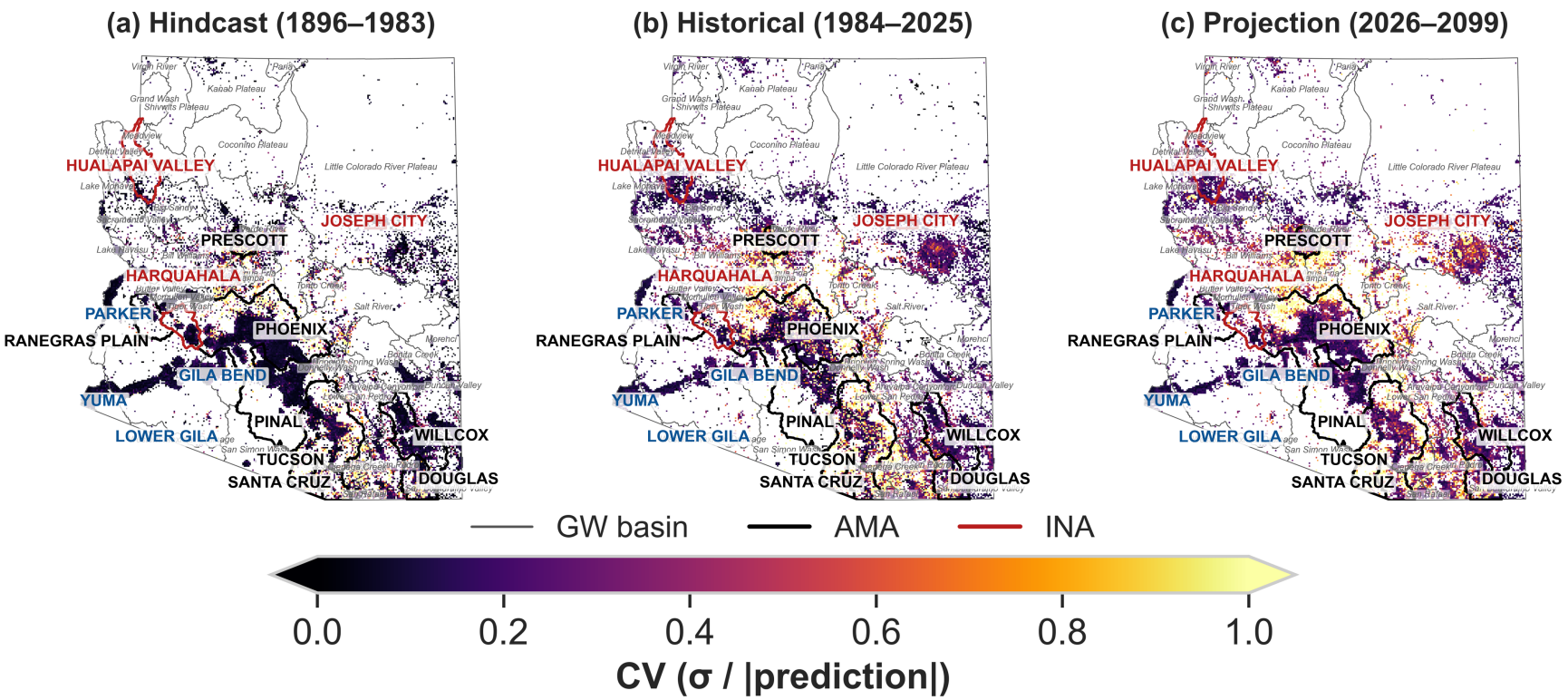


Fig. S4. Era-mean coefficient of variation (CV = σ_{total} / |prediction|) of annual total withdrawal for the (a) hindcast, (b) historical, and (c) projection eras. The color scale is capped at 1. The signal-to-noise ratio (SNR = 1/CV) is band 4 of every published raster[1].

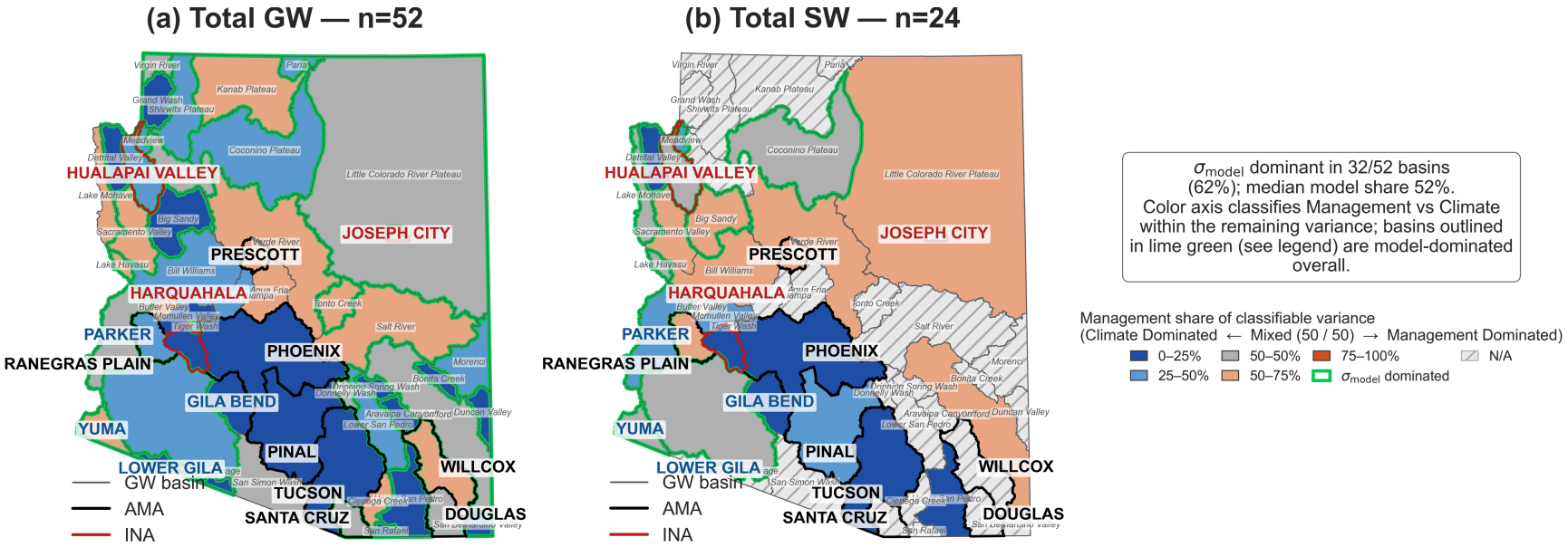


Fig. S5. Per-basin σ attribution of (a) total groundwater and (b) total surface-water withdrawal for the projection era (2026–2099), the withdrawal counterpart of the consumptive-use attribution in main-text Fig 3. Each basin is shaded by the management share of its management-plus-climate variance; basins where σ_{model} exceeds both classes are outlined in lime green, and hatched basins are not classified. Panel titles give the number of classified basins. The hindcast and historical maps and the per-year attribution series are in the Zenodo repository[1].

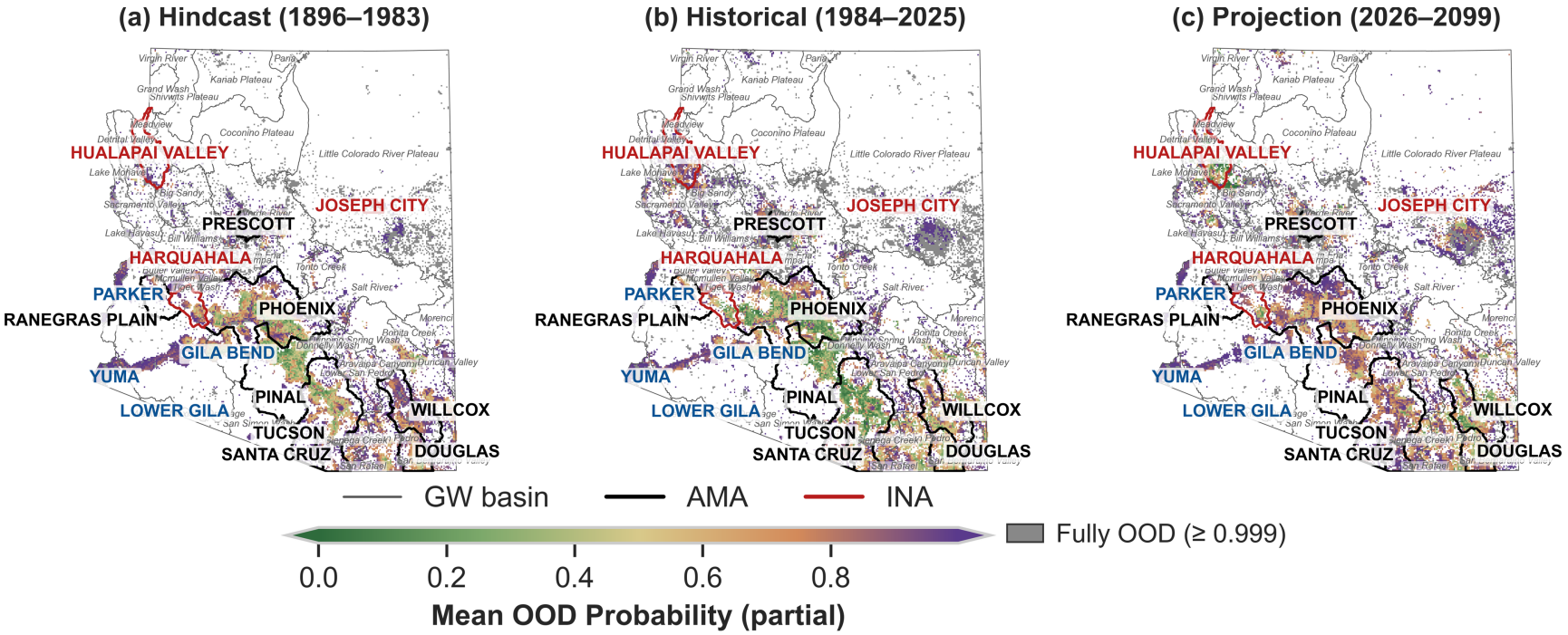


Fig. S6. Era-mean out-of-distribution (OOD) probability for the (a) hindcast, (b) historical, and (c) projection eras. The probability is the $\chi^2(17)$ cumulative distribution of the squared Mahalanobis distance between a pixel's climate and land-use predictors and those of the training data (Methods, Out-of-distribution detection): 0 means in-distribution and values near 1 mean strong extrapolation. Gray pixels have an era-mean probability of at least 0.999.

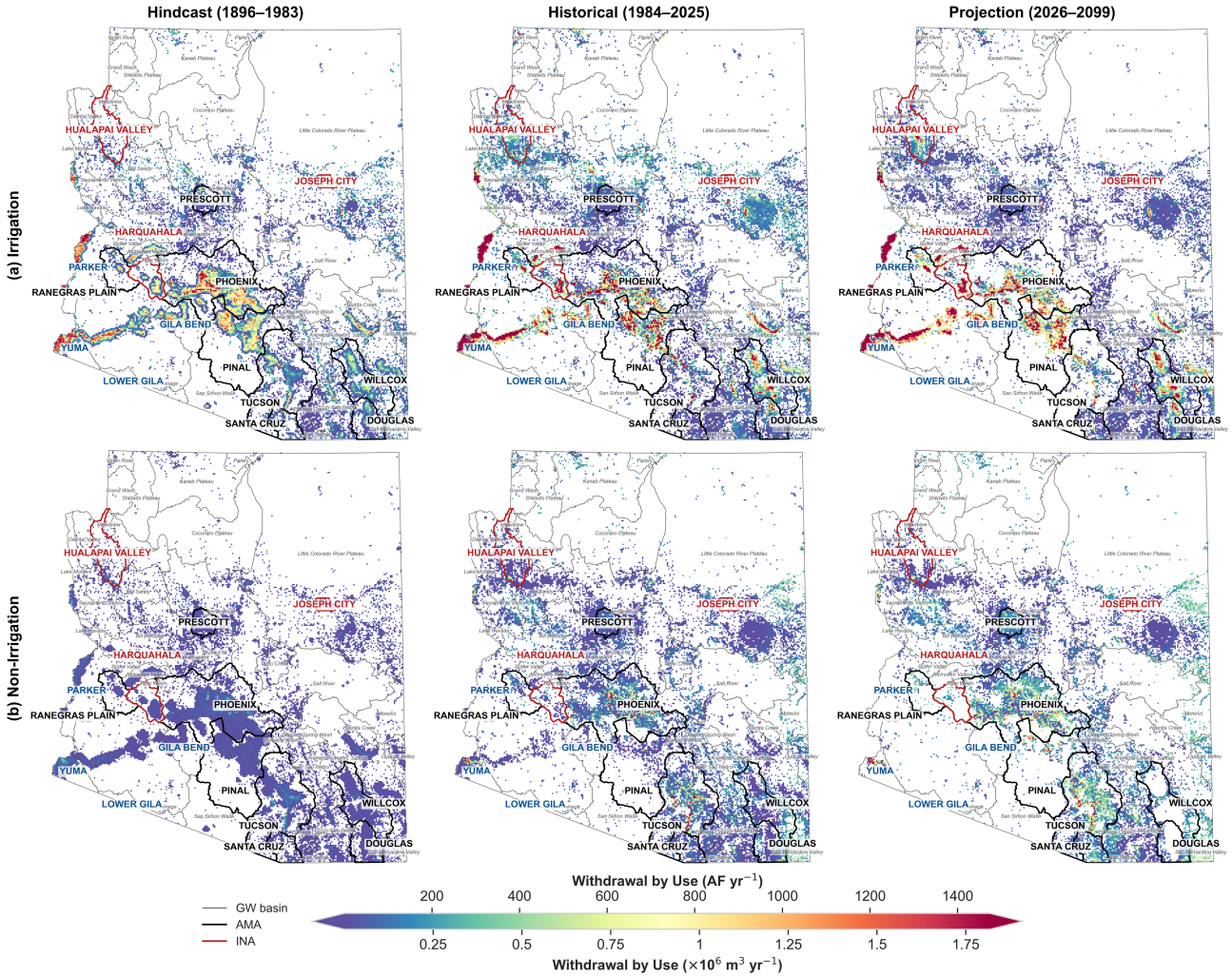


Fig. S7. Era-mean annual withdrawal volumes by use: (a) irrigation (top row) and (b) non-irrigation (bottom row), with the hindcast (1896–1983), historical (1984–2025), and projection (2026–2099) eras as columns, on a shared color scale (×10^6 m^3 yr^{-1}, bottom; AF yr^{-1}, top). Maps of the groundwater and surface-water parts of each use are in the Zenodo repository[1].

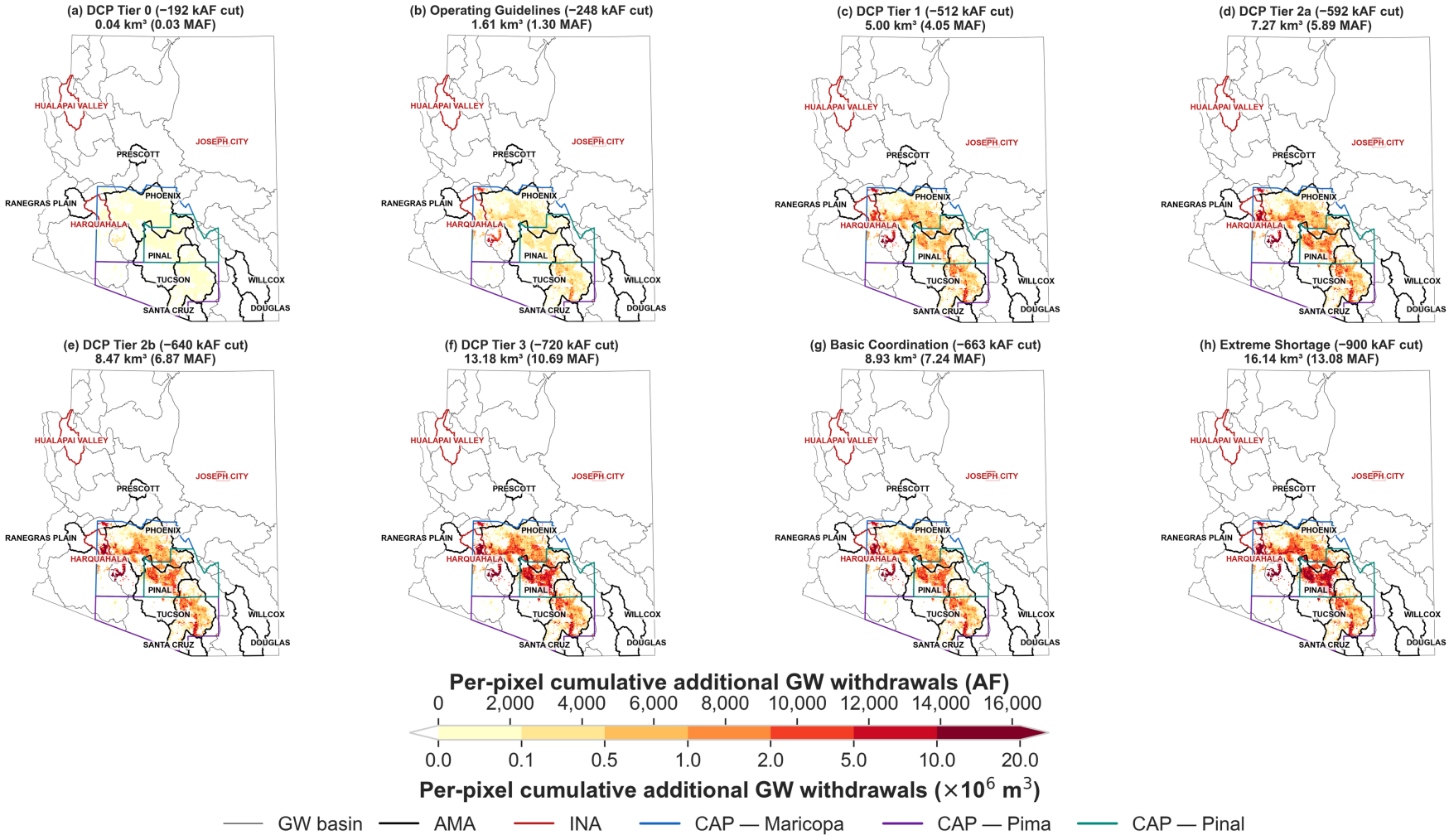


Fig. S8. Per-pixel cumulative additional annual GW pumping (ΔGW, AF per pixel) over 2027–2060 for the eight CAP shortage scenarios: (a) DCP Tier 0, (b) 2027–2028 Operating Guidelines[16], (c)–(f) DCP Tiers 1, 2a, 2b, and 3, (g) WestWater Basic Coordination, and (h) WestWater Extreme Shortage. Panel titles give each scenario's cut from the 900 kAF baseline delivery and the statewide total; the baseline, the cuts, and the pro-rata pixel distribution are as described for main-text Fig 5 and Table 12, which shows the 2027–2099 maps.

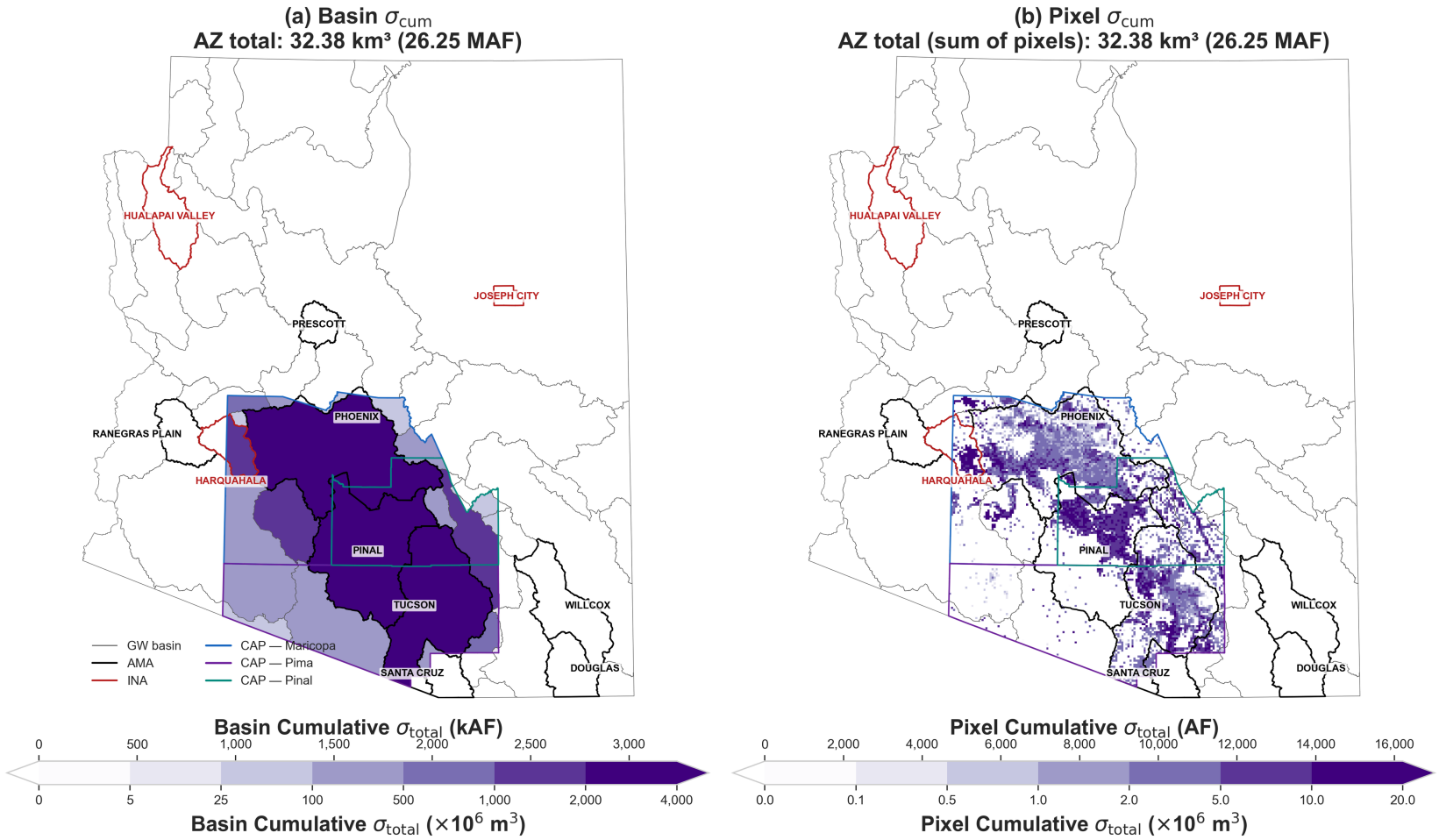


Fig. S9. Cumulative σ_{total} of groundwater withdrawal over the CAP service area, 2027–2099, (a) by basin and (b) by pixel. The CAP scenarios have no uncertainty ensemble of their own, so this central-run σ_{total} of TotalGW, restricted to CAP-service-area pixels and summed over the window, applies to every scenario (32.38 km^3, or 26.25 MAF, statewide).

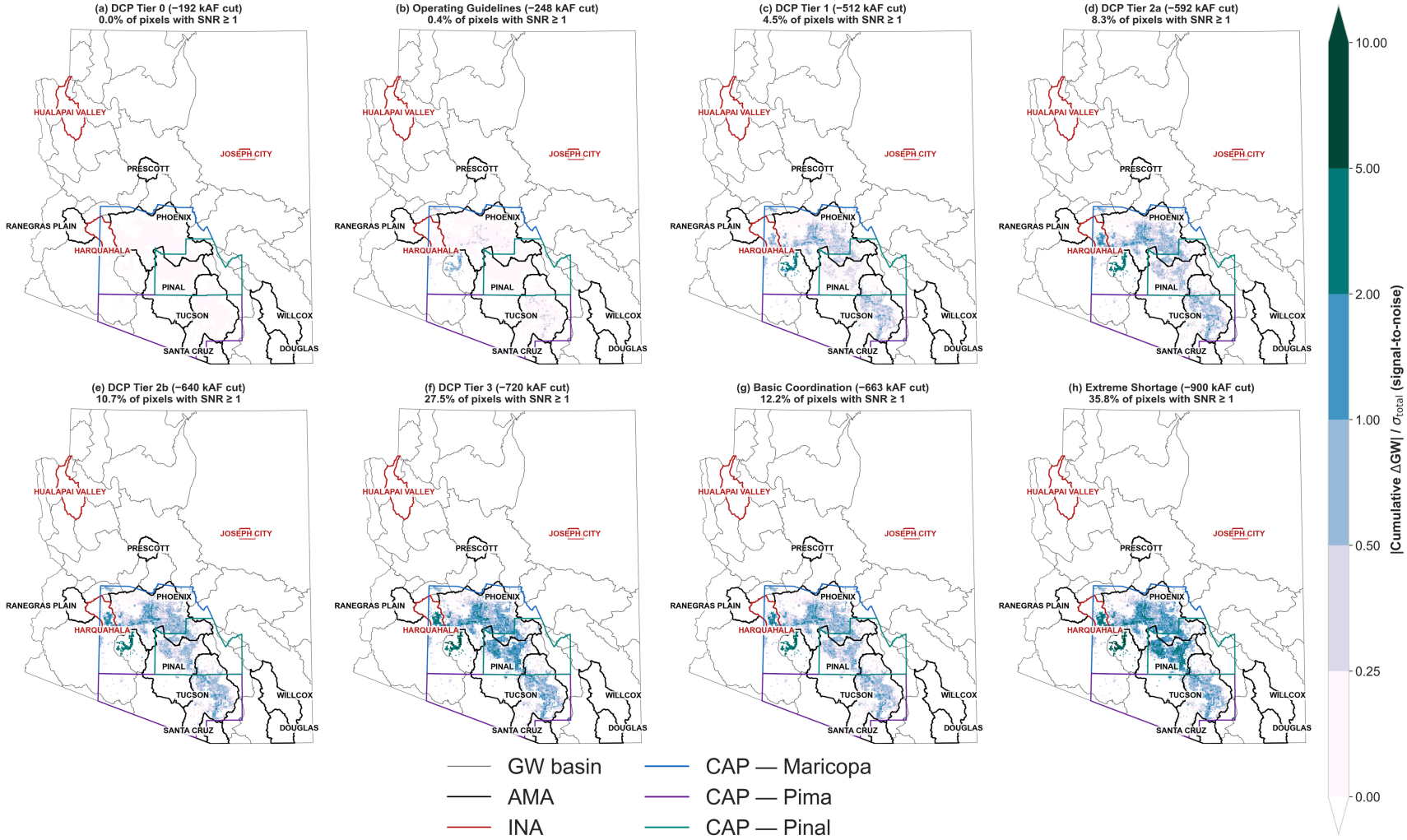


Fig. S10. Per-pixel signal-to-noise ratio of the cumulative additional groundwater pumping, SNR = $|\Delta GW_{cum}|$ / σ_{cum}, over 2027–2099 for the eight CAP shortage scenarios, with panels and cuts as in main-text Fig 5 (each cut relative to the 900 kAF baseline delivery). SNR ≥ 1 means the scenario signal exceeds the 1σ uncertainty of Fig. S9; panel titles give the share of pixels with SNR ≥ 1. As for ΔGW, pixel values distribute the basin result in proportion to each pixel's share of TotalGW.

Supplementary References

1. Majumdar, S., Smith, R. G., ReVelle, P., Hasan, M. F., Wogenstahl, C., Tadych, D. E., & Meeker, L. (2026). *AZ-Hydro — Historical and Projected Arizona Annual Water Use: Software, Input Data, Models, Raster and Well Package Predictions, and Validation at 2 km Resolution (1896–2099)* (Version 1.2). Zenodo. https://doi.org/10.5281/zenodo.19057935

2. ADWR. (2021). *GIS Data and Maps*. https://new.azwater.gov/gis

3. CAP. (2026). *Central Arizona Project - CAP*. https://www.cap-az.com/

4. Sohl, T. L., Reker, R., Bouchard, M., Sayler, K., Dornbierer, J., Wika, S., Quenzer, R., & Friesz, A. (2016). Modeled historical land use and land cover for the conterminous United States. *Journal of Land Use Science*, *11*(4), 476–499. https://doi.org/10.1080/1747423X.2016.1147619

5. MacKichan, K. A., & Kammerer, J. C. (1961). *Estimated use of water in the United States, 1960: U.S. Geological Survey Circular 456*. https://doi.org/10.3133/cir456

6. Anning, D. W., & Duet, N. R. (1994). *Summary of ground-water conditions in Arizona, 1987-90: U.S. Geological Survey Open-File Report 94-476*. https://doi.org/10.3133/ofr94476

7. USGS. (2026). *Water Use in the United States*. https://www.usgs.gov/mission-areas/water-resources/science/water-use-united-states#publications

8. Suresh, S., Hossain, F., Mishra, V., & Hossain, N. (2026). GRAIN – a Global Registry of Agricultural Irrigation Networks. *Earth System Science Data*, *18*(3), 1855–1875. https://doi.org/10.5194/essd-18-1855-2026

9. Lisk, M. D., Grogan, D. S., Zuidema, S., Zheng, J., Caccese, R., Peklak, D., Fisher-Vanden, K., Lammers, R. B., Olmstead, S. M., & Fowler, L. (2024). Harmonized Database of Western U.S. Water Rights (HarDWR) v.1. *Scientific Data*, *11*(1), 598. https://doi.org/10.1038/s41597-024-03434-6

10. Lisk, M. D., Grogan, D. S., Zuidema, S., Caccese, R., Peklak, D., Zheng, J., Fisher-Vanden, K., Lammers, R., Olmstead, S., & Fowler, L. (2024). *HarDWR — Harmonized Database of Western U.S. Water Rights (v2.0)*. MSD-LIVE Data Repository. https://data.msdlive.org/records/z0h32-ne023

11. Autobee, R. (1993). *The Salt River Project*. Denver, Colo.: Bureau of Reclamation History Program. https://www.usbr.gov/projects/pdf.php?id=183

12. Salt River Project. (2026). *A history of canals in Arizona*. https://www.srpnet.com/about/history/canal-history

13. Pima-Maricopa Irrigation Project. (2002). *Building the Florence-Casa Grande Project Canals*. https://www.gilariver.com/lessons/sancarloslesson33.pdf

14. Bureau of Indian Affairs. (2026). *About the San Carlos Irrigation Project*. https://www.bia.gov/programs-services/power-utilities/scip-power/about-scip

15. ADWR. (2025). *ADWR Annual Report 2025*. https://www.azwater.gov/sites/default/files/2025-08/2025_ADWR_ANNUAL_REPORT_web.pdf

16. USBR. (2026). *Operating Guidelines: Colorado River Guidelines for Coordinated Operations of Lake Powell and Lake Mead, Operating Years 2027 and 2028*. U.S. Department of the Interior. https://www.usbr.gov/ColoradoRiverBasin/post2026/decision-doc/2027-2028OperatingGuidelines_Final.pdf